ERDC/CERL TR-15-6

US Army Corps
of Engineers®
Engineer Research and
Development Center

ERDC
INNOVATIVE SOLUTIONS
for a safer, better world

*Military Facilities Engineering Technology*

# Multifunctional Nanocomposites for Improved Sustainability and Protection of Facilities

Dongsheng Mao, Igor Pavlovsky, Richard L. Fink, Jonathan C. Trovillion, Veera M. Boddu, L.D. Stephenson, Debbie J. Lawrence, and Ashok Kumar

May 2015

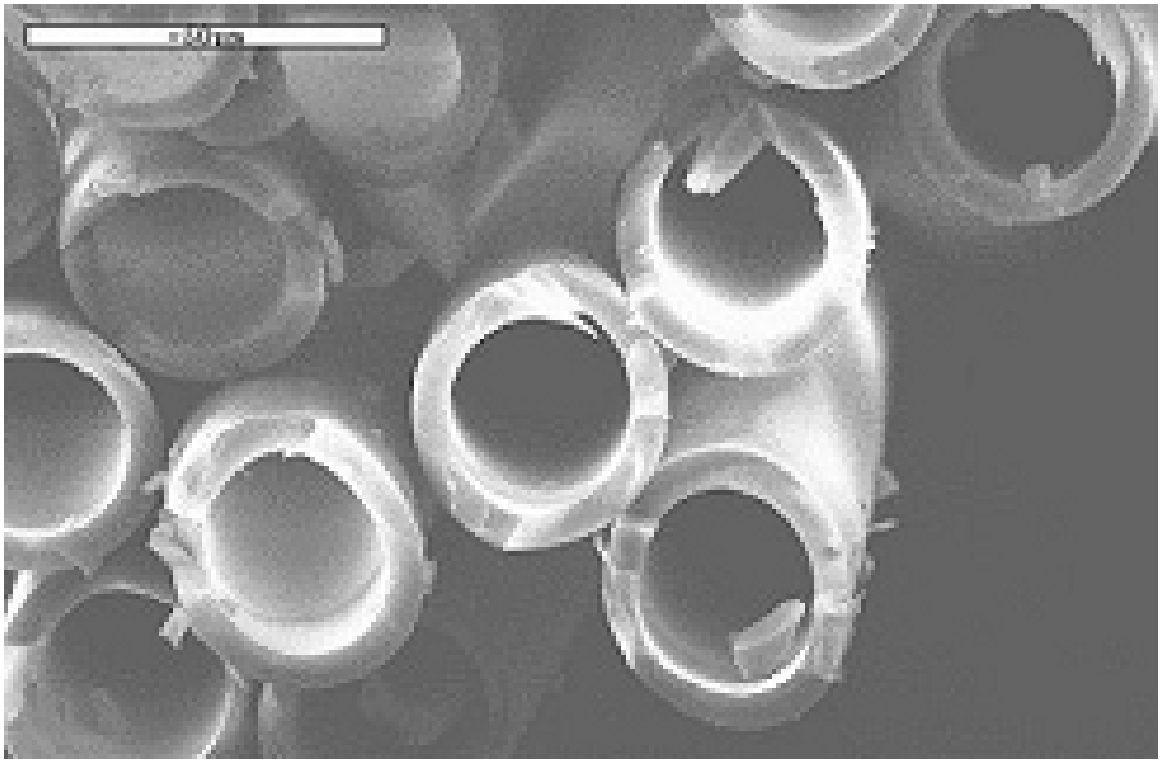

Construction Engineering
Research Laboratory

**The US Army Engineer Research and Development Center (ERDC)** solves the nation's toughest engineering and environmental challenges. ERDC develops innovative solutions in civil and military engineering, geospatial sciences, water resources, and environmental sciences for the Army, the Department of Defense, civilian agencies, and our nation's public good. Find out more at www.erdc.usace.army.mil.

To search for other technical reports published by ERDC, visit the ERDC online library at http://acwc.sdp.sirsi.net/client/default.

ERDC/CERL TR-15-6
May 2015

# Multifunctional Nanocomposites for Improved Sustainability and Protection of Facilities

Jonathan C. Trovillion, Veera M. Boddu, L.D Stephenson,
Debbie J. Lawrence and Ashok Kumar

*Construction Engineering Research Laboratory*
*U.S. Army Engineer Research and Development Center*
*2902 Newmark Drive*
*Champaign, IL 61822*

Dongsheng Mao, Igor Pavlovsky, and Richard L. Fink

*Applied Nanotech, Inc.*
*3006 Longhorn Blvd., Suite 107*
*Austin, TX 78758*

Final report



Prepared for U.S. Army Corps of Engineers
Washington, DC 20314-1000

Under Project #157067, "DEFEAT-Defeat of Emerging Adaptive Threats"
Project #331695, "High Performance Materials Research Program"

# Abstract

The U.S. Army makes worldwide use of high-performance ballistic-resistant fiberglass composite panels for force protection and other applications. This widespread use creates a need for an improved panel material that offers better bullet resistance at a lighter weight while still meeting existing ballistic resistance standards. The team's work to solve the Army's need included conceiving, developing, and validating a new nanocomposite material that is made of epoxy resin blended with functionalized carbon nanotubes (CNTs) that exhibits highly improved flexural strength and electrical conductivity for improving ballistic resistance in lighter weight glass fiber reinforced polymer (GFRP) ballistic panels. In addition, the team's work tested various options for adding self-healing, CNT reinforcement, EMI shielding, and self-decontaminating properties for GFRP panels. Results of separate studies included in this report are: loading panels with CNTs by using different mass fractions and functionalization methods; introducing a self-healing agent directly to the matrix or contained in embedded hollow glass fibers; using layers of proprietary CNT sheeting in the GFRP composite; testing the electromagnetic impulse (EMI) shielding effects of introducing conductive materials; and adding a biocide-containing coating to finished panels.

# Contents

# Figures and Tables

## Figures

## Tables

# Preface

This study was conducted for Headquarters, U.S. Army Corps of Engineers under Research, Development, Test, and Evaluation (RDT&E) Program Element 622784 T41, "Military Facilities Engineering Technology," Project #157067, "DEFEAT–Defeat of Emerging Adaptive Threats" and Project #331695, "High Performance Materials Research Program." The technical monitor was Pamela Kinnebrew (ERDC-GSL).

The work was performed by the Materials and Structures Branch (CF-M) of the Infrastructure Division (CF), U.S. Army Engineer Research and Development Center, Construction Engineering Research Laboratory (ERDC-CERL). At the time the work was done, Vicki L. Van Blaricum was Chief, CEERD-CF-M; L. Michael Golish was Chief, CEERD-CF; and Kurt Kinnevan, CEERD-CV-T, was the Acting Technical Director for Adaptive and Resilient Installations. The Deputy Director of ERDC-CERL was Dr. Kirankumar Topudurti, and the Director was Dr. Ilker Adiguzel.

At the time of publication, LTC John T. Tucker III was the Commander of ERDC, and Dr. Jeffery P. Holland was the Director.

# Unit Conversion Factors

| Multiply | By | To Obtain |
|---|---|---|
| feet | 0.3048 | meters |
| foot-pounds force | 1.355818 | joules |
| gallons (U.S. liquid) | 3.785412 E-03 | cubic meters |
| inches | 0.0254 | meters |
| microns | 1.0 E-06 | meters |
| ounces (mass) | 0.02834952 | kilograms |
| ounces (U.S. fluid) | 2.957353 E-05 | cubic meters |
| pounds (mass) | 0.45359237 | kilograms |
| square feet | 0.09290304 | square meters |

# Executive Summary

The U.S. Army Engineer Research and Development Center, Construction Engineering Research Laboratory (ERDC-CERL) led a series of studies designed to improve the high-performance composite ballistic-resistant panels used worldwide by the Army for force protection, physical security, and other applications. The principal thrust of the research was to reduce the weight and cost of standard panels by improving their material properties to meet established protective standards at reduced thickness. In opening panel material formulations and configurations to advanced development, the research was leveraged to investigate the introduction of other improvements in order to create a new category of multifunctional composite materials for military applications.

Efforts to improve the mechanical and physical properties of the basic GFRP panel, and to add new functionalities to it, were executed in a series of separate but related studies. These studies involved the reformulation of the composite polymer matrix, introduction of carbon nanotubes (CNTs) in both particle and sheet form, development and addition of a self-healing agent to panel components, introduction of conductive materials to serve as electromagnetic interference (EMI) shielding, and an amendment to self-decontaminate panel surfaces exposed to harmful biological substances. Private-sector participants in these studies included Applied Nanotech, Inc. (ANI) in Austin, Texas; and Armortex in Schertz, Texas.

Different CNT loadings and functionalization methods within the epoxy and polyester resins were studied in order to achieve optimized mechanical property improvement of the matrix. The following results were achieved:

- **For -COOH functionalized CNTs at a loading of 1.0 wt% in the polyester resin**: 23% improvement of flexural strength, 4% improvement of the flexural modulus, 26% improvement of compression strength, and 10% improvement of compression modulus were achieved. However, the impact strength decreased by about 48%.
- **For -OH functionalized CNT at a loading of 0.5 wt% in polyester resin**: 18% improvement of flexural strength, 4% improvement of the flexural modulus, 22% improvement of compression strength, 10%

improvement of compression modulus, and 24% improvement of the impact strength were achieved.
- **For CNT-reinforced epoxy GFRP panels**, a 5% improvement of the V50 ballistic resistance was achieved. For CNT-reinforced polyester GFRP panels, the improvement was minimal.

A proprietary CNT sheeting product was also studied to improve the ballistic resistance of the GFRP panels. The number of the CNT sheets used and their position in the multilayer GFRP laminate were studied for improvement of the ballistic resistance. The observed improvement was marginal, and the same level could be achieved more cost-effectively using other approaches such as mixing CNTs into the polymer matrix.

To add a self-healing factor to GFRP panels, hollow glass fibers (HGFs) filled with a self-healing agent were investigated. Different sizes of the HGFs, loading of the self-healing agent, and the position of the self-healing layers were studied. The following ballistic testing results were noted:

- Panels with HGF were weaker than the control panels that did not have HGF, showing a 5–10% decrease of the V50 value.
- The placement of the self-healing agent may affect the ballistic resistance of the panels.
- For panels that were shot and then given time for the self-healing agent cure, performance in the V50 test exceeded the performance of virgin panels using HGF, and it came close to the performance of the control panels with no HGF.

After ballistic testing, the mechanical properties of self-healing panels with HGF, the following results were observed:

- The effect of different loadings (2.5%, 5.0%, and 10.0%) of self-healing agent on the self-healing efficiency was studied, and it was found that a loading of 2.5% has the best self-healing efficiency.
- The compression strength of the GFRP panels with 2.5% loading of the self-healing agent without impact was 50.0 MPa.
- The compression strength after an impact energy of 30 J, tested within 1 hour after the impact, was 35.2 MPa. This means that the strength of the GFRP panel was decreased by about 30% after the impact. It was

concluded that the self-healing agent will not effectively react with the catalyst within 1 hour.
- The compression strength of the GFRP panel with 2.5% loading of the self-healing agent after an impact energy of 30 J, tested a week after the impact, was 48.1 MPa. The self-healing efficiency in this test was 96%, and the panel recovered to nearly the full compression strength of the undamaged panel (50.0 MPa).

In order to introduce EMI shielding to ballistic GFRP panels, additions of copper mesh screen, conductive carbon coating, and Exclucent material to the matrix were investigated, with the following results:

- For the GFRP panels incorporated with copper mesh screen, the EMI shield achieved 60–66 dB between 0.1 to 1000 MHz frequencies. It was shown to have less shielding at the 8-10 GHz range.
- For the GFRP panel coated with a conductive carbon layer, EMI shielding was on the order of 5–10 dB. At 0.1 MHz and 1 MHz the average was less than 1 dB, and at 10 MHz the average shielding was found to be 5.17 dB. At higher frequencies the shielding was at an average of 23 dB.
- The average shielding was found to be 4.33 dB at 100 kHz, 16.3 at 1 MHz, and 39 dB at 10 MHz for the GFRP panel incorporated with an Exclucent film on its surface.

In the investigation of a biocidal functionality for GFRP panels, the results showed that biocides added to a topcoat were not efficient for spore decontamination. This result was attributed to chemicals in the paint that blocked the active surface sites or chemical groups of the agent or the added photocatalysts. The photocatalysts sprayed over the dried topcoat offered much better performance. The spore inactivation rate achieved over 180 min of exposure of sunlight was as high as 97.2% for PhotoScrub V (log kill = 1.56), and it was lower for ZnO-based compositions.

Finally, a number of full-size GFRP panels (4 x 8 ft x 0.5 in.) were fabricated with different functionalities to provide evidence that production could be scaled up for commercialization.

(This page intentionally blank.)

# 1 Introduction

## 1.1 Background

The U.S. Army uses high-performance ballistic-resistant fiberglass panels for force protection and other applications, both within the United States and at numerous locations overseas. This type of panel is a composite material made from woven glass fibers integrated with a thermosetting polymer material such as polyester, epoxy, or vinyl ester. Such panels are designed for architectural applications and automotive armor.

A typical ballistic-resistance standard for these panels is the UL 752 Standard's Level 3 criteria, providing projectile capture and retention capabilities to avoid ricochet (2005). A panel meeting this standard (0.5 in. nominal thickness) can withstand multiple shots from a .44 Magnum firearm discharging a 240-grain projectile at 1,450 feet/second with no penetration. In other words, these panels capture bullets within the plies of the laminate material; steel, aluminum, and ceramic armor panels, by comparison, pose a high potential for ricochet.

A typical composite panel (96 x 48 x 0.5 in.) meeting the UL 752 Level 3 standard weighs 165 lb, which is 25% the weight of sheet steel of the same dimensions. A typical panel consists of approximately 40% resin and 60% glass fiber by volume, and tends to be very expensive. The U.S. Army has a need for an improved fiberglass composite panel material that offers better bullet resistance (a 30% improvement in ballistic resistance is sought) at a lighter weight. In meeting that need, the panel also would be easier to install, would lower the risk of structural damage, and would cost less to procure.

## 1.2 Objectives

A comprehensive approach to improving the ballistic performance of protective structural panels must involve both the reinforcing fiber and the polymer resin matrix. Material design at this level also presents opportunities for introducing other performance-enhancing capabilities such as blast resistance, degradation resistance, shielding against electromagnetic interference (EMI), and even surfaces that self-decontaminate from the attachment of harmful biological agents.

The principal objective of this work was to investigate material formulations or configurations that would allow at least a 25% decrease in composite panel weight while maintaining conformance to the UL 752 Level 3 standard for ballistic resistance. Secondary objectives included investigating ways to add material that would add self-healing capabilities, EMI shielding, and biocidal properties.

## 1.3 Approach

A series of investigations was performed by the U.S. Army Engineer Research and Development Center, Construction Engineering Research Laboratory (ERDC-CERL). Private-sector participants in this work were Applied Nanotech, Inc. (ANI) of Austin, Texas; and Armortex of Schertz, Texas. These investigations were leveraged through related studies intended to evolve the panels into multifunctional materials that could enhance physical security and force-protection applications.

An extensive literature review related to the ballistic resistance of composites was performed (Chapter 2). Over 200 publications were investigated as well as presentations and news articles from both industrial and academic sources related to ballistic resistance. Key properties of the polymer matrix were identified as potentially critical for improving ballistic resistance of the composite, and this information served as a primary focus for ANI. Based on the literature review, this work's primary properties for testing were impact strength, compression strength and modulus, and glass transition temperature. Secondary properties for testing were flexural strength and modulus, interlaminar shear strength, and toughness.

This project focused on improving the mechanical and physical properties of the carbon nanotube (CNT)-reinforced polymer matrix. Polyester was selected as the matrix because it is one of the most popular thermosetting materials for ballistic-resistant fiberglass reinforced polymer (FRP) composite panel manufacturing; it is the material of choice for Armortex, the project's panel manufacturing subcontractor. EPON™ Resin 828[1] epoxy was used in the feasibility study since study authors had considerable mechanical data and experience with this material system. This approach allowed for testing the ballistic-resistance benefit of functionalizing a resin with CNT materials. The feasibility study work, under the Broad Agency

[1] EPON 828 is an undiluted clear difunctional bisphenolA/epichlorohydrin-derived liquid epoxy resin, manufactured by Hexion Specialty Chemicals.

Announcement (BAA) Phase I program (W9132T-09-T-0139), demonstrated that the ballistic resistance of the glass-fiber reinforced polymer (GFRP) panels could be improved by using an Epon 828 matrix with CNT reinforcement (Trovillion et al. 2010). A 5% improvement of the ballistic resistance was achieved under V50 testing for the GFRP panels using CNTs (see Figure 1 and Table 1). While these numbers fell short of the 30% improvement goal set for this program, obtaining an improvement of 5% over the neat resin panels is a very encouraging initial result.

Figure 1. A 0.50 in. fragment simulating projectile (FSP), showing the tapered edges of the strike face.

Table 1. Results from V50 ballistic testing.

| Designation | V50 (ft/sec) | Max Span (ft/sec) | Increase (%) |
|---|---|---|---|
| Neat Resin (No CNTs) | 1768 | 74 | -- |
| 0.5wt% CNTs with Functionalization-A | 1775 | 99 | 0.4 |
| 1.5wt% CNTs with Functionalization-B | 1856 | 60 | 5.0 |

It was learned that the epoxy material may not be the best material for manufacturing large ballistic-resistant panels. Equipment needed for curing the epoxy is more expensive, and the viscosity of the epoxy material is too high for use in common hot-press equipment. Polyester was chosen for

the Phase II study since it is the typical material of choice for ballistic-resistant panels.

Commercial partner Armortex incorporated the CNT-enhanced polyester material into their "hot press" process. Steps explored to make the panel fabrication process easier and recommended options for scale-up consist of the following:

1. Determined and quantified the factors (mechanical and physical properties) that will lead to improvement of the ballistic resistance of the composite glass fiber panels.
2. Proposed an experimental design significantly improved the factors of the polymer matrix determined in step 1. A series of CNT-reinforced nanocomposites (resins only) were synthesized. Mechanical and physical properties of the samples were characterized.
3. Based on the unique properties of the CNT-reinforced resins achieved in Step 2, preparation of CNT-reinforced thermosetting resin was completed and sufficient quantities were delivered to Armortex for fiberglass panel fabrication.
4. Multiple FRP composite panels at standard and reduced thicknesses were prepared by Armortex.
5. Demonstrated improved ballistic resistance of the CNT-reinforced composite panel, showing that ballistic resistance can be maintained with a panel of reduced weight.

# 2 Literature Review

An extensive literature review was performed on topics related to the ballistic resistance of composite materials. The information was from the following sources:

- Nerac[1] (www.nerac.com; keywords: ballistic resistance, composite) and
- World Wide Web (using standard Internet search engines).

Based on the Nerac search, a total of 93 pieces of information were obtained which included published journal articles, papers from conference proceedings, and issued patents and publications. Additional information was also achieved based on the Internet search, and over 200 of those publications were investigated. A number of presentations and news articles from both industrial and academic areas were also studied related to ballistic resistance. All information investigated was published from the early 1980s to present. In summary, intensive research and development on the ballistic resistance of composites was conducted during the last three decades.

The publications covered a wide range of materials that were chosen for ballistic-resistant applications. Those materials included:

- metal (Vanark et al. 1996; Polito et al. 1998)
- steel (Reddy and Mohandas 1996; Showalter et al. 2008)
- alloy (Anderson and Dannemann 2002; Gogolowski and Morgan 2001)
- ceramic (Gilde and Adams 2005; VietnamGear.com 2006; Franks 2008)
- concrete (Ben-Dor et al. 2009; Zhong et al. 2008)
- polymeric materials (Kohlman 1995; Edwards and Waterfall 2008; Wright et al. 1993)

Fibers were also synthesized or fabricated based on materials such as:

- steel (Nycon n.d.; Takazuka 1979)
- carbon (Aliabadi et al. 2006)
- glass (PPG Industries n.d.; Total Security Solutions n.d.)

[1] Nerac of Tolland, Connecticut, is a research services company.

- kevlar (DuPont n.d.; Karahan et al. 2008)
- nylon (Tatum 2015)
- polyethylene (Honeywell 2015)

In a majority of cases, these materials were combined with each other to form a single uniform composite (Colakoglu et al. 2007; Naik et al. 2005: Harel et al. 2002; Gooch and Burkins 2001; Ahmad et al. 2007). Sandwich or laminate structures were also designed and utilized in order to achieve improved ballistic resistance of the composites (Xu et al. 2008; Patel et al. 2004; Reyes-Villanueva and Cantwell 2004). Fibers could be unidirectional, woven, or non-woven fabrics which could be either integrated with matrix or standing by themselves.

A large portion of the publications were focusing on the ballistic impact behavior and related modeling of the specific materials to try to understand the mechanism of the damage based on different ballistic testing methods (Sun and Potti 1996; Ben-Dor et al. 2005; Naik et al. 2005; Kyziol 2007; Gamma et al. 2005; Velmurugan et al. 2006). Hence, only a few of these publications can supply the direction needed for the target of Task 1. No publication was found that presented a systemic study of the relationship between the mechanical properties of the composites and their ballistic resistance. Table 2 shows factors affecting the ballistic resistance of different materials and ballistic testing methods that were mentioned in publications listed in the table.

Table 2. Factors to affect the ballistic resistance of the composites.

| Material system | Reference | Ballistic testing method | Factors |
|---|---|---|---|
| Carbon nanotube fiber | Rincon 2007 | - | Strength |
| Carbon nanotube mat | Nanocomp Technologies, Inc. of Merrimack, New Hampshire | - | Strength |
| Multi-walled carbon nanotube (MWNT) / glass fiber / vinyl ester epoxy | Grujic et al. 2007 | 0.50 caliber FSP (605 m/s) | Interfacial bond strength between CNTs and matrix |
| Carbon nanotube / polycarbonate | Abdelkader et al. 2002 | FSP depth of penetration | Compressive strength |
| $SiO_2$ nanoparticle / ethylene glycol / Kevlar fabrics | Lee et al. 2003 | FSP (244 m/s) | Shear thickening effect/rigidness |

| Material system | Reference | Ballistic testing method | Factors |
|---|---|---|---|
| $WS_2$ nanocomposite | Genuth and Yaffee 2006 | Steel projectile (1.5 km/s) | Rigidness |
| $TiO_2$ nanoparticle / polyurethane foam | Udden et al. 2009 | FSP high-velocity test (800 m/s) | Improved mechanical properties |
| Layered silicate / nylon 6 | Ostermayer et al. 2001 | V50 | Toughness |
| Nanoparticle / epoxy | Raju et al. 2006 | Simulation modeling | Strength and modulus |
| CBDO co-polyester | Booth et al. 2006 | FSP V50 (up to 355 m/s) | Impact strength |
| Glass fiber / polyester | Horsfall et al. 2007 | NATO standard 7.62 x 51 mm ammunition | Compressive strength |
| Kevlar fiber / Polybenzoxazine alloys | Pathomsap et al. 2006 | 9 mm handgun | Glass transition temperature |
| Cloth ballistic panel | Prosser et al. 2000 | 0.22 caliber projectiles | Heat |
| Polyolefin / Kevlar KM2 laminates | Walsh et al. 2007 | 4.1 g FSP | Lower stiffness, better performance |
| FRP composites | Faur-Csukat 2005 | Prediction | High modulus, high impact strength |
| Fiber fabrics / resin | Walker 2001 | Modeling | Bending strength |
| GFRP composite | Quan and Birnbaum 1999 | Smooth particle hydrodynamics simulation/projectile striking | Interlaminar delamination |
| S2 glass /epoxy | Sevkat et al. 2007 | V50 (300, 500, 950 m/s) | Delamination |
| Glass fiber / epoxy | Roberts et al. 2002 | Wedge-shaped titanium projectile (259 m/s) | Delamination |
| Glass fiber/polypropylene<br>Glass fiber/vinyl ester | Chen et al. 2007a | FSP V50 (200–600 m/s) | Delamination capability |
| Glass fiber (vinyl ester, unsaturated polyester, and epoxy) | Chen et al. 2007b | V50 (200–600 m/s) | Delamination capability |

| Material system | Reference | Ballistic testing method | Factors |
|---|---|---|---|
| Carbon / epoxy / Kevlar | Gama et al. 2006 | Low-velocity impact test | Wetting between epoxy and Kevlar |
| Glass fiber / polymer | Jensen and McKnight 2004 | Not disclosed | Adhesion between fiber and matrix |
| Glass fiber / epoxy | Jensen et al. 2004 | Drop weight testing | Sizing between fiber and epoxy |
| Polyethylene /epoxy | Brown et al. 1991 | — | Bonding between fiber and matrix |
| Hemp / epoxy random mat; Jute /epoxy plain weave laminate | Santulli and Caruso 2009 | Falling weight impact (11.4 kg mass, 19.8 mm diameter impactor) | Direction of fiber |
| Braided fiber fabrics / epoxy | Hosur et al. 2007 | Low-velocity impact tests/high strain rate compression | Structure of fiber fabrics |
| Glass fiber / sandwich | Mantena et al. 2010 | Natl. Inst. of Justice standard, Level III impact | Direction of fiber |
| Fiber / toughened epoxy | Brown and Sevkat 2008 | Low-impact test (40–100 J energy) | Structure of the system |
| Glass fiber / epoxy | Hong and Liu 1989 | Steel projectile (impact velocity 20–100 m/s) | Fiber orientation |

## 2.1 CNTs for improved ballistic resistance

Fiber or yarn consisting of carbon nanotubes is another very promising ballistic material because of their excellent strength. Both the British and American militaries have expressed interest in carbon fiber woven from carbon nanotubes that was developed by Prof. Windle's group at Cambridge University in Cambridge, United Kingdom, for the potential use in body armor (see Figure 2; Rincon 2007). The CNT-made carbon fibers created at Cambridge are very strong, lightweight, and good at absorbing energy in the form of a fragment travelling at very high velocity. The CNT fibers have better performance than Kevlar fibers in all respects. In 2009, large format CNT sheets (4 x 8 ft) began being produced at Nanocomp

Technologies (Nanocomp 2009). The carbon nanotube mats are lighter and stronger than aluminum.

Figure 2. Carbon nanotube fibers are lightweight, but exceptionally strong (Rincon 2007).

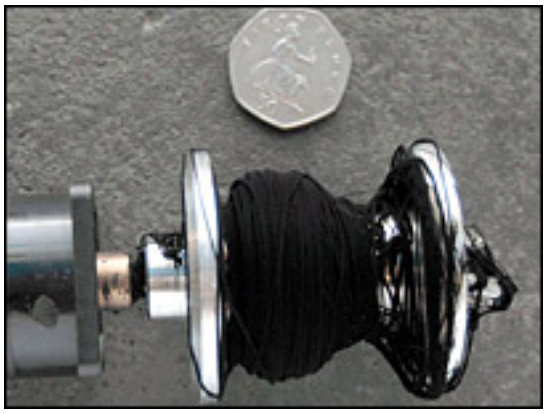

There are other publications related to carbon nanotube reinforcement of composites for ballistic applications. Based on the work of Clemson University in Clemson, South Carolina, the location and thickness of MWNT reinforced poly-vinyl-ester-epoxy matrix composite mats within a hybrid armor based on E-glass reinforced poly-vinyl-ester-epoxy composite laminates affect the ballistic performance of the armor (Grujici et al. 2007). The optimal hybrid armor design is associated with thicker (100 μm) MWNT-reinforced poly-vinyl-ester-epoxy matrix composite mats placed near the front face of the armor. The U.S. Army cooperated with MER Corporation of Tucson, Arizona, for the investigation of the CNT-reinforced polycarbonate nanocomposites for lightweight armor materials (Abdelkader et al. 2002). Dispersion of the nanotubes free of agglomerates was achieved by solvent mixing and dry blending as witnessed in scanning electron microscope (SEM) imaging. At the CNT/polycarbonate ratio of 30 wt%, the compressive strength reached the highest point (more than 50% improvement over the neat polycarbonate). The ballistic performance based on fragment-simulating projectile (FSP) penetration depth was also at a maximum at this loading; thus, the improvement of the compressive strength of the CNT-reinforced polycarbonate was consistent with the performance of the ballistic resistance (Figure 3).

Figure 3. Correlation of compressive strength with ballistic performance of CNT-polycarbonate nanocomposite (Abdelkader 2002).

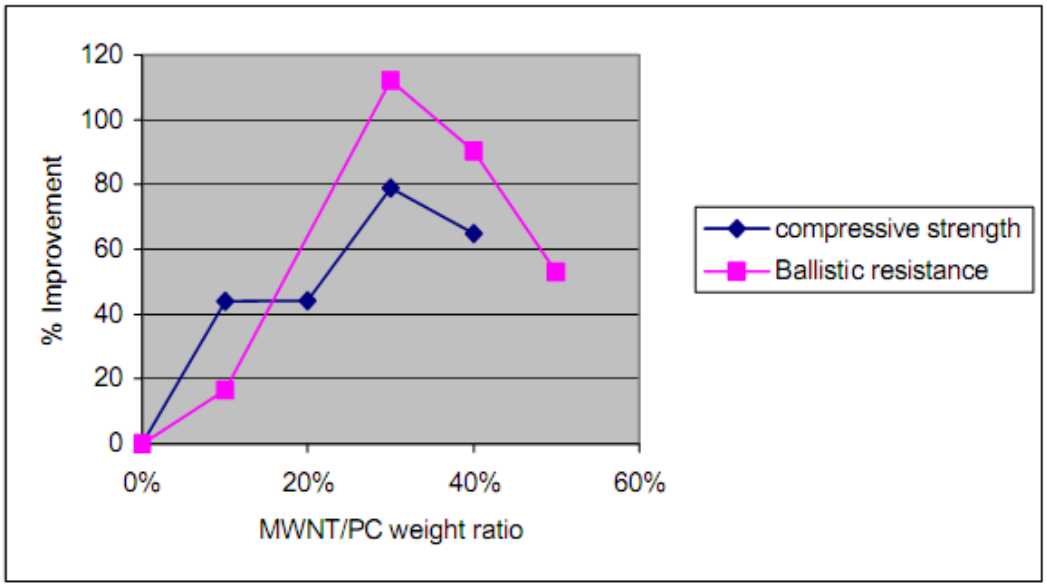


## 2.2 Other nanotechnologies for improved ballistic resistance

Currently, there are a number of methods by which nanomaterials are being implemented into body armor production. The first, developed at the University of Delaware in Newark, Delaware, is based on silicon dioxide ($SiO_2$) within the suit that becomes rigid enough to protect the wearer as soon as a kinetic energy threshold is surpassed (Lee et al. 2003). These coatings have been described as shear thickening fluid which is an aqueous suspension containing $SiO_2$ nanoparticles (446 nm average size) at a concentration of about 40 wt%. The suspension was impregnated with Kevlar woven fabrics. This material demonstrated improved ballistic resistance based on a NATO standard FSP at a velocity of 244 m/s. The incorporation of the $SiO_2$ nanoparticles makes the Kevlar woven fabrics more rigid (also called shear thickening effect) to achieve enhanced ballistic performance. These nano-infused fabrics were licensed by United Kingdom-based BAE Systems; no products have been released based on this technology.

In 2005 ApNano, an Israeli company, developed a material that was always rigid (Figure 4; Genuth and Yaffee 2006). It was announced that this nanocomposite based on tungsten disulfide ($WS_2$) nanotubes was able to withstand shocks generated by a steel projectile traveling at velocities of up to 1.5 km/s. The material was also reportedly able to withstand shock pressures generated by the impacts of up to 250 metric ton force per square centimeter. During the tests, the material proved to be so strong

after impact that the samples remained essentially unmarred. Additionally, the material was tested under isostatic pressure and found to be stable up to at least 350 metric ton force per square centimeter.

Figure 4. Tungsten disulfide nanotube's unique structure is responsible for its remarkable strength and durability (Genuth and Yaffee 2006).

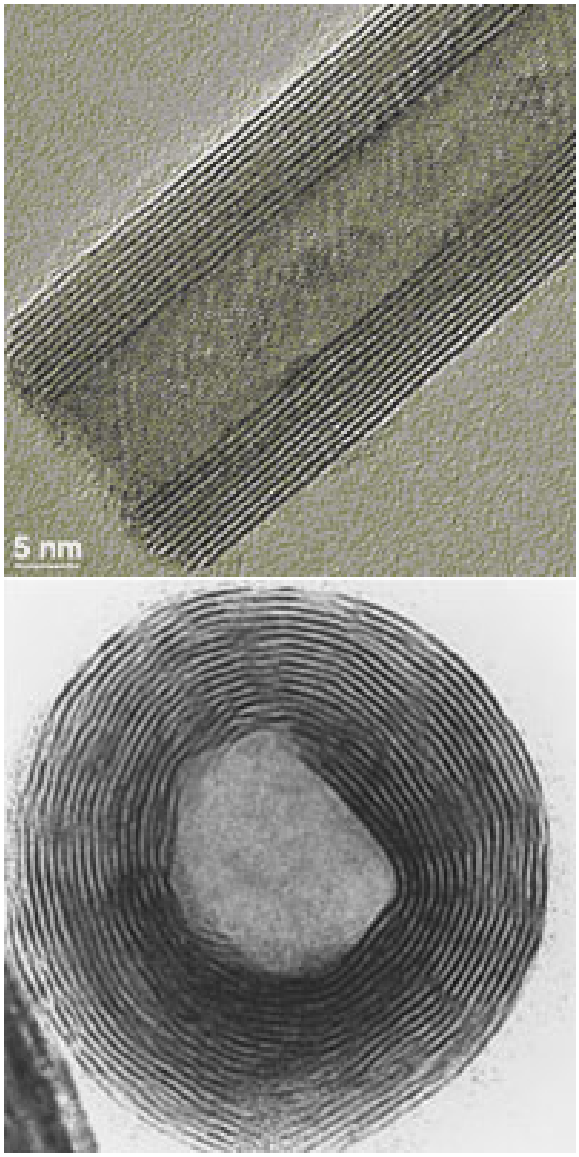


Purdue University achieved improved ballistic resistance of polyurethane foam by titanium dioxide ($TiO_2$) nanoparticle reinforcement (Uddin et al. 2009). The $TiO_2$ nanoparticles were dispersed through a sonic cavitation process and the loading of particles was 3 wt% of the total polymer weight. The material was impacted with FSP in a 1.5 in. gas gun. Projectile speed was set up to have complete penetration of the target in each experiment. Test results indicated that nano-enhanced material absorbed about 20%

more kinetic energy than its neat counterpart. The corresponding increase in ballistic limit was around 12% over the neat control samples. It is believed that improvement of the ballistic resistance is due to the improvement in the "mechanical properties" of the matrix using nanoparticle reinforcement (specific mechanical properties were not specified by the authors).

Layered silicate (nanoclay)-reinforced Nylon 6 nanocomposite was also prepared for ballistic study based on V50 testing method (0.22-cal. FSP) (Ostermayer et al. 2001). The results of the ballistic testing showed that the unmodified material had a higher V50 436 ft/s, then the nanocomposite material, which had a V50 of 338 ft/s. Both samples displayed significant spalling and radial fracture. It was concluded that the lower V50 of the clay-modified Nylon 6 nanocomposite was brittle and had lower toughness than that of the neat Nylon 6.

Ballistic resistance of nanoparticle reinforced epoxy nanocomposites was studied based on simulation (Raju et al. 2006). Based on a unit cell model created for nanoclay-epoxy composites, the effect of nanoparticle distribution on the maximum stress developed in epoxy resin was investigated using the Meshfree Particle Method-based simulation tool developed at MKP Structural Design Assoc. of Dexter, Michigan. The ensemble average of mechanical property for nanoclay-epoxy composite was also studied. Several armor samples reinforced with nanoclay-epoxy composites were fabricated and ballistic tests were conducted on the nanoclay-reinforced composite armors. It was found that higher mechanical properties, such as modulus and strength, will help to improve the performance of composite armor systems.

## 2.3 Factors affecting ballistic resistance of conventional reinforced composites

Texas State University at San Marcos, Texas, studied ballistic resistance for a unique copolymer called CBDO (2,2,4,4-tetramethyl-1,3-cyclobutanediol; Booth et al. 2006). This material displayed a notched-Izod value of 1070 J/m while maintaining $T_g$ near 100 °C. This is almost a 30% improvement of the impact strength compared to that of the bisphenol A (BPA) polycarbonate (850 J/m). FSP V50 (up to 355 m/s) showed that the CBDO copolymer performed with better ballistic resistance than polycarbonate.

Ballistic impact tests were performed on E-glass weave fabric polyester composite based on NATO's standard 7.62 x 51 mm ammunition (Horsfall et al. 2007). The strength of the panels was determined by compression testing after impact test and conformed to Suppliers of Advanced Composite Materials Association (SACMA) Recommended Method (SRM) 2R-94 (SACMA 1994). The compressive strength of the panels was determined in the "as manufactured" and impacted conditions. It was shown that the loss in panel strength was directly proportional to the kinetic energy absorbed from the projectile, irrespective of whether the panel was perforated.

A comparison study of the ballistic resistance of three materials was performed using Kevlar/epoxy, Kevlar/BA (benzoxazin), and Kevlar/PU (urethane elastomer) (Pathomsap et al. 2006). The ballistic test results are shown in Figure 5 (20 plies for each composite panel). Figure 5a exhibits the damaged area of Kevlar-reinforced epoxy, which showed complete penetration and very small delaminated area. Figure 5b shows the improvement of the energy absorption appearance of composites observed from the increase of the delaminated area of polybenzoxazine composite. The composite was still not able to resist the penetration of the bullet. Figure 5c presented the ballistic resistance of Kevlar-reinforced BA/PU alloy composite showing the best result. The curing behavior of the BA/PU alloys was found to occur at higher temperature with increased glass transition temperature, which resulted in significant energy absorption.

Heat can be critical in the ballistic resistance of composites. It was demonstrated that heat plays a role in the penetration of cloth ballistic panels by 0.22 caliber projectiles (Prosser et al. 2000). Heat is generated by friction between the surface of the projectile and the yarns, between yarns, and between filaments within a yarn in advance of and in the path of the projectile. Evaluations by light microscopy, polarized light microscopy, and scanning electron microscopy show heat-induced damage in fibers in the path of and several layers preceding the layer at which a 0.22 caliber projectile comes to rest. Heat is an energy sink, and depending on how, when, and where it is generated, can degrade the ballistic performance of the yarns. It is confirmed that increasing the glass transition temperature of the composite can potentially improve the ballistic resistance.

Figure 5. The ballistic tests of Kevlar-reinforced composites using a 9 mm bullet: (5a) Kevlar-reinforced epoxy composite; (5b) Kevlar reinforced benzoxazine composites; and (5c) Kevlar-reinforced benzoxazine alloy composite (Horsfall et al. 2007).

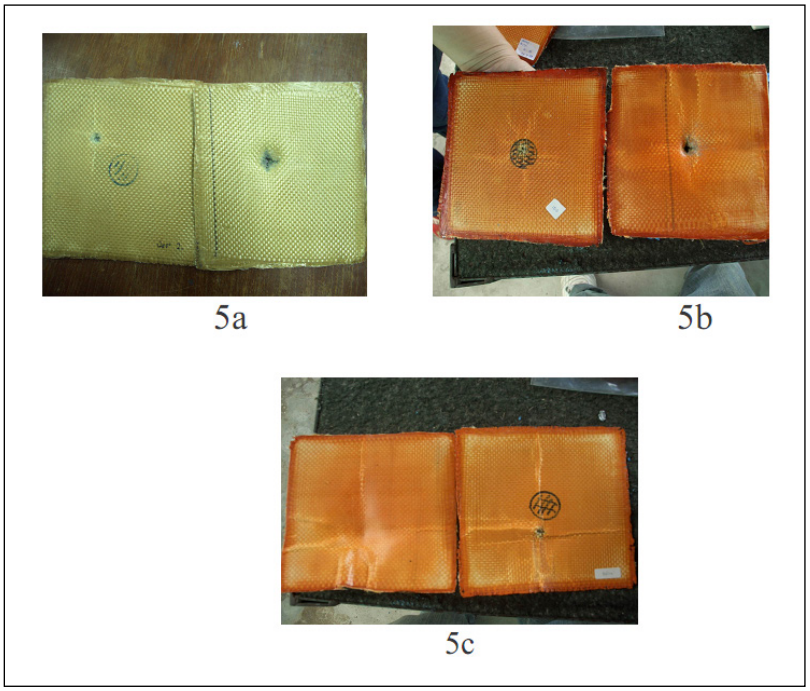


The Army Research Laboratory (ARL) studied the ballistic resistance of fiber-reinforced composite laminates (Walsh et al. 2007). Figure 6 presents the observed relationship between a laminate's stiffness and its ballistic resistance to a 4.1 g steel FSP. Overall, as suggested by this data, those materials that deflect easily (low stiffness) during impact may have the greatest ballistic efficiency. Thermoplastic matrices will lower the stiffness of the composite significantly depending upon resin content and the modulus of the neat thermoplastic matrix itself. Based on the same polymer matrix, the ballistic resistance may be improved if the stiffness is increased (e.g., K49/epoxy). For the K29/VE composite, the ballistic resistance is decreased if the flexural stiffness is increased. Different material systems may give totally different trends between the ballistic resistance and the flexural stiffness.

Figure 6. Relationship between ballistic efficiency (V50) and a laminate's stiffness (Walsh et al. 2007).

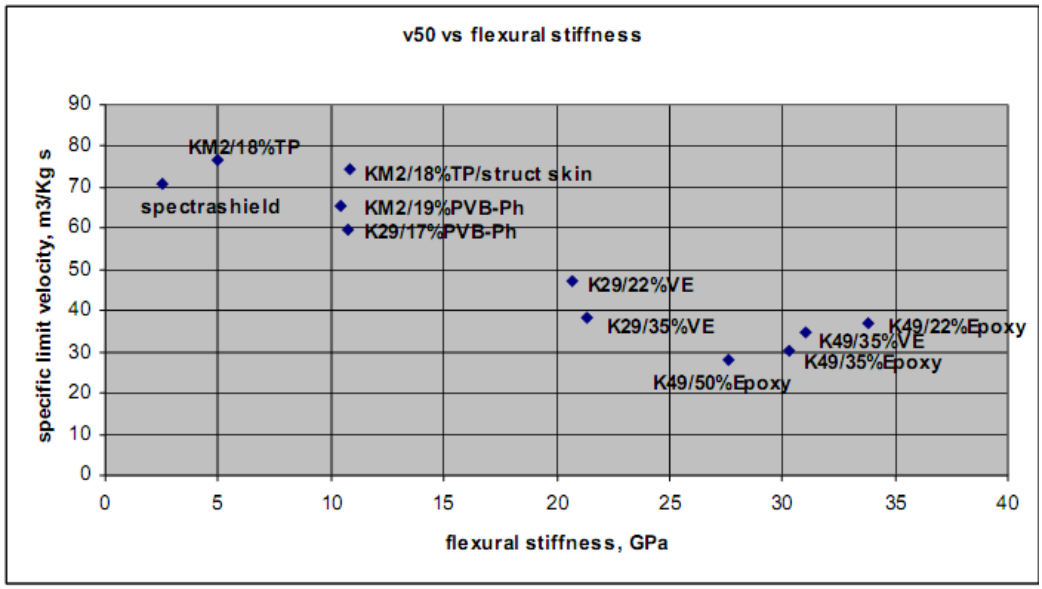


Bay Zoltan Institute for Materials Science and Technology in Budapest, Hungary, is developing fiber-reinforced ballistic composites at low weight that are able to absorb high energy of impacts and could be used for production of bulletproof doors and structures (Faur-Csukat 2005). Researchers claimed that, in order to achieve good performance, ballistic materials should have high impact resistance, high modulus, and low density. The plasticity of matrix polymer could be modified in order to improve energy absorption capacity. It was shown that the impact strength of the matrix resin highly affects the energy absorption capacity of the composites.

Southwest Research Institute of San Antonio, Texas, studied the ballistic resistance of the fiber fabrics reinforced resin composites and provided an equation to predict the ballistic limit curve of the fabric/resin composite panel (Walker 2001). The equation is also compared to experimental data for Kevlar 29/resin composite panels. One of the important conclusions is that the increased bending strength of the composite leads to an increase in the transverse wave speed, thus reducing the strain and increasing the ballistic limit. Also, a hardener panel deforms the projectile, leading to an increase in the presented area of the projectile and thus leading to an increase in the ballistic limit. It also claimed to be possible that for larger amounts of resin, the harder panel will rigidly hold the fabric, allowing the fibers to be sheared by the projectile rather than failing in tension, thus leading to a reduction in ballistic limit.

A smooth particle hydrodynamics (SPH) numerical technique was used to simulate the ballistic resistance (impact and penetration) of the glass fiber reinforced plastics (Quan and Birnbaum 1999). The simulation was also compared with the experimental results based on the ballistic resistance of the woven E-glass/epoxy and S2-glass/phenolic composites. It was found that, during penetration and perforation of laminated composites, interlaminar delamination is an important failure mode that affects the structural behavior of the damaged laminates. In order to improve the ballistic resistance, it is important to improve the interlaminar delamination strength of the GFRPs. Other publications showed that the ballistic resistance of the glass fiber reinforced resins (epoxy, unsaturated polyester, vinyl ester) highly depended on the delamination capability (Sevkat et al. 2007; Roberts et al. 2002; Chen et al. 2007a, 2007b).

It was also found that the bonding between the fiber and resin matrix is important to improve the ballistic resistance of the composites.[59-62] The V50 increased if the fibers were sized to improve the bonding between the fibers and the resin matrix. The direction of the fibers in the matrix could play an important role in the ballistic resistance (Santulli and Caruso 2009; Hosur et al. 2007; Mantena et al. 2010; Brown and Sevkat 2008; Hong and Liu 1989).

## 2.4 Properties affecting ballistic resistance

In the Army's BAA for this work package, the following factors for ballistic resistance in FRP composites were listed:

- flexural strength and modulus
- compression strength and modulus
- impact strength (may have close relationship with the ballistic resistance)
- interlaminar shear strength
- toughness
- thermal conductivity (heat dissipation may affect the ballistic resistance)
- glass transition temperature (the ability to resist higher temperatures may improve the ballistic resistance).

Based on the literature review of materials for ballistic protection, it was decided to focus this work on the properties of impact strength, compression strength and modulus, and glass transition temperature. Secondary

properties for testing were flexural strength and modulus, interlaminar shear strength, and toughness.

# 3 Characterization and Optimization of CNT-Reinforced Polymer Matrix

Factors affecting the ballistic resistance of the glass fiber composite panels were identified. Table 4 shows mechanical and physical properties along with the number of specimens needed of the neat and CNT-reinforced polyester nanocomposites for different functionalization and loadings. All mechanical testing of the specimens was completed in July 2010 (flexural strength, modulus, compression strength, impact strength). Early in the work, an experimental design was needed to select those properties necessary for functionalization of CNT materials and CNT-reinforced polyester nanocomposites. Armortex provided 50 lb of the polyester with correspondent catalyst.

Table 3. Mechanical/physical properties selected for characterization of the CNT-reinforced polyester nanocomposites.

| Mechanical/physical properties | Testing method | Number of specimens tested |
|---|---|---|
| Impact strength | ASTM D256 (tested by ANI) | 8 |
| Compression strength and modulus | ASTM D695 (tested by ANI) | 6 |
| Flexural strength and modulus | ASTM D790 (tested by ANI) | 6 |
| Interlaminar shear strength | (tested at Texas State University for ANI) | 6 |

As shown in Table 4, the focus was placed on three different functionalization groups for CNTs (-COOH, -OH, and -NH2), with four different loading levels (0.5, 1.0, 2.0, and 3.0 wt%) in the polyester matrix. Higher loading of the CNTs was attempted but was constrained by the viscosity increase of the polyester-CNT matrix.

All the necessary mechanical test specimens of the neat polyester were fabricated as required. The CNT-reinforced polyester nanocomposites were fabricated by using different functionalizations of CNTs and loadings. The polyester resin was mixed with the catalyst (1.3%) and cured at 112 °C for 20 min.

Table 4. Properties of the CNT-reinforced polyester for different functionalization groups and loading levels.

| Samples as wt% of CNT and (Functionalization) | Flexural Strength (MPa) | Flexural Modulus (GPa) | Compression Strength (MPa) | Compression Modulus (GPa) | Impact Strength (J/m) |
|---|---|---|---|---|---|
| 0 (neat polyester) | 109.5 | 3.77 | 115.6 | 2.38 | 235 |
| 0.5 (-COOH) | 123.9 | 3.84 | 132.5 | 2.45 | 151 |
| 1.0 (-COOH) | 134.8 | 3.91 | 145.6 | 2.62 | 113 |
| 2.0 (-COOH) | 83.6 | 4.07 | 124.3 | 2.45 | 72 |
| 0.5 (-OH) | 129.0 | 3.92 | 142.0 | 2.61 | 292 |
| 1.0 (-OH) | 117.3 | 4.13 | 146.9 | 2.75 | 177 |
| 2.0 (-OH) | 102.5 | 3.60 | 121.5 | 2.57 | 136 |
| 3.0 (-OH) | 83.8 | 3.58 | 118.6 | 2.38 | ——— |
| 0.5 ($-NH_2$) | 86.0 | 3.70 | 132.2 | 2.62 | 96 |
| 1.0 ($-NH_2$) | 77.5 | 4.05 | 138.9 | 2.70 | 120 |
| 2.0 ($-NH_2$) | 70.8 | 3.54 | 133.8 | 2.48 | 77 |

CNT-reinforced polyester resins were made by ANI and sent to Armortex which used them to prepare four sets of the GFRP panels as follows (and shown in Figure 7):

- 5 panels with neat resin
- 5 panels with 0.5% -OH functionalized CNT
- 5 panels with 1.0% -OH functionalized CNT
- 5 panels with 3.0% -OH functionalized CNT.

The neat resin panel set was the benchmark panel. The 0.5% and 1.0% OH panel sets represented a good combination of mechanical properties, as shown in Table 5. A 3.0% panel set was chosen to continue the testing in the -OH family but at a high-loading extreme. There was some indication from the author's previous work with GFRP for sporting goods that this idea might be successful even though the resin-only data indicated a decrease. Chesapeake Defense Service, Inc. tested V50 ballistic resistance, and the results are listed in the Table 5.

Table 5 shows that ballistic resistance decreased for all three different loading samples when -OH functionalized CNT-reinforcement was added.

Figure 7. E-glass/polyester composites for ballistic testing (from left: neat polyester, 0.5 wt% CNT-OH, 1.0 wt% CNT-OH, and 3.0 wt% CNT-OH polyester composite panels).

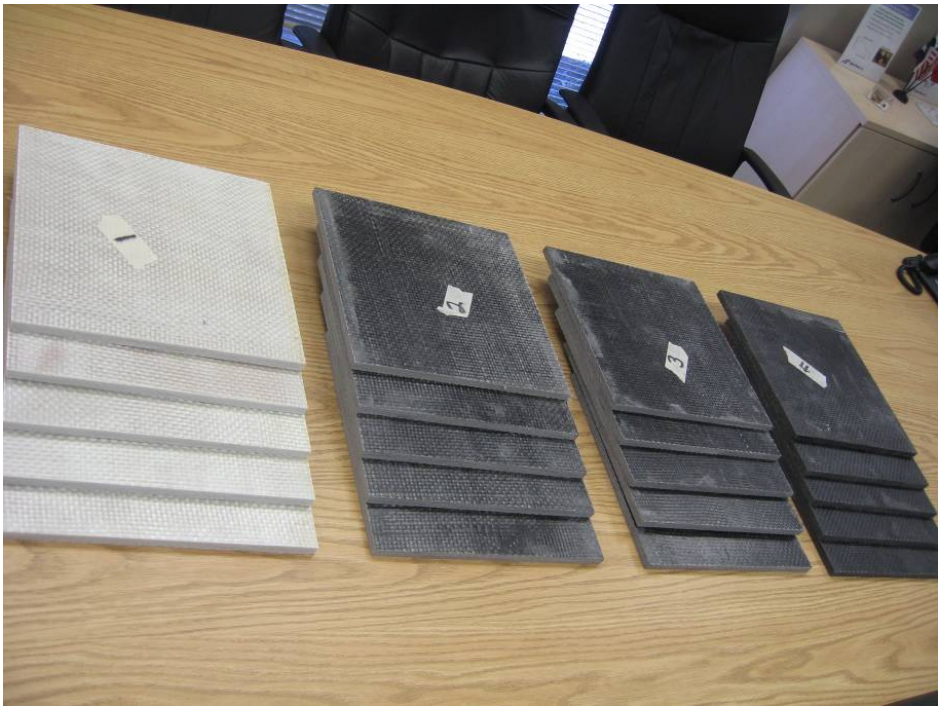

Table 5. V50 ballistic testing results of the GFRP panels with -OH functionalized CNT.

| GFRP Samples as wt% of CNT and showing (OH functionalization) | V50 (ft/s) | |
|---|---|---|
| | Thickness of GFRP panel = 1.0 in. | Normalized at thickness of 0.5 in. |
| 0 (neat polyester) | 1876±147/0.465 | 2018 |
| 0.5 (-OH ) | 1864±116/0.469 | 1986 |
| 1.0 (-OH ) | 1879±120/0.473 | 1985 |
| 3.0 (-OH ) | 1704±105/0.485 | 1824 |

# 4 Ballistic Testing of CNT-Reinforced GFRP Panels

## 4.1 CNT-reinforced materials

A larger quantity of the –COOH functionalized CNT-reinforced polyester resins were made at different loadings of 0.5, 1.0, and 2.0 wt%. –COOH functionalized CNT-reinforced polyester has the highest flexural strength improvement at a loading of 0.5 and 1.0 wt% of CNT compared to other samples. A 2.0 wt% loading was also added to see the trend of the ballistic resistance. As part of the task, 15 GFRP panels were made for each of the samples (panel size: 12 x 12 x 0.5 in.). Armortex completed fabrication of the panels at the end of November 2010. Five panels of each sample were sent to Chesapeake Defense Services, Inc. in Maryland for primary V50 ballistic testing. Then 10 panels of each sample were kept by ANI for detailed V50 ballistic testing. The initial result of the V50 ballistic testing results from Chesapeake is shown in Table 6. The ballistic resistance of the GFRP panels was not improved by using –COOH functionalized CNT reinforcement (Table 7).

Table 6. V50 ballistic testing results of the GFRP panels at Chesapeake Defense Service on –COOH functionalized CNT panels.

| GFRP Samples (wt% of CNT; -COOH functionalized) | V50 (ft/s) | |
|---|---|---|
| | Thickness of GFRP Panel = 1.0 in. | Normalized at Thickness = 0.5 in. |
| 0 (Neat polyester) | 2038±93/0.520 | 1958 |
| 0.5 | 1972±113/0.516 | 1910 |
| 1.0 | 2078±114/0.521 | 1995 |
| 2.0 | 1983±120/0.505 | 1962 |

In additional to the above samples, modified resins were prepared for four sample lots of the CNT- and clay-reinforced polyester resins for GFRP panel preparation (Table 7). GFRP panels were made in January 2011 and tested by Chesapeake in February 2011.

Table 7. GFRP panels prepared for ballistic resistance testing at Chesapeake Defense Services.

| Description | V50 (ft/s)/Thickness of GFRP panel (in.) | V50 (ft/s) normalized at thickness of 0.5 in. |
|---|---|---|
| 1% clay nanoparticles | 1799±114/0.473 | 1900 |
| 1% clay + 1% CNT (-COOH functionalized) | 1739±94/0.475 | 1831 |
| 1.0% long double-walled carbon nanotubes (DWNTs) | 1859±70/0.485 | 1918 |
| 1.0% long MWNTs | 1723±125/0.469 | 1837 |

Based on the results, ANI completed the mechanical testing of a ballistic panel loaded with CNT to see the correlation between the mechanical properties and ballistic resistance of the GFRP panels. A CNT-COOH (1.0 wt%) reinforced polyester GFRP panel (1/8 in. thickness) was prepared. For comparison, a neat polyester GFRP panel of the same thickness was prepared (Figure 8). ASTM-standard samples were prepared for testing mechanical properties (flexural, compression, delamination shear strength).

Figure 8. E-glass/polyester GFRP panels without (left) and with (right) CNT-COOH (1.0%) reinforcement.

Table 8 shows mechanical properties of the neat and CNT-reinforced polyester GFRP specimens, along with the percentage change.

Table 8. Comparison of mechanical properties of the GFRP panels with 1% -COOH CNT reinforcement.

| Samples | Flexural Strength (MPa) | Flexural modulus (GPa) | Compression Strength (MPa) | Interlaminar Shear Strength (MPa) |
|---|---|---|---|---|
| Neat GFRP | 315.8 | 20.4 | 202.0 | 95.4 |
| CNT-COOH (1.0%) GFRP | 340.7 | 22.6 | 202.6 | 87.5 |
| Difference: reinforced over neat | 8%↑ | 11%↑ | 0% | 8%↓ |

Flexural strength and flexural modulus increased by 8% and 11% with CNT-COOH loading, while the interlaminar shear strength decreased by about 8%.

## 4.2 Preparation of GFRP panels using CNT sheet reinforcement

GFRP panels using CNT sheet reinforcement for improving ballistic resistance were made. The effort included the characterizations listed below.

1. **Mechanical property characterization of polyester resin.** Specimens of the designated polyester resin were prepared. Tensile strength and modulus of the specimens were tested based on ASTM D3039; tensile strength and modulus are crucial for reinforcement of the ballistic performance of the fibers and fabrics.
2. **Mechanical property characterization of CNT sheet-reinforced polyester resin.** Specimens of the CNT sheet-reinforced polyester resins were prepared. Tensile strength and modulus (ASTM D3039) were tested and the results were compared to the samples made without CNT sheet reinforcement. A number of CNT sheets were folded to integrate with the polyester. The target loading of the CNT sheets was 50%–60% by volume.
3. **Mechanical property characterization of E-glass fiber reinforced polyester.** Specimens of the E-glass reinforced polyester were prepared, and tensile strength and modulus were tested. The loading of the E-glass fiber fabric was controlled at 50%–60% by volume. The tensile strength and modulus were obtained based on ASTM D3039.

4. **Mechanical property characterization of the CNT sheet-reinforced E-glass fiber polyester.** Specimens of the E-glass reinforced polyester were prepared with different numbers of layers of CNT sheets in them. Tensile strength and modulus were tested based on ASTM D3039. The loading of the E-glass fiber fabric was controlled at 50%–60% by volume. Again, the tensile strength and modulus was tested based on ASTM D3039.

Figure 9. Position of the CNT sheets in the GFRP panels (each GFRP panel contains 22 layers of the E-glass fiber fabric).

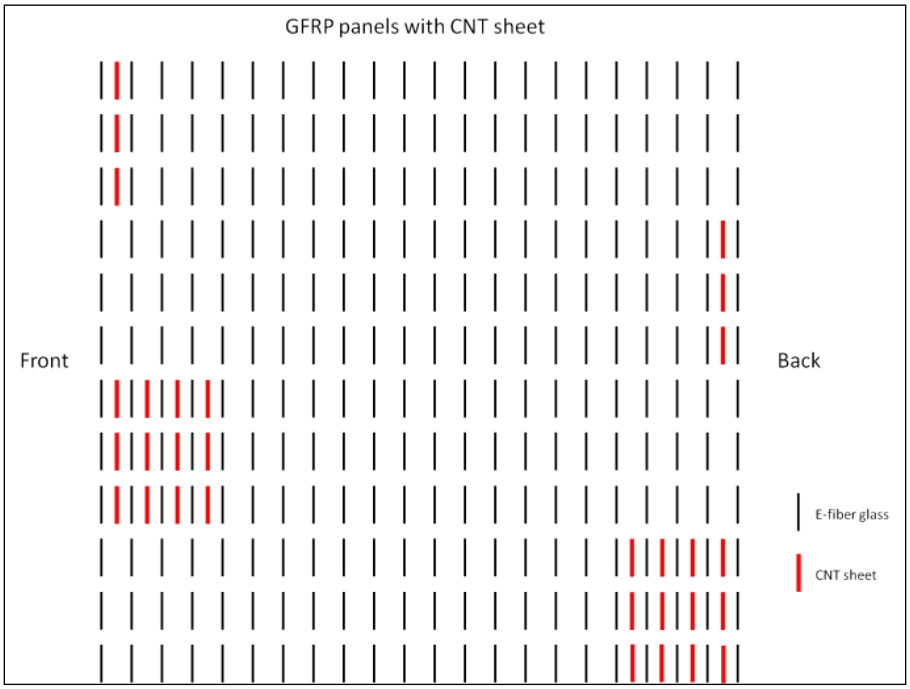


The CNT sheet-reinforced GFRP panels were fabricated by Armortex. In March 2011, a large quantity (>75 sq ft) of CNT sheets were purchased from Nanocomp Technologies for this effort. The ballistic resistance of the panels was evaluated by ERDC-CERL.

The following numbers and types of sample panels were prepared for tensile testing and analysis (samples shown in Figure 10):

- Polyester (6 dog-bones for tensile testing)
- CNT sheet/polyester (7.5 x 7.5 in. with 10 CNT sheets included; content of the CNT sheets is about 21% [CNT sheets: 5 g, polyester: 19 g])
- E-glass fiber/polyester (7.5 x 7.5 in. with 2 layers of E-glass fiber fabric included; content of the E-glass fiber fabric was 50 wt%)

- CNT sheet/E-glass fiber/polyester (7.5 x 7.5 in. with 2 layers of E-glass fiber fabric and 10 layers of the CNT sheets between; content of the E-glass fiber fabric/CNT sheet was 50 wt%)

Figure 10. Samples prepared for tensile testing, based on ASTM D3039.

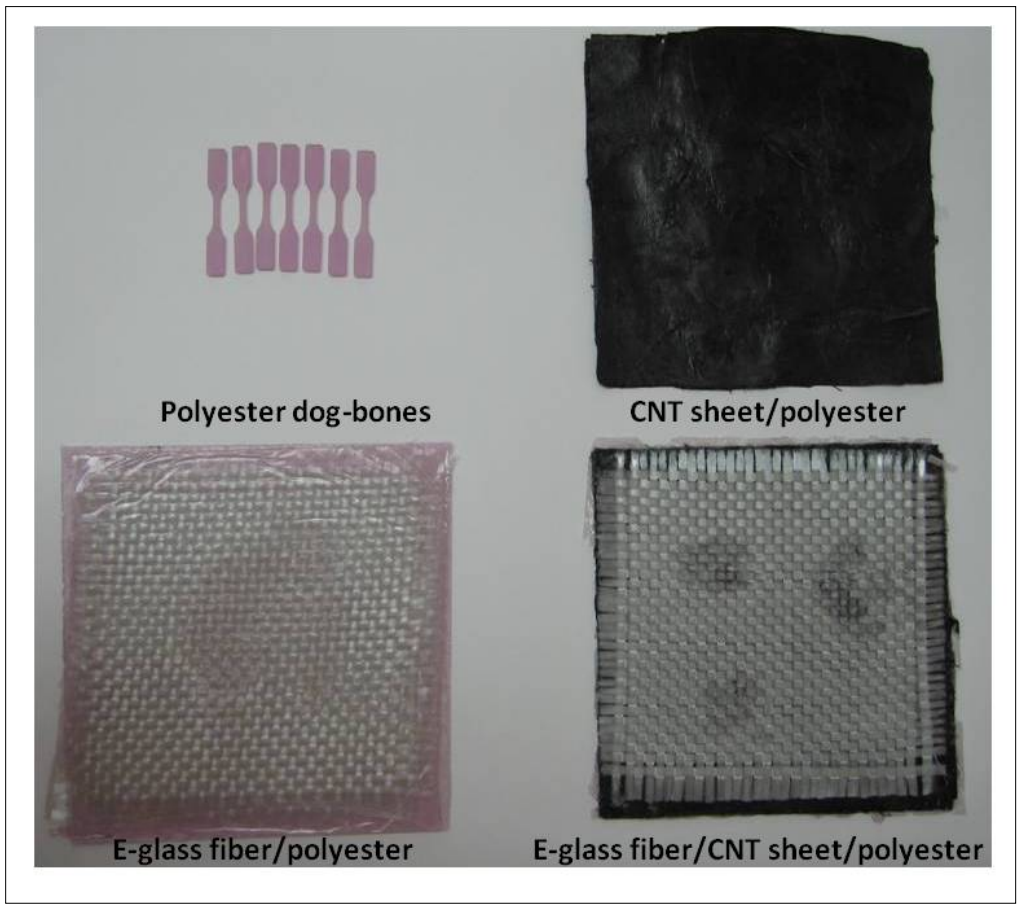


During the V50 testing for ballistic resistance, the bullet was shot from the front to the back side of the panels (schematic of panels is shown from left to right in Figure 11).

Figure 11. Schematic diagram of the GFRP panels incorporated with CNT sheets.

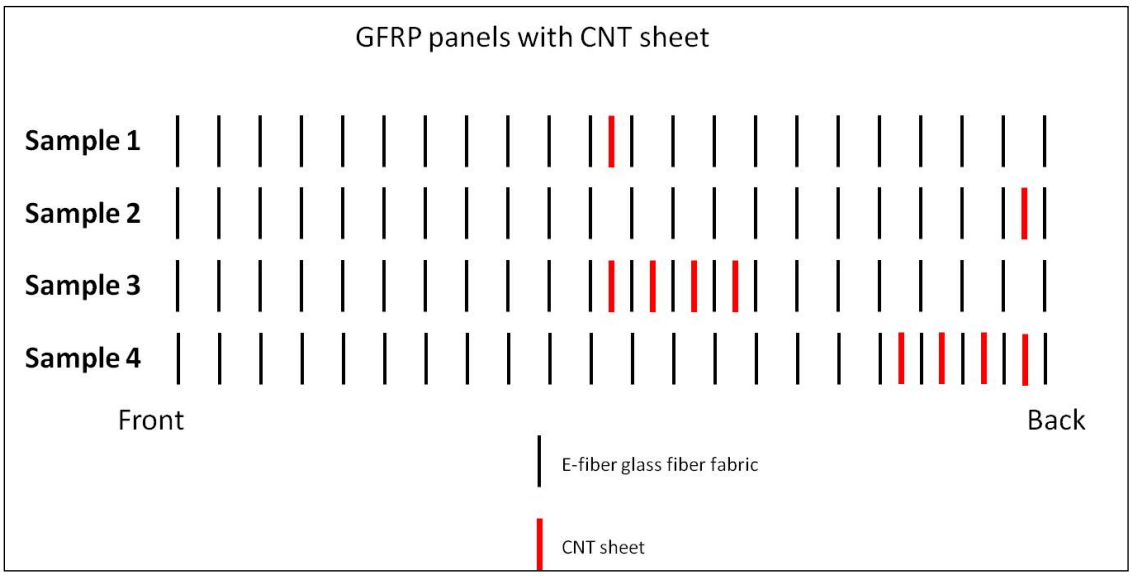


Table 9 shows that Sample 3 exhibited the best ballistic resistance, measuring around 5% improvement in ballistic resistance compared with the reference sample without CNT sheet, when normalized for thickness. The location and number of the CNT sheets may have an effect on ballistic resistance of the GFRP panels; however, the differences are small and may be within the uncertainty of the measurement.

Table 9. V50 ballistic testing results of the GFRP panels with CNT sheet-reinforced GFRP Panels.

| GFRP Samples | V50 (ft/s)/Thickness of GFRP panel (in.) | V50 (ft/s)- Normalized at thickness of 0.5 in. |
|---|---|---|
| Sample 1 | 2042±75/0.546 | 1870 |
| Sample 2 | 2051±89/0.544 | 1885 |
| Sample 3 | 2020±80/0.485 | 2082 |
| Sample 4 | 2019±74/0.495 | 2039 |
| Reference (no CNT sheet) | 2002±100/0.505 | 1982 |

# 5 Ballistic Testing of Self-Healing GFRP Panel

## 5.1 Self-healing materials

Composite materials are ideal for structural applications where high strength-to-weight ratio and stiffness-to-weight ratios are important. Weight-sensitive applications such as construction, aircraft, and space vehicles are the primary consumers of composites, especially fiber-reinforced polymer matrix composites. However, use of these composites is limited due to the difficulty in damage detection and repair, as well as lack of resistance to extended fatigue and impact. One way to protect material degradation is to incorporate materials that create a self-healing ability.

Polymer composites have been attractive candidates to introduce the autonomic healing concept into modern-day engineering materials. There has been significant research in self-healing polymeric materials, and numerous studies specifically in fiber-reinforced polymers. A breakthrough in the study of self-healing materials was reported in 2001 by a research group at University of Illinois (White et al. 2001). White's team first introduced the incorporation of microcapsules containing a polymer precursor into the matrix material of a non-fiber-reinforced polymer composite for self-healing purposes. The polymer precursor was contained in microcapsules and embedded into the matrix. The matrix contained a randomly dispersed catalyst that was supposed to react with the precursor flowing through any crack that was formed due to damage and initiate polymerization. The polymer was then supposed to bond the crack face closed. The investigators overcame several challenges in developing microcapsules that were weak enough to be ruptured by a crack but strong enough not to break during manufacture of the composite system. The researchers showed it was possible to recover up to 75% of the maximum tensile strength of the virgin composites. The most successful work was done by Bond and co-workers (Trask et al., 2007). The use of functional repair components stored in HGFs (Hollow Glass Fiber) placed with glass fiber/epoxy and carbon fiber/epoxy laminates can effectively mitigate dam-

age occurrence and restore mechanical strength (Trask et al. 2007). Figure 12 shows HGF used by Prof. Bond's group.

Figure 12. Typical HGF (35 μm external diameter with 55% hollowness fraction).

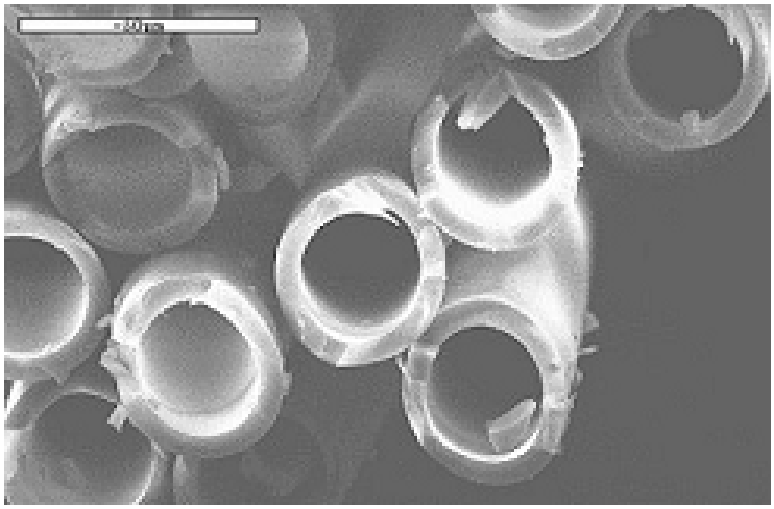

The benefit is very obvious if the self-healing material can be successfully incorporated into the CNT-reinforced GFRP composite panels; those panels can then serve a longer time with better performance. Self-healing materials embedded in the glass fiber-reinforced composite or laminate showed considerable restoration of mechanical properties such as flexural strength, compressive strength, and impact resistance, plus a highly efficient recovery of matrix strength.

An additional task was to apply the self-healing material into the CNT-reinforced GFRP ballistic-resistant composite panels. The task's purpose was to self-repair the damage area of the panels by using the self-healing material that is integrated into the GFRP composite. The approach using the HGFs has the advantage of significantly increasing the amount of catalyst and polymer available for the self-repair process resulting from severe damage from ballistic impact to the panel. This approach can increase the service life of the panel and recover its performance soon after initial damage.

The feasibility of self-healing processes in GFRP composites, including CNT-reinforced GFRP composites, was determined by using electrospun, HGF tubes filled with polymer resin suitable for healing the composite. In this process, a monomer and a catalyst were encapsulated in the separate

HGF tubes, and the tubes were embedded together within the thermosetting polymer resin of the GFRP at a predetermined ratio/concentration.

The following numbers and types of sample panels were prepared for the self-healing process effort:

- Neat polyester GFRP panels with vinyl ester/ methyl ethyl ketone peroxide (MEKP) as the self-healing agent—five panels
- Neat polyester GFRP panels with CNT/vinyl ester/MEKP as the self-healing agent—five panels
- Neat polyester GFRP panels without the self-healing agent—five panels.

The reason a vinyl ester/MEKP system was chosen for the self-healing effort is that the vinyl ester can be cured at room temperature when it is mixed with the catalyst MEKP. Self-healing of the ballistic GFRP panels was developed based on the variable parameters discussed below.

### 5.1.1 Dimension of HGFs

The initial focus was on the small-diameter HGF fabricated by Schott North America, Inc. of Elmsford, New York. These HGFs had 8 in. length, 66 μm inner diameter (ID), and 90±10 μm outer diameter (OD). Those dimensions yielded a hollowness fraction of approximately 54%. However, this type of HGF was very expensive ($10,000 was spent for 2 lb). Schott does not regularly manufacture this type of HGF, but made it for this project in company's R&D laboratory. The fiber's high cost may be an issue in the future commercialization process for self-healing of GFRP panels.

As an alternative, large-diameter HGFs also were used, both to lower the cost and to improve performance for the self-healing effort. A number of companies were found which manufacture or supply large-diameter HGFs. For example, Sutter Instrument Co. of Novato, California, supplied HGFs with IDs of 0.5–1.56 mm, ODs of 1.0–2.0 mm, and lengths of 7.5–15 cm. For the glass fiber with ID of 0.69 mm and outer diameter of 1.20 mm at length of 15 mm, the price was $41 for 250 pieces. This cost is almost 20 times lower than the smaller-diameter HGFs made by Schott for the same volume storage of self-healing material. The price is expected to be even lower if a large quantity of the larger-diameter HGF is purchased.

### 5.1.2 Loading of the self-healing resin in the GFRP panel

It has been observed in the work of other researchers that the mechanical strength of the GFRP panels may be degraded when integrated with the HGFs. This degradation may also affect the ballistic resistance. This work studied the loading of the self-healing material which depends on the loading of the HGF (dimension and hollowness fraction) in the GFRP panels. The purpose is to find the optimal loading of the self-healing material in the GFRP panels to (1) add the self-healing property, and (2) not to degrade the ballistic resistance of the GFRP panels. This work selected loadings of 2.5 wt% and 5.0 wt% for the self-healing resin of the matrix resin (polyester).

### 5.1.3 Placement of HGF filled with self-healing resin

The GFRP panels fabricated by Armortex for ballistic application are ½ in. thickness which combines 22 plies of the glass fiber fabric. In this work, two different HGF distributions were wound directly onto uncured GFRP plies prior to lamination to investigate the effort of HGF on the host laminate properties and the healing efficacy of different healing agent volumes. Figure 13 shows images of the HGFs provided by Schott NA.

Figure 13. Images of HGFs: (a) a bundle contains 30,000 HGFs; (b) optical microscope magnification of an HGF; (c) cross-section view of an HGF (images courtesy of Schott NA).

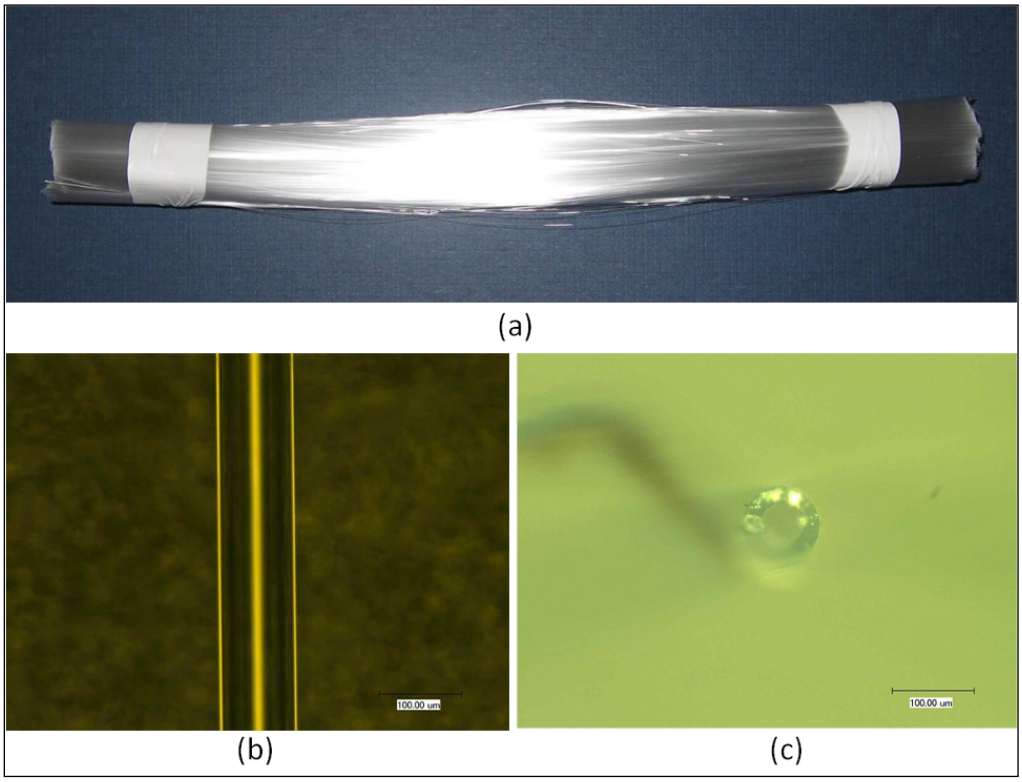


The HGFs were first sealed at one end by silicone sealant purchased from Master Bond, Inc. of Hackensack, New Jersey. The fibers were then immersed into the vinyl ester liquid under a vacuum chamber to allow the vinyl ester to penetrate the inner side of the HGF. Eventually, the other end of the HGFs was sealed. The same process was utilized to fill the MEKP catalyst in the separated tubes. Photographs show HGFs sealed with the silicone sealant (Figure 14) and self-healing agents (Figure 15).

Figure 14. HGFs sealed with silicone sealant at the end.

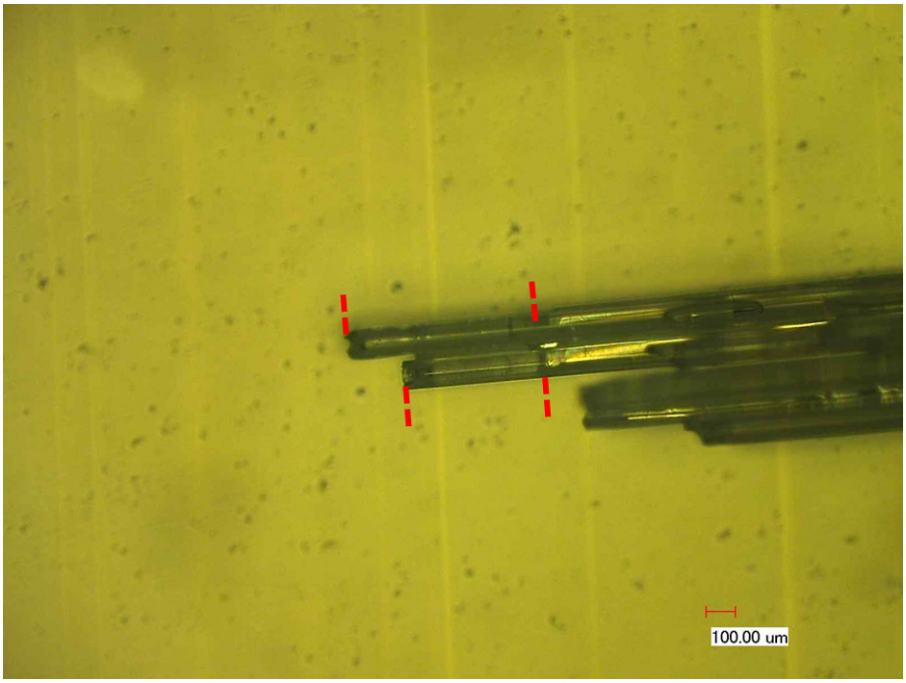


Figure 15. As marked in the photo, HGFs in original state (top); filled with neat vinyl ester (middle); and filled with CNT-reinforced vinyl ester (bottom).

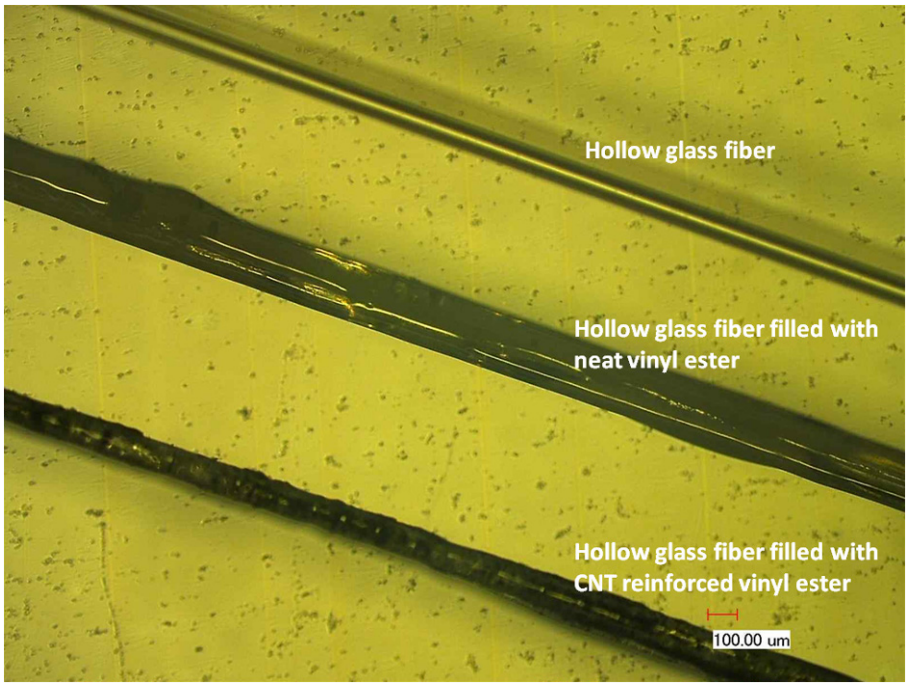


Figure 16 shows that a layer of HGFs was placed on an E-glass fiber fabric for GFRP panel preparation. The loading ratio of the vinyl ester to MEKP was 95:5. The HGFs filled with vinyl ester and MEKP were evenly distributed in the whole layer. The position of the self-healing layer for the case

of 12 x 12 x 3/8 in. size of the GFRP panels is shown in Figure 17 schematic.

Figure 16. Layer of small HGFs filled with neat vinyl ester (top); and CNT reinforced vinyl ester (bottom) were placed on an E-glass fiber fabric for GFRP panel preparation.

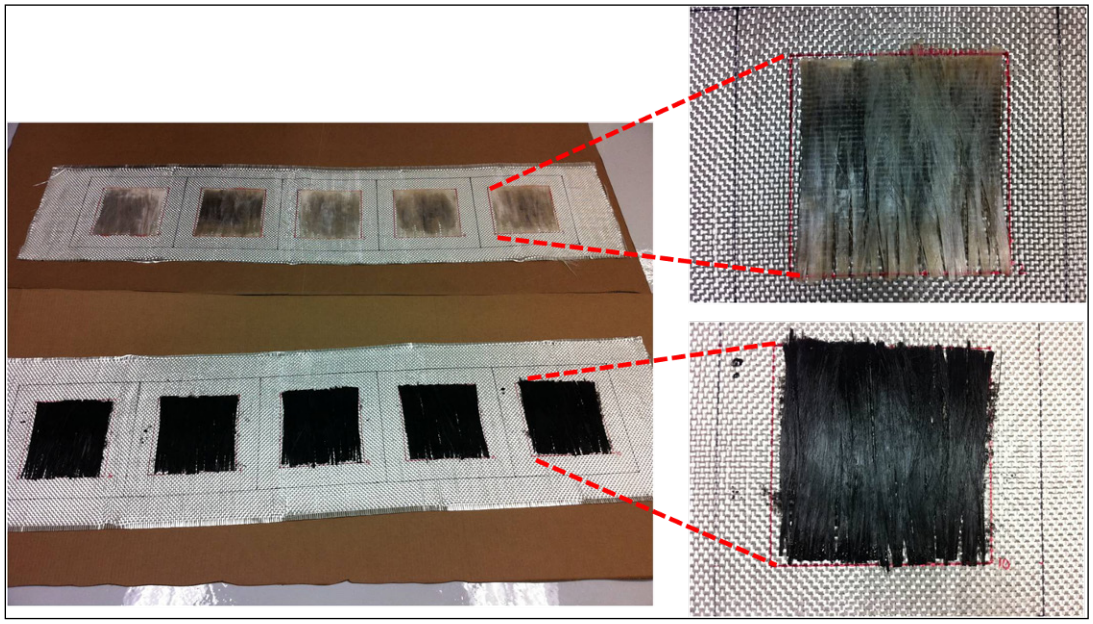

Figure 17. Schematic diagram of the self-healing GFRP panels for ½ x 1/2 x 3/8 in. size.

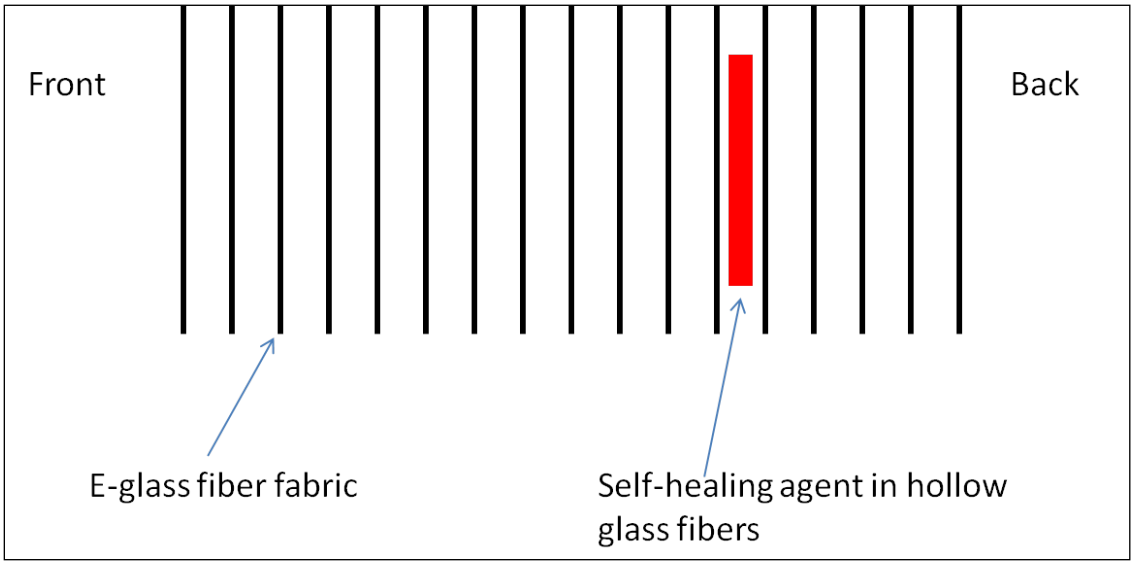


As shown in Figure 17, each panel contained 17 layers of E-glass fiber fabric. The HGF layer with self-healing agent and catalyst was placed between

the 12th and 13th layers of the E-glass fiber fabric. During ballistic testing, the projectile was supposed to be shot from the front of the panel.

As stated, large-diameter HGF was purchased from Sutter Instrument. The HGFs were 4 in. long with an ID of 860 μm and OD of approximately 1500 μm. That size HGF yielded a hollowness fraction of approximately 33%. Figure 18 shows some images of the HGFs filled with self-healing agent. Figure 19 shows the position of the self-healing agent on the E-glass fiber fabric.

Figure 18. From left to right and top to bottom: large diameter HGF, HGF sealed with silicone sealant at the end, HGF filled with vinyl ester, and HGF filled with MEKP catalyst.

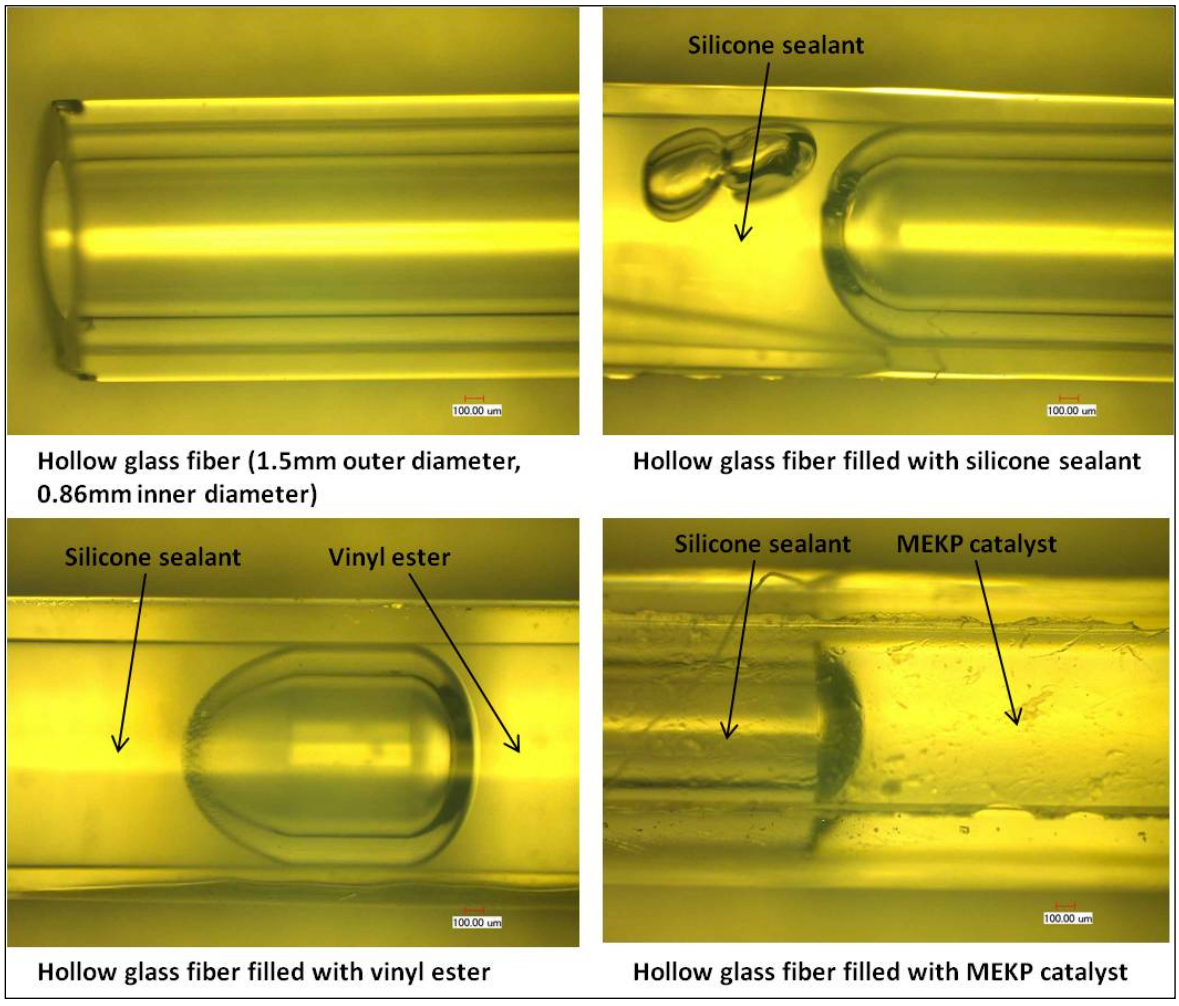

Figure 19. Layer of large HGFs filled with neat vinyl ester.

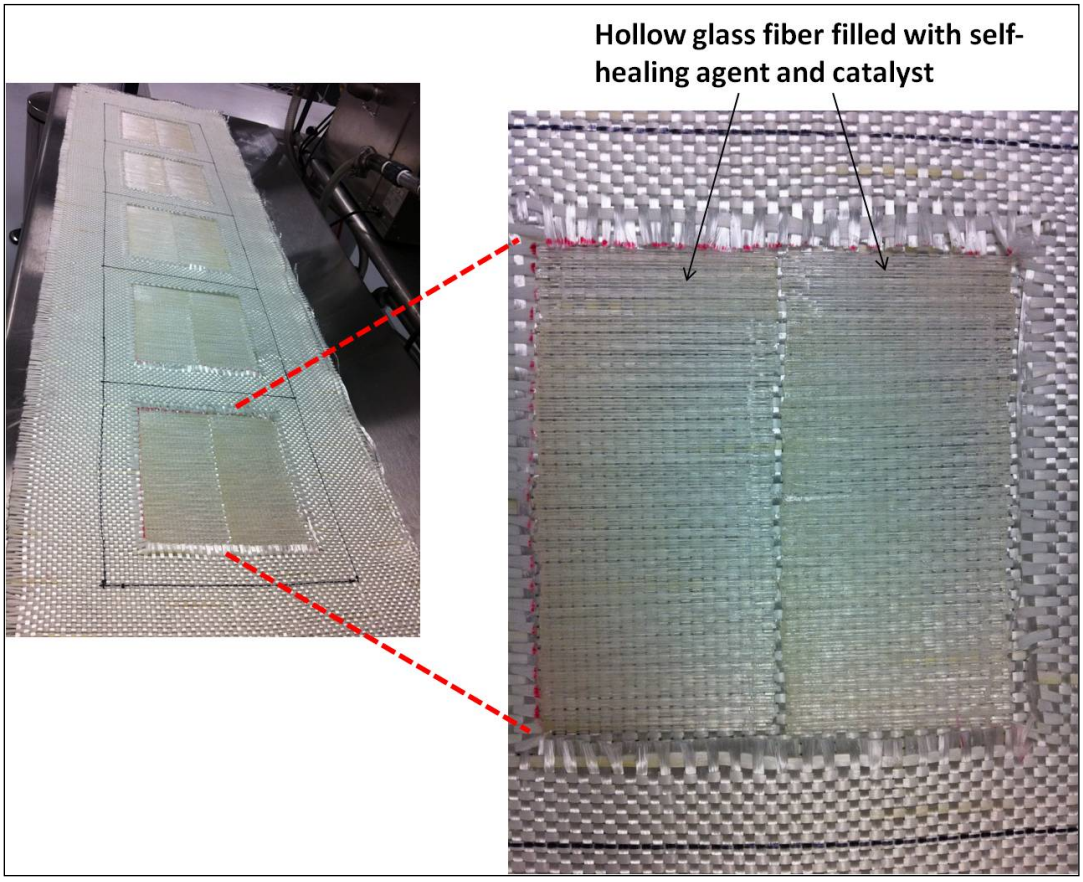


As mentioned above, the vinyl ester/MEKP system was chosen for the self-healing agent because the vinyl ester can be cured at room temperature when it is mixed with the catalyst MEKP. Ten sets of five panels each were tested that were loaded with self-healing agent material. Eight of those sets are 0.5 in. thick panels, two of those sets are 3/8 in. thick panels. In addition, there was a set of control panels (no healing agent, no HGFs) for each thickness, making a total of 12 sets. Again, each set has five panels (see Table 10).

Table 10. Fabrication of self-healing GFRP panels.

| Self-Healing GFRP Panels | Wt% of Self-Healing Resin | Placement of HGF (see footnote for explanation) | Number of Panels Fabricated (per set unless noted) |
|---|---|---|---|
| Control (Polyester GFRP) | 0 | — | 40 |
| GFRP with small-diameter HGFs | 2.5 | * | 5 |
| | 2.5 | ** | 5 |
| | 5.0 | * | 5 |
| | 5.0 | ** | 5 |
| GFRP with large-diameter HGFs | 2.5 | * | 5 |
| | 2.5 | ** | 5 |
| | 5.0 | * | 5 |
| | 5.0 | ** | 5 |

*F/GF/GF/GF/HGF/GF/GF/GF/GF/GF/GF/GF/HGF/GF/GF/GF/GF/GF/GF/GF/GF/GF/GF

**F/GF/GF/GF/HGF/GF/GF/GF/GF/GF/GF/GF/GF/GF/GF/GF/GF/GF/HGF/GF/GF/GF/GF

## 5.2 Requested test protocol

Figure 20 shows the sketch of each panel and the planned placement of each shot for the V50 testing. The V50 tests were performed with a 0.30 caliber FSP.

**First round of shots.** For each set, there were 3 shots each panel (15 total). All of these shots can be used to establish a V50 test result (V50-A). All 15 shots were fired. The location of these shots was close to the dots marked "X" in the map (red dots, Figure 20).

**Second round of shots.** Within 1 hour of the first round of shots, 7–8 shots were made that are near (1 in.) the original shots. Those 7–8 shots were used for another V50 test (V50-B). *Note: Only 7–8 shots were done for this test because the remaining 7–8 shots were used in the third round of V50 testing (see below).*

**Third round of shots.** After 1 week from the first round of shots (V50-A), another 7–8 shots were made that were also near (1 in.) the original shots. Those 7–8 shots were used for another V50 test (V50-C). Thus all original shots had a neighboring shot that was distanced about 1 in. from

the original. Each panel should have six shots, three original (V50-A) and three for either V50-B or V50-C testing.

Figure 20. Planned placement of each shot for the V50 testing.

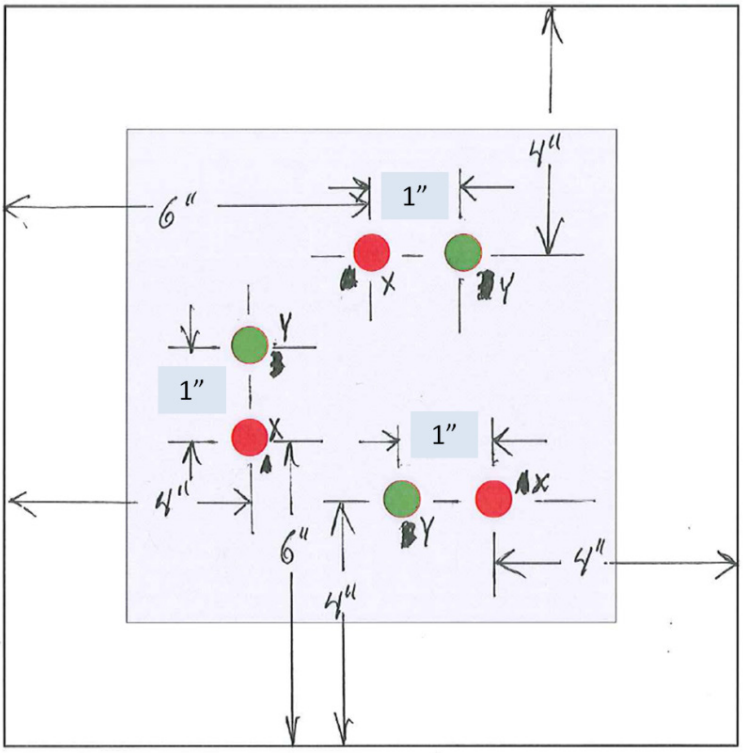


Table 11 shows V50 results of all the self-healing GFRP panels.

Table 11. V50 ballistic testing results of the self-healing GFRP panels. The configurations for placement of HGFs are shown in footnotes at the bottom of the table.

| GFRP Panel | Sample Lot # | Loading of Self-Healing Agent | Placement of HGF* | 1st V50 (V50-A) | | 2nd V50 (V50-B) | | 3rd V50 (V50-C) | |
|---|---|---|---|---|---|---|---|---|---|
| | | | | V50 (ft/s) / Thickness of GFRP Panel (in.) | V50 (ft/s) Normalized at 0.5 in. Thickness | V50 (ft/s) / Thickness of GFRP Panel (in.) | V50 (ft/s) Normalized at 0.5 in. Thickness | V50 (ft/s) / Thickness of GFRP Panel (in.) | V50 (ft/s) Normalized at 0.5 in. Thickness |
| GFRP w/ small-diameter HGF and ½-in. panel | 1 | 2.5 | a | 1964±88/0.581 | 1690 | 2018±76/0.582 | 1737 | 2010±92/0.565 | 1779 |
| | 2 | 2.5 | b | 1906±141/0.562 | 1696 | 1943±121/0.562 | 1729 | 2046±96/0.562 | 1820 |
| | 3 | 5.0 | a | 1956±111/0.565 | 1730 | 1984±72/0.565 | 1756 | 2046±79/0.565 | 1811 |
| | 4 | 5.0 | b | 1967±111/0.547 | 1798 | 2015±101/0.547 | 1842 | 2085±68/0.547 | 1906 |
| | 5 | control (no HGF) | n/a | 1929±98/0.515 | 1873 | 1983±113/0.515 | 1925 | | |
| GFRP w/ large-diameter HGF and ½-in. panel | 1 | 2.5 | a | 1997±138/0.577 | 1731 | 2049±89/0.577 | 1776 | 2080±140/0.577 | 1802 |
| | 2 | 2.5 | b | 2226±84/0.702 | 1585 | 2162±92/0.702 | 1540 | 2266±111/0.703 | 1614 |
| | 3 | 5.0 | a | 2074±145/0.582 | 1730 | 2080±61/0.582 | 1756 | 2137±121/0.582 | 1836 |
| | 4 | 5.0 | b | 2263±123/0.698 | 1621 | 2155±39/0.698 | 1544 | 2295±116/0.714 | 1607 |
| | 5 | control+ | n/a | 1929±98/0.515 | 1873 | 1983±113/0.515 | 1925 | | |
| Initial 3/8 in. panel | 1 | 2.5 (neat#) | c | 1891±122/0.547 | 1729 | 1920±89/0.547 | 1756 | 1968±117/0.547 | 1799 |
| | 2 | 2.5 (CNT-reinforced agent) | c | 1839±143/0.511 | 1799 | 1885±100/0.511 | 1844 | 1871±80/0.505 | 1830 |
| | 3 | control | n/a | 1645±101/0.402 | 2046 | 1654±142/0.402 | 2057 | | |

* Placement a: GF/GF/GF/GF/HGF/GF/GF/GF/GF/GF/GF/GF/HGF/GF/GF/GF/GF/GF/GF/GF/GF/GF/GF

Placement b: GF/GF/GF/GF/HGF/GF/GF/GF/GF/GF/GF/GF/GF/GF/GF/GF/GF/GF/HGF/GF/ GF/GF/GF

Placement c: GF/GF/GF/GF/GF/HGF/GF/GF/GF/GF/GF/GF/GF/GF/GF/GF/GF/GF

The bullet was shot from the right side for all the cases above.

\+ "Control" means no self-healing agent and not CNT reinforcement in the GFRP panel.

\# "Neat" means 2.5% loading of the self-healing agent and no CNT reinforcement in the GFRP panel.

Figure 21 shows the V50 results normalized to thickness and plotted with no normalization to thickness. (V50-A were panels tested on the first shot, V50-B were second round of samples within 1 hour, and V50-C were samples tested after 1 week from V50-A).

Figure 21. V50 test results for the different GFRP panels with self-healing agent normalized to thickness (right-side graphs) and plotted with no normalization to thickness (left-side graphs). As stated, V50-A panels are those tested on the first shot, V50-B panels are second round of samples fired within 1 hr of the first shots, and V50-C are samples tested after 1 week from V50-A test).

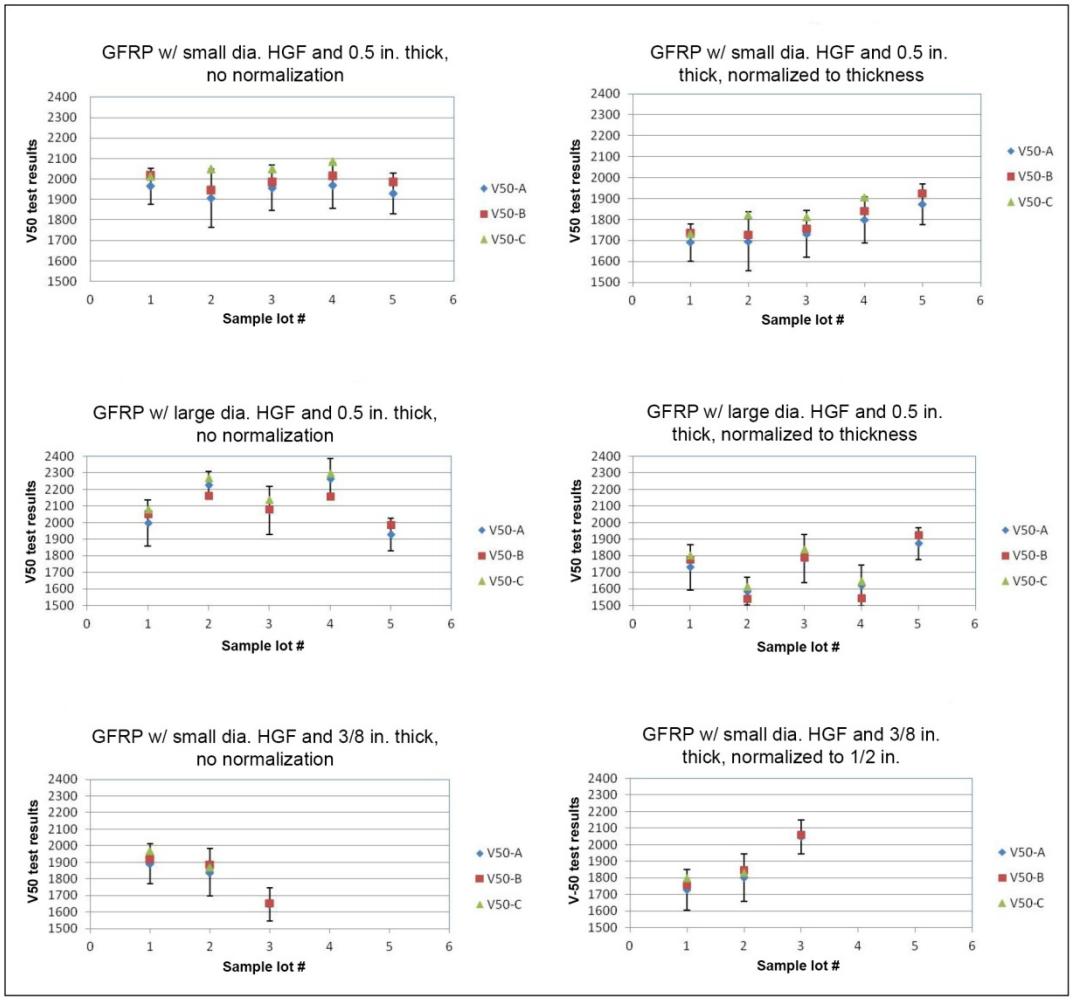


Below is a summary of the results shown by the graphs in Figure 21.

- Panels with HGFs were weaker than the control panels that did not have HGFs (e.g., V50 = 1873 which was larger than all panels with HGF). *Note: The "control set" for the small-diameter and the large-diameter HGF sets is the same.*
- Higher loading of the self-healing agent (2.5% vs. 5%) did not improve the ballistic resistance.
- The placement of the self-healing agent between layers of E-glass fiber fabric (placement "a" vs. "b;" refer to footnote in Table 11) may have had an effect on the ballistic resistance of the GFRP panels. In the case

of the small-diameter HGF loaded with self-healing agent, placement "b" had better ballistic resistance. For the large-diameter HGF loaded with self-healing agent, placement "a" had better ballistic resistance. It was not clear if this placement difference was significant.

- There was no obvious difference between the V50-A and V50-B tests; however, it was obvious that V50-C test performance was better than V50-A and V50-B. The panels with *cured* self-healing agent (V50-C tests) exceeded the performance of even virgin panels using HGF and came close to the performance of the control panels with no HGF.

Three samples were chosen for cross-section investigation:

1. GFRP with small-diameter HGF (placement "b"), 5% loading of self-healing agent, ½ in. thickness.
2. GFRP with large-diameter HGF (placement "a"), 5% loading of self-healing agent, ½ in. thickness.
3. GFRP with small-diameter HGF (placement "c"), 2.5% loading of self-healing agent, 3/8 in. thickness.

Figure 22 shows the GFRP with small-diameter HGF with 5% loading of self-healing agent at ½ in. thickness, after being cut. The cross-section cut for deeper analysis is shown in Figure 23. When the panels were cut for cross-sectional analysis, there was no flow-out of the self-healing agent seen from the HGFs, either close or far away from the bullet shooting area. This means that the entire collection of HGFs filled with self-healing agent was most likely fully cured after the V50 testing (i.e., the whole layer of HGFs was damaged, and the self-healing agent was allowed to flow and be cured). It was also found that the delamination was more serious close to the bullet impact area.

Figure 22. GFRP with small-diameter HGF with 5% loading of self-healing agent at ½ in. thickness, after being cut. Bullet impact areas are indicated by solid red pointer lines, and the location of the area that was cut out and removed for deeper cross-sectional investigation is indicated by the dashed red pointer lines.

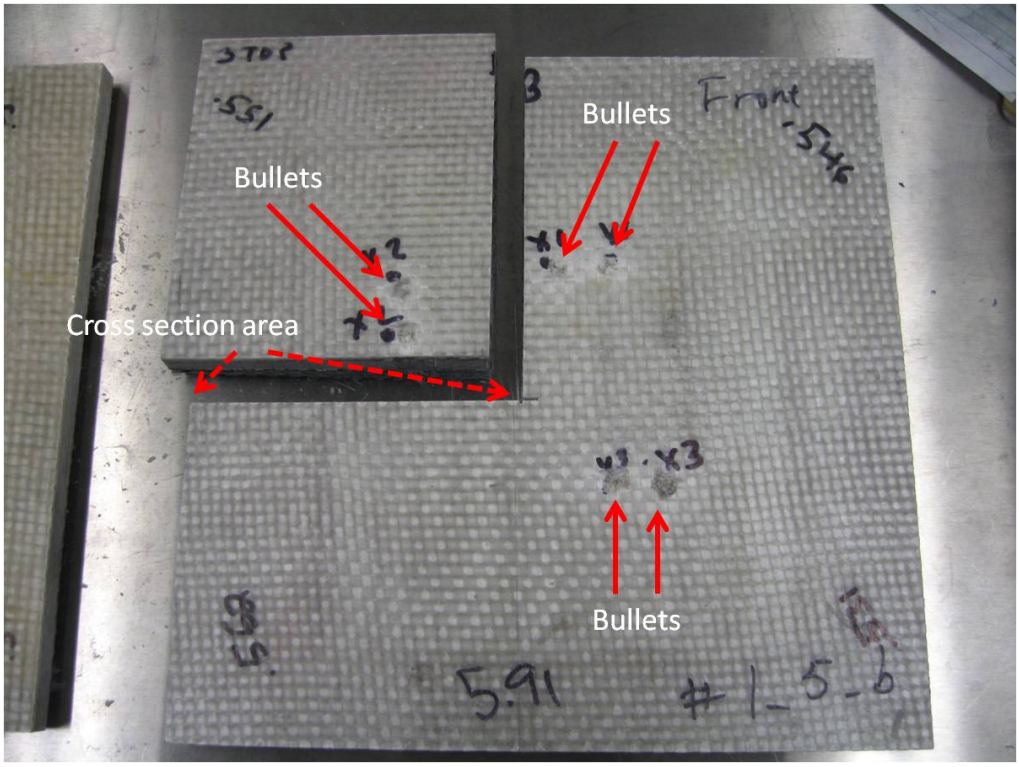


Figure 23. GFRP with small-diameter HGF (placement "a"), 5% loading of self-healing agent, ½ in. thickness. Bullet direction in the image was from top of image to bottom.

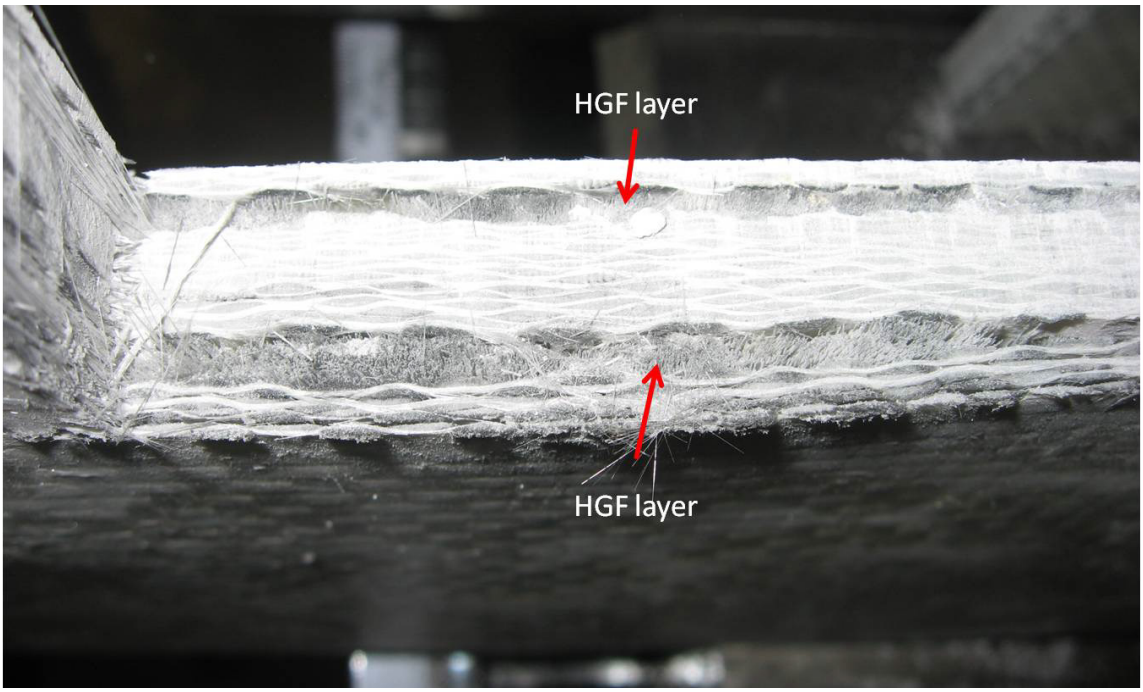

Figure 24 shows the GFRP with large-diameter HGF with 5% loading of self-healing agent at ½ in. thickness, after being cut. The cross section area was pointed out for deep investigation. The cross-section cut for deeper analysis is shown in Figure 25. Again, when the panels were cut for cross-sectional analysis, there was no flow-out of the self-healing agent seen from the HGFs, either close or far away from the bullet shooting area, showing again that the entire collection of HGFs filled with self-healing agent was most likely fully cured after the V50 testing. It was also found again that delamination was more serious close to the bullet impact area.

Figure 24. The GFRP with large-diameter HGF with 5% loading of self-healing agent at ½ in. thickness, after being cut.

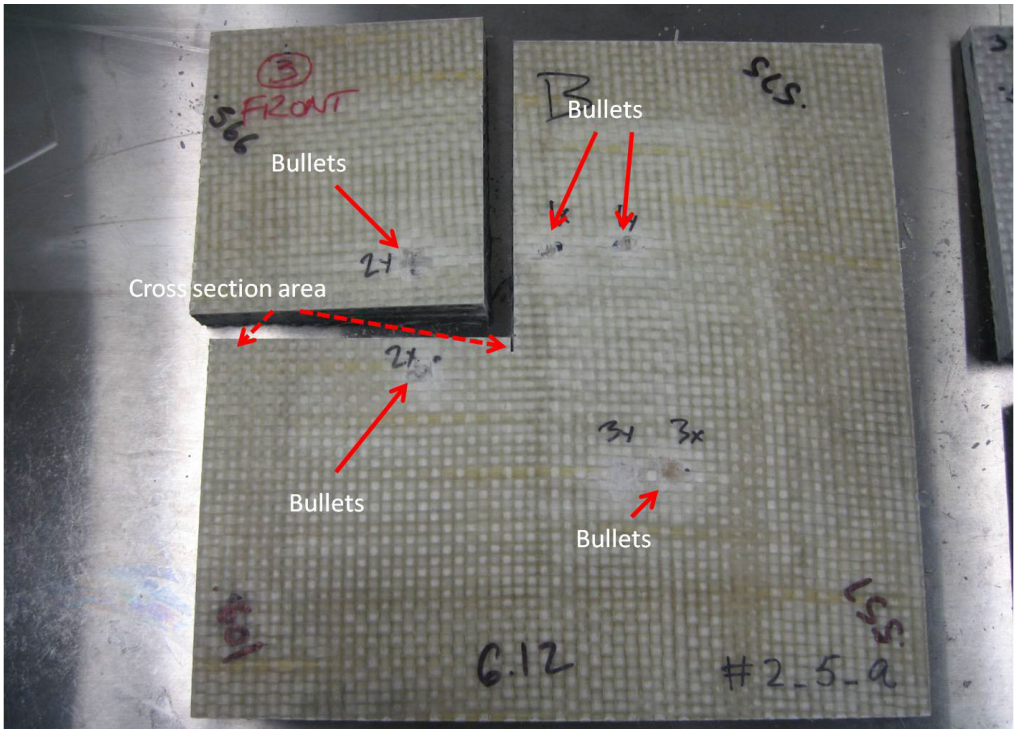


Figure 25. GFRP with large-diameter HGF (placement "a"), 5% loading of self-healing agent, ½ in. thickness. Bullet direction in the image was from top of image to bottom. (Left image taken closer up to bullet impact than right image.)

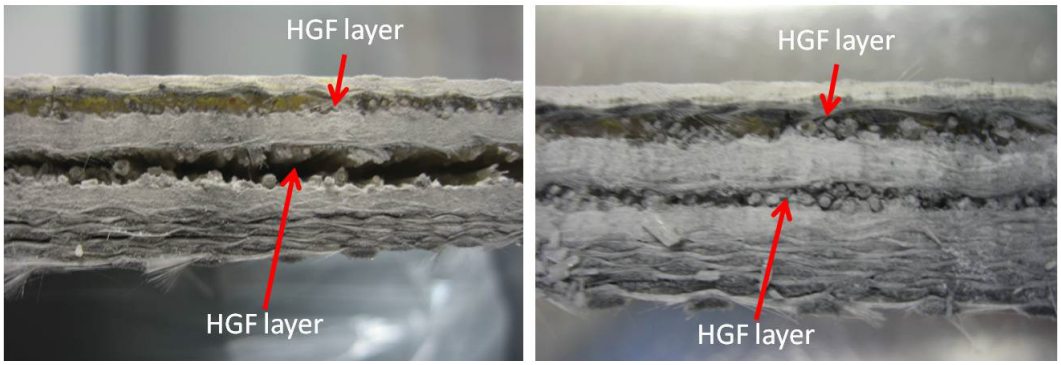

Additional pictures of the GFRP with smaller diameter HGF are shown in Figure 26 and Figure 27.

Figure 26. The GFRP w/small diameter HGF with 5% loading of self-healing agent at ½ in. thickness after being cut (V50-A and V50-B).

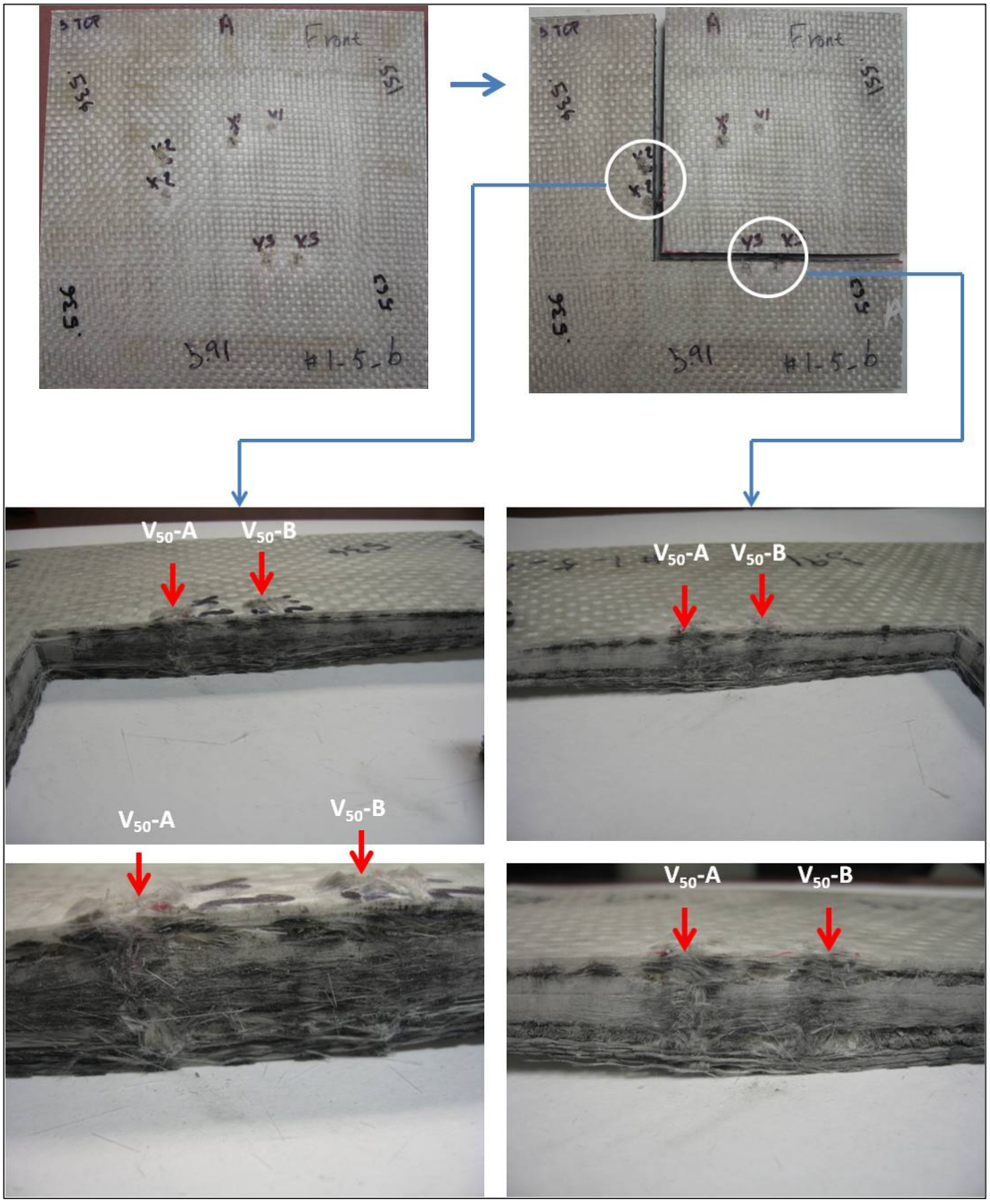

Figure 27. The GFRP with small-diameter HGF with 5% loading of self-healing agent at ½ in. thickness, after being cut (V50-A and V50-C).

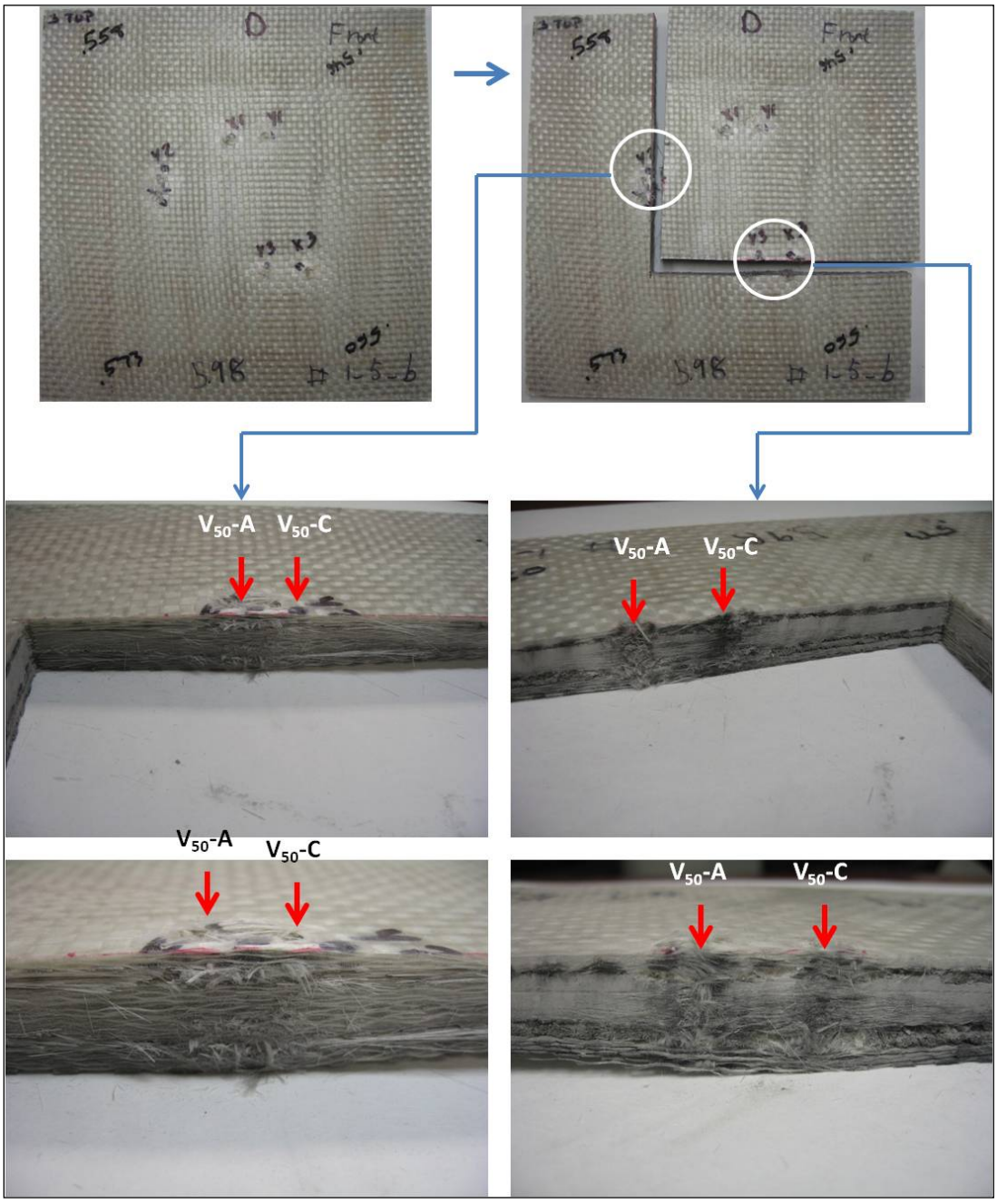

# 6 Mechanical Properties of Self-Healing GFRP Panels

This work achieved promising results in ballistic testing of the GFRP panels with self-healing properties, as shown in Chapter 5. As discussed in that chapter, the panels with the self-healing agent included in HGFs that were embedded in the panels showed improved V50 test results after ballistic impact and after one week of self-healing repair when compared to virgin panels using HGFs, and the panels came close to the performance of the control panels with no HGF.

The next step was to investigate the change of mechanical properties resulting from integrating the self-healing agent in the GFRP panels. The GFRP panels with HGF were observed to be weaker than the control panels with no HGF. It is generally known that the mechanical properties of the GFRP panels (normalized for panel thickness) will be decreased when HGFs or other carriers of the self-healing agent are integrated in the panel. It is also known that there is a connection between mechanical properties and ballistic resistance, although the relationship can be complex. Based on previous results, the investigation considered the parameters listed below.

1. **Mechanical tests focused on compression and compression after impact** (CAI) for the GFRP panels integrated with self-healing agents (based on ASTM D7137). It is known that mechanical properties during compression testing are more susceptible to damage than during tension and flexural testing and thus, structural changes are amplified (damage, healing, etc). The dimensions of the specimens for CAI testing are shown in Figure 28. The polyester and E-glass fiber (PPG's Hybon 2006 direct draw roving, 24 oz) continued to be used as the matrix materials for the base ballistic panels in this study.
2. **Loading of the self-healing agent in the GFRP panels** was chosen at 2.5 and 5 wt% loadings of the self-healing agent. No obvious difference in ballistic resistance between those two loadings was seen, so it would be of interest to look at lower loading levels such as 0.5, 1.5, and 2.5 wt% loadings of the self-healing agent. Using the vinyl ester/MEKP resin system as the self-healing agent was considered be-

cause of promising results shown in the BAA-0020 program (Fink 2011).

3. **Use of small- or large-diameter HGFs**[1] in making the GFRP panels did not cause significant differences in ballistic performance. Large-diameter HGFs were used for this work because they were much lower in cost than the small-diameter HGFs.
4. **Distribution and position of the self-healing agent** play an important role for both mechanical and ballistic performance of the GFRP panels. Both factors were considered when preparing the GFRP panels.

Figure 28. Diagram of the specimen size (based on ASTM D7136) for the after-impact compression testing (based on ASTM D7137). The specimen's thickness was close to 0.2 in., and four plies of the E-glass fiber fabric were utilized. The self-healing layer was placed in the middle of the specimens.

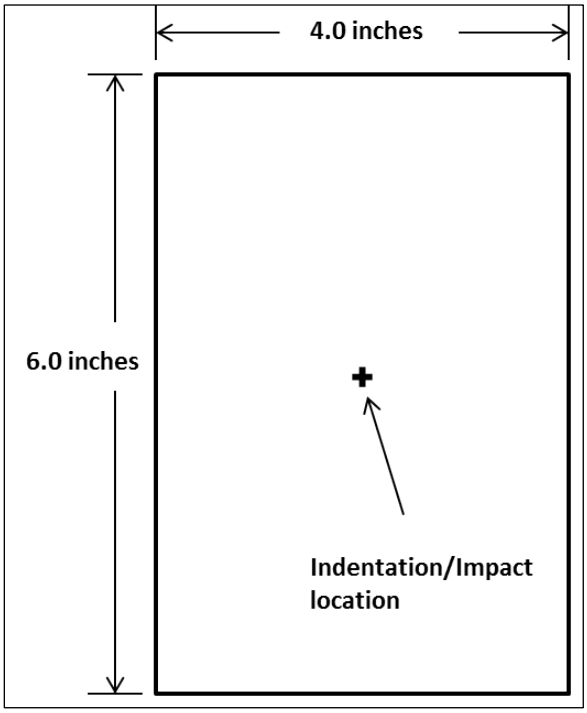


Figure 29 shows the process of cutting an E-glass fiber sheet into specimen-size sheets.

[1] Small diameter HGFs = 66 μm ID and 90±10 μm OD. Large diameter HGFs = ID of 860 μm and OD of around 1500 μm.

Figure 29. E-glass fiber sheet was cut into 4 x 6 in. pieces.

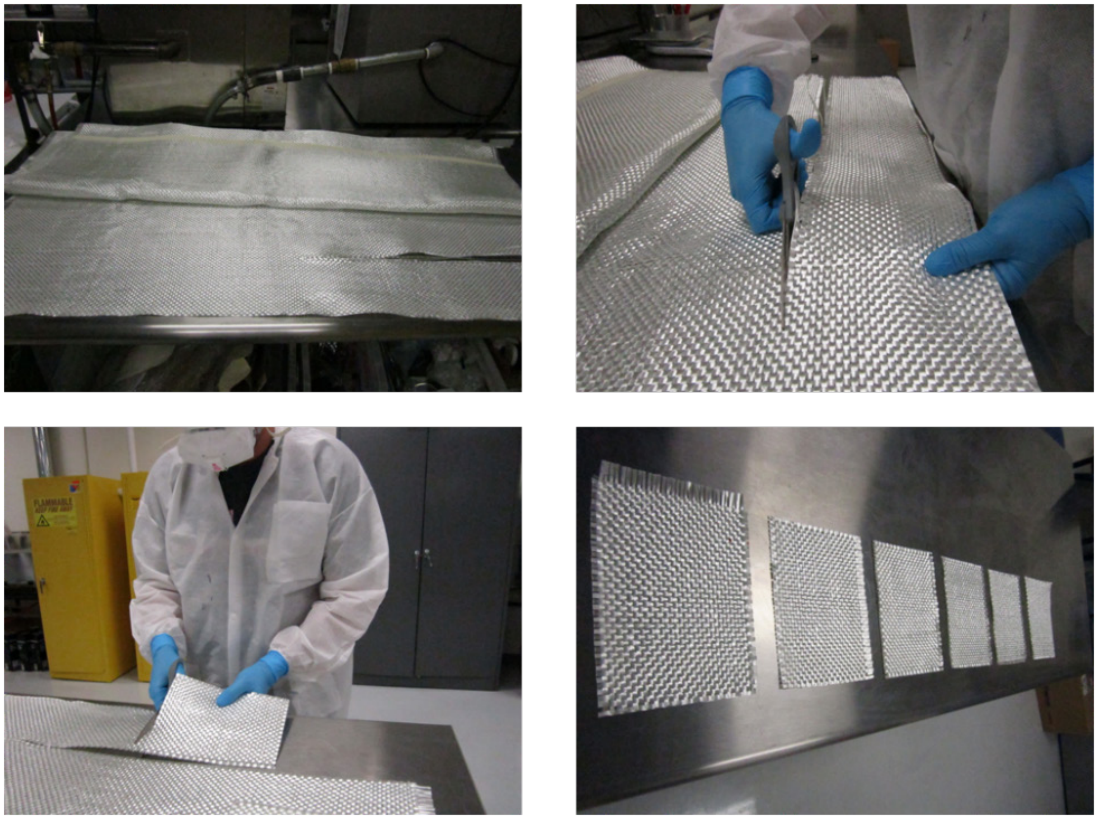

## 6.1 Testing facility

The Department of Manufacturing at Texas State conducted the mechanical testing of materials. The lab there has a fully instrumented low-velocity impact (Instron) machine. The main specifications of the machine were:

- Energy: 0.3–405 J
- Drop height: 0.03–1.1 m
- Impact velocity: 0.77–4.85 m/s

For this study, some test coupons (both reference and self-healing GFRP samples) were first made to find the optimized low-velocity impact energy for the samples. The resulting optimized energy level was used for the remainder of this effort.

Several U.S. labs were contacted in relation to testing impact and compression after impact of the samples. As a result, Accutek Testing Laboratory in Fairfield, Ohio, was found to have the capability to perform both tests.

## 6.2 Specimen preparation

Table 12 shows results of the panels made for mechanical testing. Panels were analyzed before and after mechanical testing.

Table 12. Proposed fabrication of self-healing GFRP specimens.

| Self-Healing GFRP panels | Wt% of Self-Healing Resin |
|---|---|
| Control (polyester GFRP) | 0 |
| GFRP samples with large-diameter HGFs | 2.5 |
| | 5.0 |
| | 10.0 |

Each sample group shown in Table 12 included at least 12 specimens for mechanical testing that focused on the properties listed below.

- Change of mechanical properties after introducing HGF
- Degree of damage that was repaired after introducing self-healing agent (the behavior before and after the self-healing agent was cured after impact testing was also observed)
- Damage behavior of the panels by introducing self-healing agent (e.g., length of cracks, delamination)

GFRP samples with self-healing agent were prepared. The E-glass fiber fabric was cut to pieces (see Figure 29). Each HGF was filled with self-healing agent and catalyst. HGFs were then sealed with silicone sealant (see Figure 30).

GFRP samples were made using a hot-pressing process. Each specimen contained four plies of the E-glass fiber fabric with the polyester matrix. The specimens were hot-pressed at 115 °C for 30 minutes (Figure 31). There were 12 baseline samples (without self-healing agent) (Figure 32). The size of each specimen is 4 x 6 in. (Figure 33).

GFRP samples with self-healing agent were also prepared. Each specimen contained four plies of the E-glass fiber fabric with the polyester (see Figure 34). The HGFs filled with self-healing agent were placed between the second and third plies of the E-glass fiber fabric (based on the weight ratios mentioned in Table 12).

ANI fabricated all the GFRP panels for the four samples. Each of the samples contained 12 GFRP specimens (see Figure 35). These samples were sent immediately to Accutek Testing.

Figure 30. Process of filling HGFs with self-healing agent: (a) one end of the HGF is sealed with silicone sealant; (b) HGF is filled with self-healing agent under vacuum; and (c) other end of the HGF is sealed with silicone sealant.

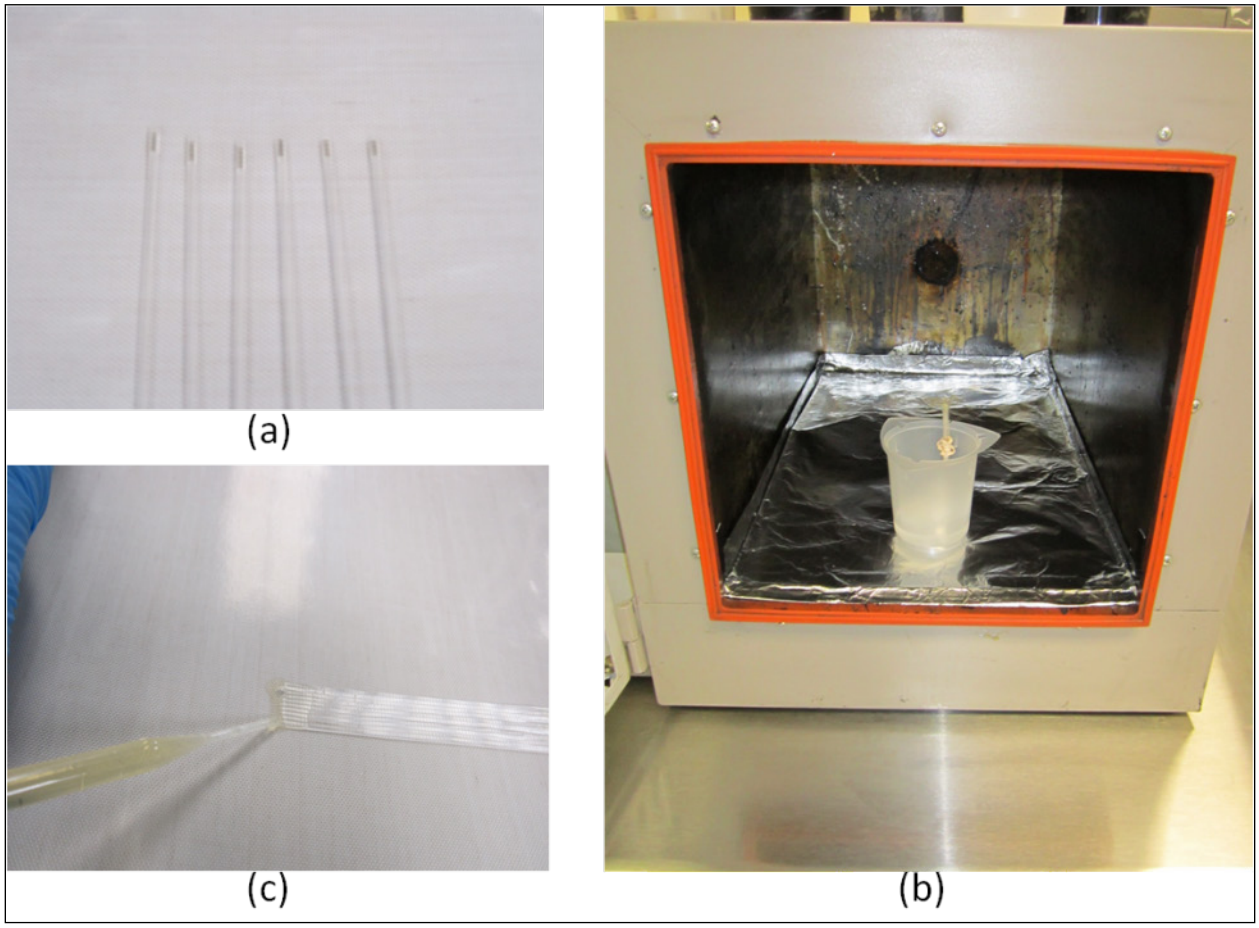

Figure 31. GFRP samples were made using a hot-pressing process. Each specimen contained four plies of the E-glass fiber fabric with the polyester matrix. The specimens were hot-pressed at 115 °C for 30 minutes.

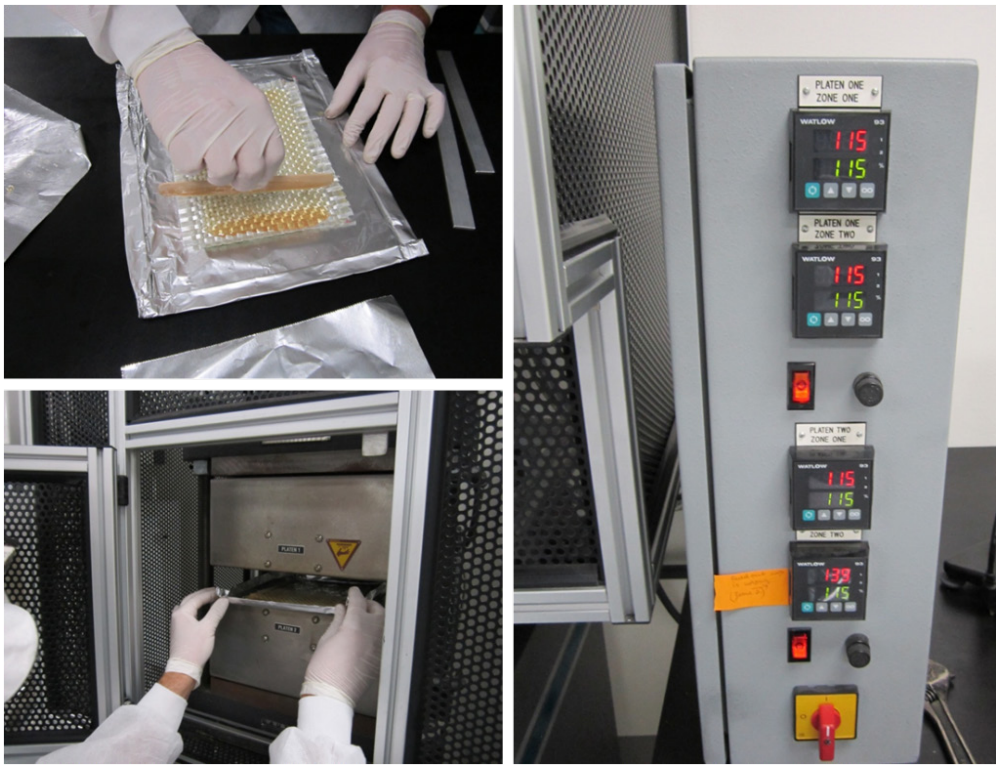


Figure 32. Baseline GFRP sample specimens without self-healing agent.

Figure 33. Each baseline sample specimen measured 4 x 6 in.

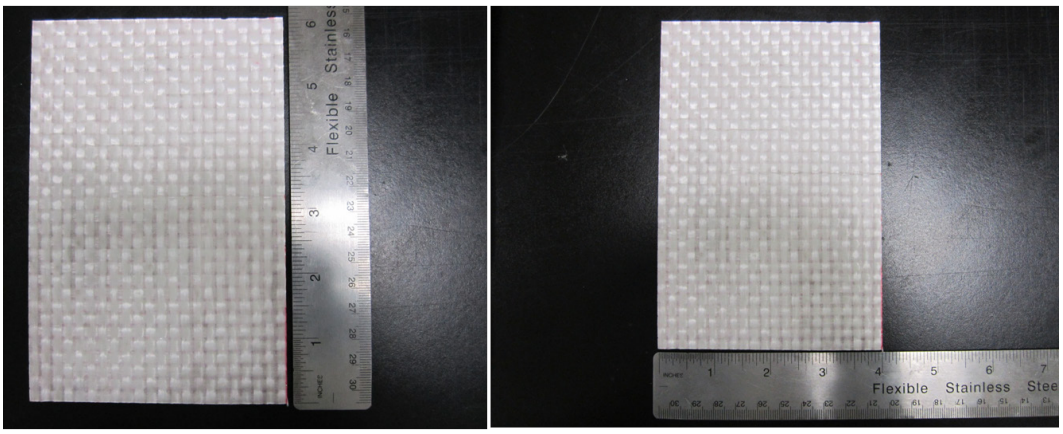


Figure 34. Preparing a GFRP sample with self-healing agent (left); completed GFRP sample with 2.5% self-healing agent (right).

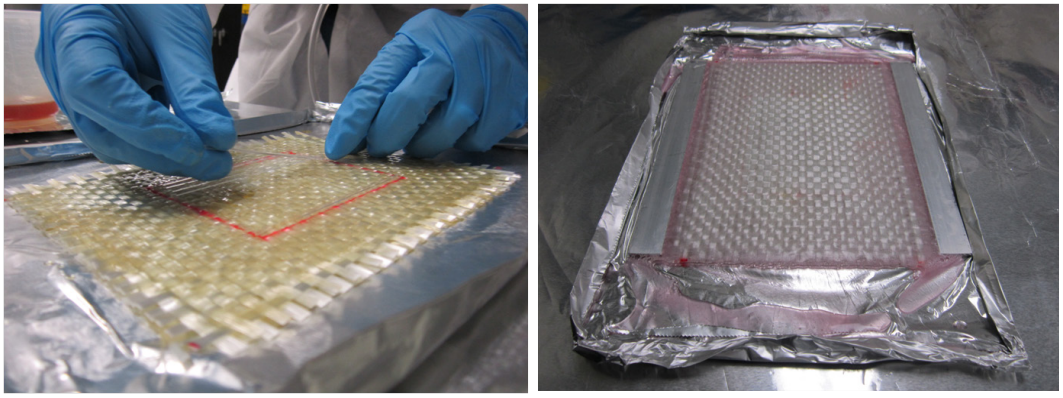

Figure 35. Four samples of GFRP panels including the control, 2.5%, 5.0%, and 10.0 wt% of self-healing agent were made for testing impact and compression after impact. (Each sample has 12 specimens).

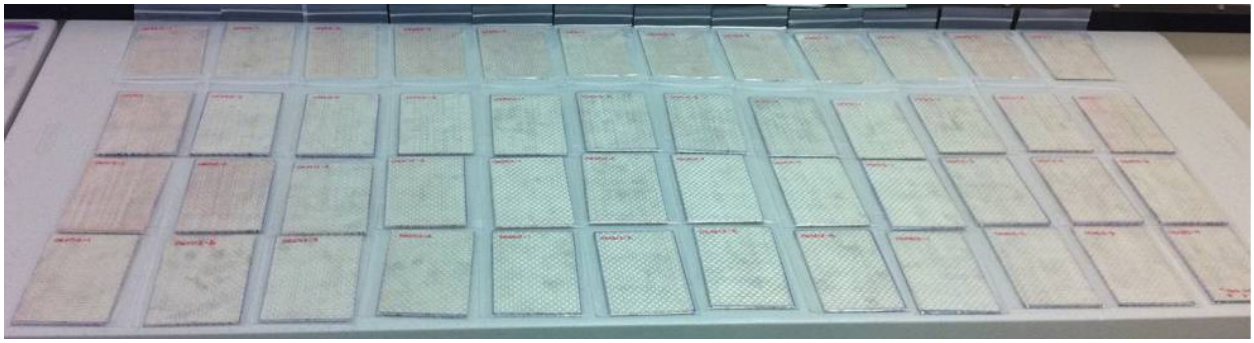

## 6.3 Testing program and results

The test procedures for evaluating the GFRP samples are shown in Table 13. For the samples with self-healing agent, six specimens of each sample were tested under impact. Then the compression-after-impact test was

performed within an hour. The remaining six specimens of each sample were tested for compression after impact a week after the impact testing.

Table 13. Fiber-reinforced polymer matrix composite test instruction for Accutek.

| Sample ID | Sample Description | Quantity | Task | Allowed Testing Timeframe (ASTM 7136) | Note |
|---|---|---|---|---|---|
| 1.1–1.2 | Compression test coupons | 2 | Set up for ASTM D7137 | N/A | To find the baseline strength of undamaged samples |
| 1.3–1.6 | Impact test coupons | 4 | Set up for ASTM D7136 | N/A | To determine optimized impact force for the composite. Accutek sent test results and photos of the damage prior to testing samples 1.7–1.12 |
| 1.7–1.12 | Control samples for base line | 6 | Set up for ASTM D7136 and D7137 | N/A | To determine baseline of impact and compression test.<br>Accutek sent the test results and photos of the damage to ANI prior to testing the remaining samples. |
| 2.1–2.6 | 2.5% self-healing agent | 6 | Set up for ASTM D7136 and followed by ASTM 7137 within 1hr | Compression testing for each sample should be completed within 1hr. of impact testing. | |
| 2.7–2.12 | | 6 | Set up for ASTM D7136 and followed by ASTM 7137 after 1wk | N/A | |
| 3.1–3.6 | 5.0% self-healing agent | 6 | Set up for ASTM D7136 and followed by ASTM 7137 within 1hr | Compression testing for each sample should be completed within 1hr. of impact testing. | |
| 3.7–3.12 | | 6 | Set up for ASTM D7136 and followed by ASTM 7137 after 1wk | N/A | |
| 4.1–4.6 | 10.0% self-healing agent | 6 | Set up for ASTM D7136 and followed by ASTM 7137 within 1hr | Compression testing for each sample should be completed within 1hr. of impact testing. | |
| 4.7–4.12 | | 6 | Set up for ASTM D7136 and followed by ASTM 7137 after 1wk | N/A | |

Note: Specimens 1.1–1.12 are specimens without self-healing agent.

Table 14 shows mechanical properties of the GFRP specimens without self-healing agent. Specimens 1.1 and 1.2 were tested for compression strength without impact. Specimens 1.3 and 1.4 were first tested for impact under different energies, and then compression strength testing was performed. It can be seen that the compression strength after impact of the GFRP specimens was at an impact energy of 20 J or over.

Table 14. Mechanical properties of the GFRP specimens without self-healing agent

| Specimen ID | Impact Energy ( J) | Dent Depth (mm) | Avg. Thickness (mm) | Avg. Width (mm) | Ultimate Force (N) | Compression Strength (MPa) | Failure Mode |
|---|---|---|---|---|---|---|---|
| 1.1 | N/A | N/A | 2.973 | 102.22 | 20465 | 67.4 | Failure near center of specimen |
| 1.2 | N/A | N/A | 2.975 | 102.50 | 21218 | 69.6 | Failure near center of specimen |
| 1.3 | 20 | 0.338 | 2.998 | 102.34 | 11695 | 38.1 | Failure through impact damage |
| 1.4 | 15 | 0.232 | 2.990 | 102.65 | 22507 | 73.3 | Failure through impact damage and near top of specimen |
| 1.5 | 30 | 0.653 | 3.005 | 102.11 | 11746 | 38.3 | Failure through impact damage |
| 1.6 | 40 | 0.802 | 2.978 | 102.19 | 11455 | 37.6 | Failure through impact damage |

Based on the results in Table 14, it was decided to use impact energy of 20 J. Three specimens of each sample were tested to see compression after impact within an hour and after a week following the impact testing. The results were shown in Table 15.

A couple of immediate conclusions can be made based on the data in Table 15. First, it is apparent that as the loading of self-healing material in the samples increases, CAI strength decreases. Second, the difference in mechanical properties observed within one hour of impacting and one week after impacting are very similar. The decrease in strength with an increase in self-healing loading was, to some degree, expected based on the literature related to this type of self-healing system. More surprising was the minor decrease in strength after the one-week waiting period. One possible reason for this result could be that the initial impact energy was not sufficient to cause enough internal damage to the self-healing fibers and allow the self-healing material to freely flow and mingle with the catalyst.

The results from Table 15 were discussed with Accutek, and it was decided to increase the impact energy to 30 J for testing the remaining samples (three specimens each of the four sample sets). The change was made to ensure the HGFs were able to be broken during the impact so that the self-healing agent and hardener could potentially flow out and react. The results of CAI testing with self-healing agent at 30 J are shown in Table 16.

Table 15. CAI of the GFRP specimens with self-healing agent (20 J impact energy).

| Specimen ID | Self-Healing Loading (wt%) | Impact Energy ( J) | Ultimate Force (N) | Compression Strength (MPa) | Compression Timing |
|---|---|---|---|---|---|
| 2.1 | 2.5 | 20 | 14253 | 46.1 | <1 hour |
| 2.3 | 2.5 | 20 | 21050 | 66.1 | <1 hour |
| 2.4 | 2.5 | 20 | 18446 | 58.1 | <1 hour |
| | | **Average** | **17916** | **56.8** | |
| 2.2 | 2.5 | 20 | 12281 | 39.1 | 1 week |
| 2.5 | 2.5 | 20 | 17285 | 55 | 1 week |
| 2.6 | 2.5 | 20 | 21738 | 59.3 | 1 week |
| | | **Average** | **17101** | **51.2** | |
| 3.2 | 5.0 | 20 | 12339 | 35.3 | <1 hour |
| 3.3 | 5.0 | 20 | 10106 | 28.9 | <1 hour |
| 3.4 | 5.0 | 20 | 12139 | 30.1 | <1 hour |
| | | **Average** | **11528** | **31.5** | |
| 3.1 | 5.0 | 20 | 13257 | 40.1 | 1 week |
| 3.5 | 5.0 | 20 | 10286 | 25.1 | 1 week |
| 3.6 | 5.0 | 20 | 10148 | 25 | 1 week |
| | | **Average** | **11230** | **30.1** | |
| 4.2 | 10.0 | 20 | 8504 | 22.1 | <1 hour |
| 4.3 | 10.0 | 20 | 11191 | 29.3 | <1 hour |
| 4.4 | 10.0 | 20 | 11954 | 28.7 | <1 hour |
| | | **Average** | **10550** | **26.7** | |
| 4.1 | 10.0 | 20 | 11048 | 27.3 | 1 week |
| 4.5 | 10.0 | 20 | 10958 | 24.8 | 1 week |
| 4.6 | 10.0 | 20 | 10307 | 25.4 | 1 week |
| | | **Average** | **10771** | **25.8** | |

Table 16. CAI of the GFRP specimens with self-healing agent (30 J impact energy).

| Specimen ID | Self-Healing Loading (wt%) | Impact Energy (J) | Ultimate Force (N) | Compression Strength (MPa) | Compression Timing |
|---|---|---|---|---|---|
| 2.7 | 2.5 | 30 | 19722 | 54.5 | <1 hour |
| 2.8 | 2.5 | 30 | 10021 | 32.6 | <1 hour |
| 2.9 | 2.5 | 30 | 6559 | 18.4 | <1 hour |
| | | **Average** | **6823** | **35.2** | |
| 2.10 | 2.5 | 30 | 11220 | 32.2 | 1 week |
| 2.11 | 2.5 | 30 | 20663 | 60.0 | 1 week |
| 2.12 | 2.5 | 30 | 17686 | 52.1 | 1 week |
| | | **Average** | **17101** | **48.1** | |
| 3.7 | 5.0 | 30 | 7146 | 17.5 | <1 hour |
| 3.8 | 5.0 | 30 | 8343 | 21.7 | <1 hour |
| 3.8 | 5.0 | 30 | 7471 | 20.4 | <1 hour |
| | | **Average** | **7653** | **19.9** | |
| 3.10 | 5.0 | 30 | 9088 | 25.3 | 1 week |
| 3.11 | 5.0 | 30 | 10334 | 28.1 | 1 week |
| 3.12 | 5.0 | 30 | 9378 | 26.4 | 1 week |
| | | **Average** | **11230** | **26.6** | |
| 4.7 | 10.0 | 30 | 9908 | 25.3 | <1 hour |
| 4.8 | 10.0 | 30 | 10510 | 27.0 | <1 hour |
| 4.9 | 10.0 | 30 | 7223 | 18.5 | <1 hour |
| | | **Average** | **9214** | **23.6** | |
| 4.10 | 10.0 | 30 | 10096 | 25.4 | 1 week |
| 4.11 | 10.0 | 30 | 9211 | 23.3 | 1 week |
| 4.12 | 10.0 | 30 | 9679 | 23.9 | 1 week |
| | | **Average** | **9214** | **24.2** | |

It can be seen in Table 16 that, as the loading of self-healing material in the samples increases, the compression strength decreases after impacting which was similar to the results shown in the Table 15. Second, the compression strength observed one week after impacting is significantly better than within an hour after impacting. In the case of the GFRP panels with 2.5 wt% and 5.0 wt% loadings of the self-healing agent, the compression

strength after impact was increased almost 40% in a week. Thus it is believed that the self-healing agent plays an important role in healing the GFRP panels after damage. Figure 36 shows the curves of compression after impact vs. loading of the self-healing agent at different impact energy.

Figure 36. Compression after impact vs. loading of the self-healing agent at different impact energy.

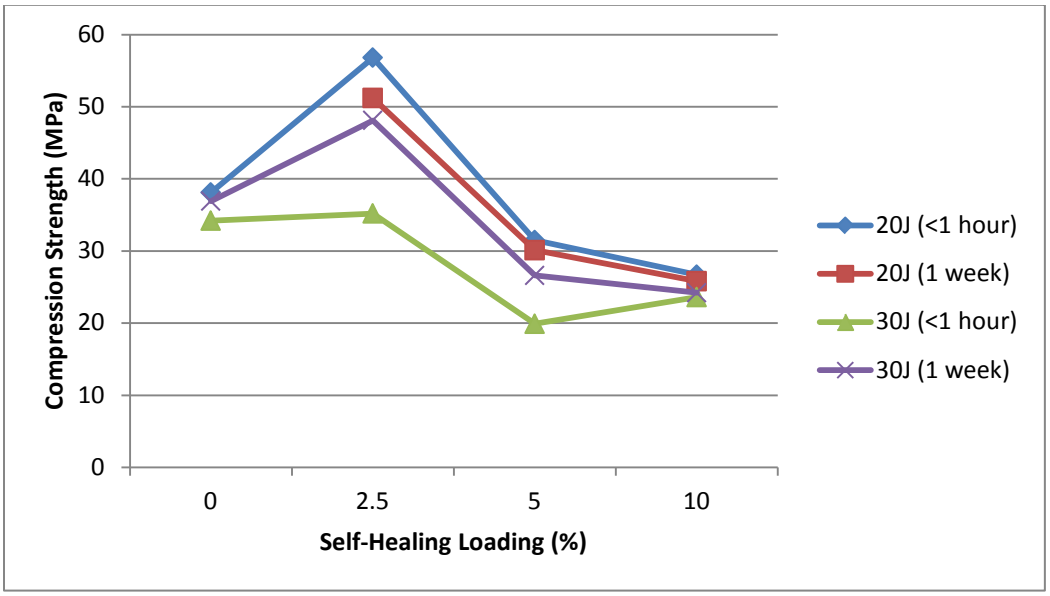


In an effort to confirm that the increased strength is a result of the self-healing materials in the panel, Accutek was asked to perform additional testing on panels without the self-healing materials. Accutek impacted six specimens and then tested three of them for compression strength within one hour of impacting and tested the remaining three for compression strength one week after impacting. The results are shown in Table 17.

Table 17. CAI of the GFRP specimens without self-healing agent (30 J impact energy).

| Specimen ID | Self-Healing | Impact Energy (J) | Ultimate Force (N) | Compression Strength (MPa) | Compression Timing |
|---|---|---|---|---|---|
| 1.7 | N/A | 30 | 11771 | 38.0 | <1 hour |
| 1.8 | N/A | 30 | 10003 | 32.6 | <1 hour |
| 1.9 | N/A | 30 | 9763 | 32.0 | <1 hour |
| | | **Average** | **10512** | **34.2** | |
| 1.10 | N/A | 30 | 12226 | 40.2 | 1 week |
| 1.11 | N /A | 30 | 11480 | 37.6 | 1 week |
| 1.12 | N/A | 30 | 10079 | 33.0 | 1 week |
| | | **Average** | **11261** | **36.9** | |

As shown in Table 17, the compression strength of the specimens tested after one week was very similar to those tested within one hour. This confirmed that the increase observed in compression strength for specimens with self-healing materials was a result of the self-healing materials being released into the panel and then curing to provide a restoration of compression strength. These results confirmed what was revealed in the testing of the panels with self-healing materials—that the self-healing materials play a significant role in healing the GFRP panels after impact damage. Data in Table 17 show that within 1 hour and 1 week there was an improvement of about 8% in CAI at impact energy of 30 J for the panels without self-healing agent. The data in Table 16 show that at 30 J of impact loading, the average increase in CAI is about 37% with 2.5 wt% self-healing agent and 34% increase in CAI with 5 % self-healing agent, but the increase is only 3% for the 10% self-healing agent. These results indicate that there is an optimum loading of self-healing agent.

Additional flexural testing was requested and conducted for panels with and without self-healing. Four sets of samples were made for flexural strength and modulus testing: GFRPs without HGFs and self-healing agent, and GFRPs with HGFs and self-healing agent at loadings of 2.5 wt%, 5.0 wt%, and 10.0 wt%, respectively. The results in Table 18 show a change of the flexural property by adding self-healing agent in the GFRP panels.

Table 18. Flexural strength and modulus of the GFRP samples with and without self-healing agent (each sample contains 6 specimens, average value was taken).

| Samples | Flexural strength (MPa) | Flexural modulus (GPa) |
|---|---|---|
| Control | 222.8 | 14.1 |
| 2.5% self-healing agent | 218.5 | 15.0 |
| 5.0% self-healing agent | 238.7 | 16.2 |
| 10.0% self-healing agent | 180.2 | 17.8 |

It can be seen in Table 18 that the GFRP sample containing 5.0% of the self-healing agent had the best mechanical properties. Based on the published information, the strength is usually decreased if the HGF filled with self-healing agent is introduced in the GFRP panels. It is interesting that the GFRP samples containing 2.5% and 10.0% of the self-healing agent had lower strength than the control. After the self-healing agent was introduced, the flexural modulus was increased. It is very possible that the modulus of the HGF is higher than that of the glass fiber fabric.

Another set of control panel tests for panels were included that have HGF but without self-healing agent (the number of the HGFs corresponded to the loadings of 2.5, 5%, and 10%, respectively related to the self-healing agent). Twenty-four panels were made (six of each of the samples including the control sample). This test did not need to include initial impact but were compression strength tested only. We assumed that we only needed to purchase enough Nanocomp material for one 4 x 8 ft panel.

Table 19 shows the compression strength of the GFRP specimens with HGF but no self-healing agent. It can be seen that the compression strength was increased when the HGFs were integrated into the GFRP panel. However, compression strength was then decreased when the loading of HGFs increased.

Table 19. Compression strength of the GFRP specimens with HGFs but no self-healing agent.

| Specimen ID | Loading of HGF (wt%) (corresponding to the self-healing agent) | Ultimate Force (N) | Compression Strength (MPa) |
|---|---|---|---|
| 8.1 | 0 | 13,330 | 43.6 |
| 8.2 | 0 | 13,062 | 43.1 |
| 8.3 | 0 | 13,565 | 44.6 |
| 8.4 | 0 | 12,109 | 39.8 |
| 8.5 | 0 | 13,123 | 43.2 |
| 8.6 | 0 | 12,024 | 39.9 |
| | | **Average** | **42.4** |
| 5.1 | 2.5 | 15,197 | 48.6 |
| 5.2 | 2.5 | 15,123 | 48.4 |
| 5.3 | 2.5 | 15,506 | 49.8 |
| 5.4 | 2.5 | 14,909 | 47.6 |
| 5.5 | 2.5 | 16,979 | 52.7 |
| 5.6 | 2.5 | 17,059 | 52.8 |
| | | **Average** | **50.0** |
| 6.1 | 5.0 | 12,854 | 35.0 |
| 6.2 | 5.0 | 12,759 | 37.9 |
| 6.3 | 5.0 | 9,059 | 25.7 |
| 6.4 | 5.0 | 12,271 | 34.2 |
| 6.5 | 5.0 | 13,215 | 36.8 |
| 6.6 | 5.0 | 10,911 | 31.2 |
| | | **Average** | **33.5** |
| 7.1 | 10.0 | 15,197 | 29.7 |
| 7.2 | 10.0 | 15,123 | 34.3 |
| 7.3 | 10.0 | 15,506 | 34.5 |
| 7.4 | 10.0 | 14,909 | 34.1 |
| 7.5 | 10.0 | 16,979 | 30.0 |
| 7.6 | 10.0 | 17,059 | 30.7 |
| | | **Average** | **32.2** |

# 7 Investigation of Biocidal Additives for GFRP Panel Surface Coatings

The surface coatings of the GFRP coatings consisted of a chemical agent resistant coating (CARC) primer as the first layer, followed by a CARC top-coat which contained quaternary ammonium compound biocide (QUAT) without germinating or nutrient agents. A shallow photocatalyst layer (for example, $TiO_2$) was deposited over the topcoat such that QUAT molecules would retain most of their active cationic sites near the surface. The photocatalytic composition also contained ionic silver to improve the biocidal activity of the coating. Alternative composition included the photocatalyst and silver along with the QUAT in the CARC topcoat.

The ballistic panel substrates ordered by Armortex were 1 gal of water-borne epoxy primer Type 1 (MIL-PRF-85582D), 1 gal of single-component CARC polyurethane paint (MIL-DTL-53039D), and 100 g of novel amphiphilic QUAT biocide.

Photocatalyst activity characterization was also performed by visible light using methylene blue (MB) aqueous solution as an activity indicator. The decomposition rate of MB under sunlight was assessed for different photocatalyst formulations so that the most active photocatalyst(s) could be identified for subsequent deposition over the CARC coating and biotests using *B. Subtilis* spores.

Ballistic panel substrates and coupons were received from Armortex at ANI. The coupons were 2 x 2 x 1/2 in. GFRP samples that were made for tests with *B. Subtilis*, and 12 x 12 x 1/2 in. panels which were prepared for delivery and evaluation at ERDC-CERL.

The coupons and panels (Figure 37 and Figure 38) were coated with two layers of waterborne primer type AD3247 HENTZEN Aquaprime (two-part primer, MIL-PRF-85582D). The primer was dried for 8 hr in air at room temperature. The coupons and panels were subsequently coated with the polyurethane topcoat containing a bioactive topmost layer combining QUAT and PhotoScrub material modified for sunlight activation (Figure 39).

Figure 37. GFRP coupons coated with MIL-PRF-85582D primer before topcoat application.

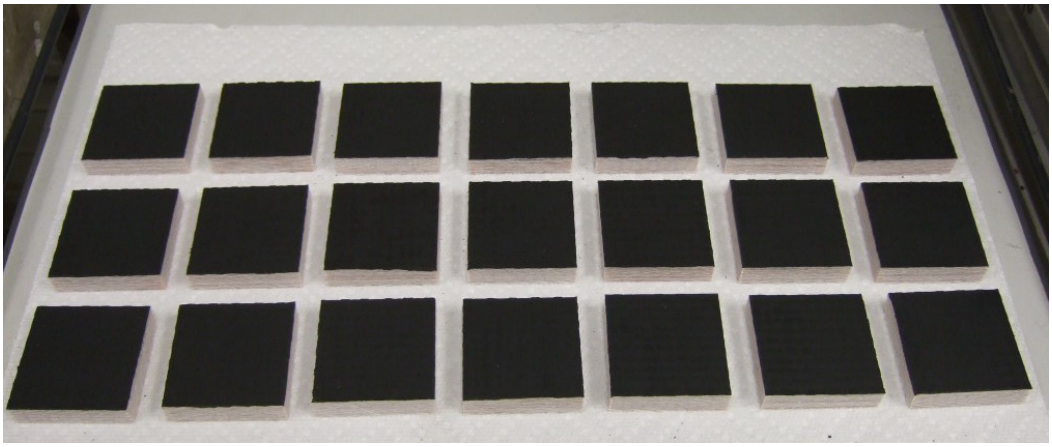

Figure 38. GFRP panels coated with MIL-PRF-85582D primer.

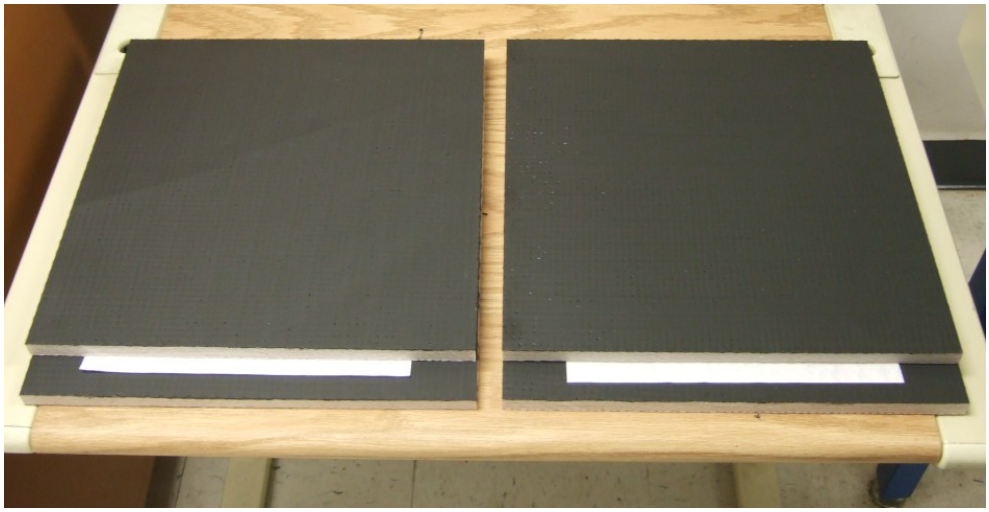

Figure 39. GFRP panels top-coated with a QUAT and PhotoScrub layer.

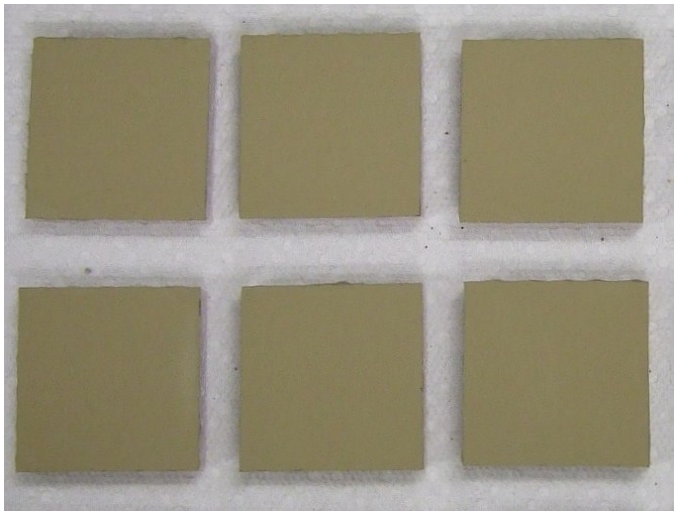

Titanium-based photocatalysts, including PhotoScrub material, were further modified to improve their biocidal efficiency under sunlight radiation (Figure 40). The modification included nitridation of anatase $TiO_2$ and oxidation of titanium nitride (TiN) nanoparticles to obtain core-shell nanostructures with high optical absorption in the visible range yet efficient photocatalytic oxidation properties ensured by the presence of active Ti:O sites on nanoparticle surface. The compositions of interest also included $TiO_2$ materials from different manufacturers.

Figure 40. System for surface modification of titanium-based photocatalytic materials.

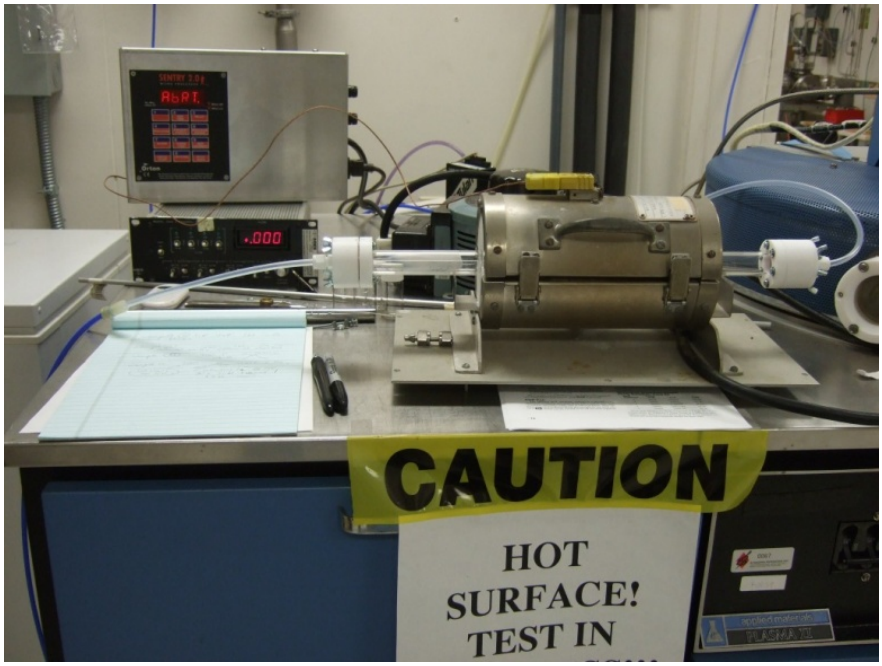


The compositions included $TiO_2$ materials from different manufacturers, as well as ammonia ($NH_3$)-treated $TiO_2$ and oxygen-treated TiN. PhotoScrub material was modified to improve its performance under visible light by using $NH_3$ treatment. The modified material is designated in this study as “PhotoScrub V.”

The data taken under sunlight are shown by the graph in Figure 41. The data shows the decomposition rate “k” of the MB dye measured after 30 min. of exposure to sunlight, assuming that the concentration of the MB decreases over time exponentially as ~exp(-k*t). The bar chart in Figure 41 displays only the significant data (i.e., where the decomposition rate is substantially higher than 0). The data also showed that ZnO nanoparticles and PhotoScrub V have the best MB decomposition performance.

Treated TiN nanoparticles were not as efficient as treated metal oxide materials.

Figure 41. Decomposition of MB by PhotoScrub V and other photocatalytic materials.

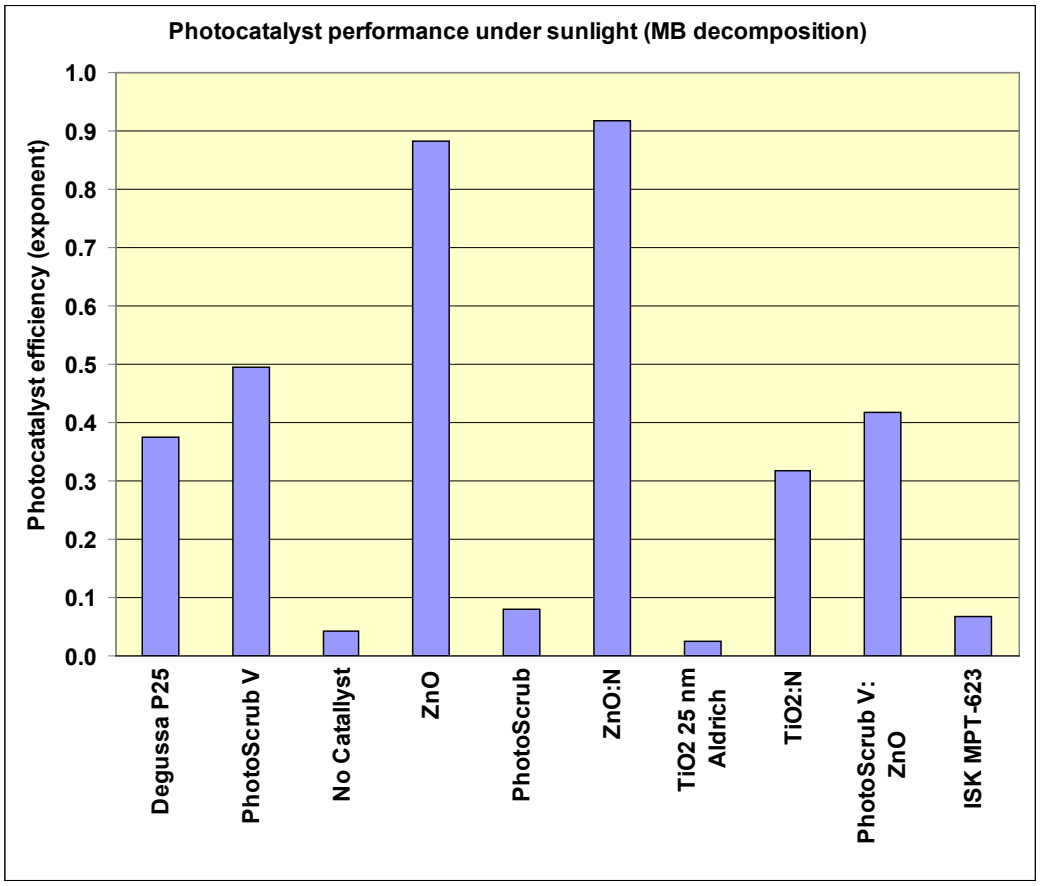


Biotests using *B. Subtilis* spores were conducted by Antimicrobial Test Laboratories in Round Rock, Texas. The test coupons were prepared in triplicate and exposed simultaneously to sunlight for 3 hr (180 min). The test data are shown in Figure 42.

The data show that the biocides added into the topcoat were not efficient for spore decontamination since it was likely that the chemicals in the paint have blocked the active surface sites or chemical groups of either QUAT or photocatalysts. The photocatalysts sprayed over the dried topcoat showed much better performance. The spore inactivation rate achieved over 180 min was as high as 97.2% for PhotoScrub V (log kill rate = 1.56), and it was lower for ZnO based compositions. The reason for including ZnO photocatalyst in the biotests' schedule was its high measured efficiency in decomposition of MB.

Figure 42. Spore inactivation under sunlight for different biocide-based surfaces.

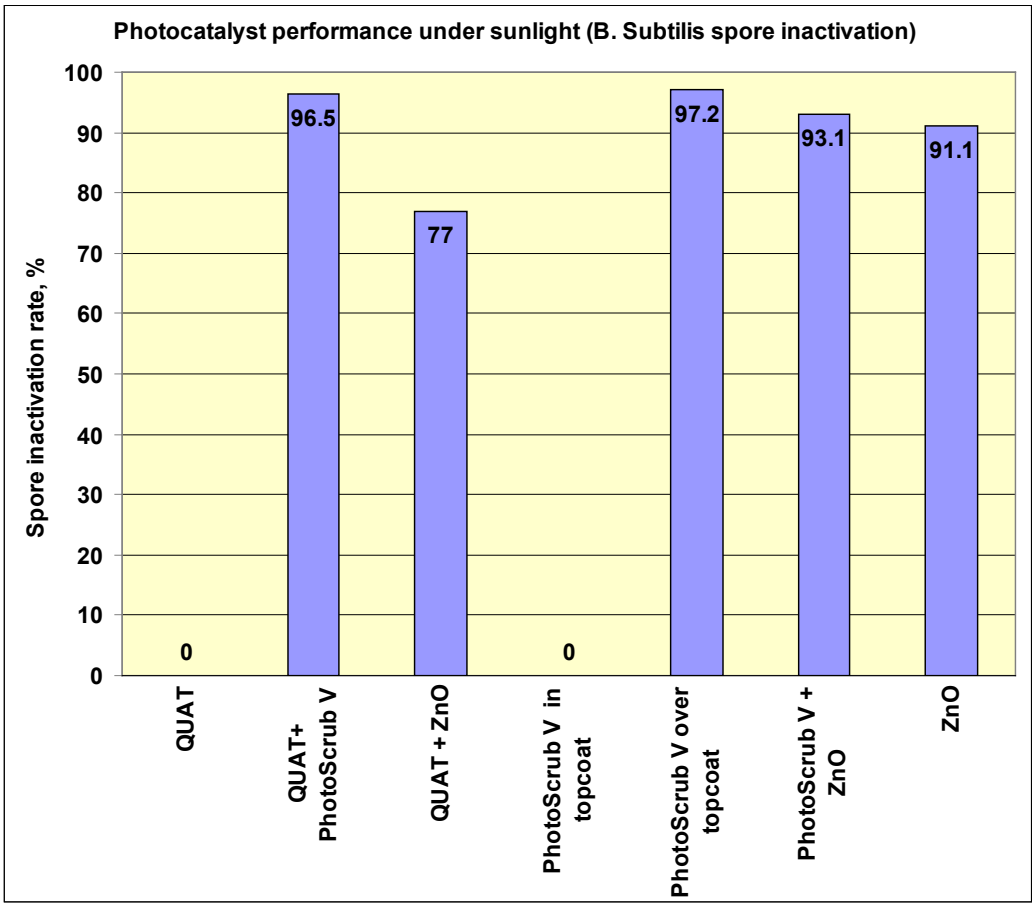

# 8 Investigation of Electromagnetic Impulse Shielding for GFRP Panels

The increasing use of composite materials in industrial and military applications necessitates intensive studies of their electromagnetic properties. An investigation of the electromagnetic properties of advanced composite materials was introduced by Allen, et al. (1976, 174–179) including their electrical constitutive parameters and electromagnetic shielding properties. The electrical and electromagnetic impacts on composites such as lightning protection, shielding effectiveness, electrical system, antenna operation, static electricity, and radar cross section were also discussed by Blake (1976, 170-173). From these studies, it has been noted that composite materials can provide only marginal conductivity but are highly anisotropic, a property which makes the study of their electromagnetic properties an important issue in electromagnetic compatibility.

Composite materials are ideal for structural applications where high strength-to-weight and stiffness-to-weight ratios are important. Weight-sensitive applications such as construction, aircraft, and space vehicles are the primary consumers of composites, especially fiber-reinforced polymer matrix composites. However they usually do not have sufficient EMI shielding capability. In many cases, structures made of composite materials, such as aircraft and buildings, need to be capable of EMI shielding for lightning strike, counter warfare, and other protections. Adding EMI shielding capability to ballistic panels will help electrically protect components inside structures armored with ballistic panels and help defend against counter warfare attack.

In this task, a metal mesh screen was incorporated in the GFRP panel to study EMI properties. The polyester GFRP panel was made and incorporated with the copper mesh screen (obtained from TWP, Inc., 4 mesh Copper, 0.047 in. wire diameter, 36 in. wide) at Armortex. The size of the panel is 32 x 56 in. (Figure 43).

The EMI shielding performance of this modified panel was tested at the U.S. Army ERDC-CERL laboratory, and results are shown in Table 20. Due to the high attenuation constant of copper, this panel was expected to provide a significant amount of shielding with both the magnetic and elec-

tric fields. This expectation held true for the lower frequencies, between 0.1 and 1000 MHz (up to 60–66 dB). However, it was shown to have less shielding at the 8-10 GHz range. This loss of shielding could be due to the location of the copper mesh or the size of the mesh.

Figure 43. Polyester GFRP panel (32 x56 in.) incorporating copper mesh screen (left), and cross-section showing copper mesh screen in middle of panel (right).

Table 20. EMI shielding performance of a GFRP panel incorporating copper mesh screen for EMI shielding.

| Panel C | | | | | | | | | | | | | |
|---|---|---|---|---|---|---|---|---|---|---|---|---|---|
| Date | 7/13/2011 | | | | | 7/15/2011 | | | | | | | |
| Type | Calibration | | Panel C | | | Calibration | | Panel C | | | | | Standard |
| Frequency (MHz) | Signal | Noise | Signal | Noise | | Signal | Noise | Signal | Noise | | | Avg. | Deviation |
| 0.1 | 80 | -19 | 52 | -26 | 28 | 80 | -19 | 55 | -26 | 25 | | 26.5 | 2.1213 |
| 1.0 | 74 | -13 | 43 | -15 | 31 | 74 | -12 | 46 | -14 | 28 | | 29.5 | 2.1213 |
| 10.0 | 54 | -12 | 19 | -13 | 35 | 54 | -13 | 21 | -13 | 33 | | 34 | 1.4142 |
| 0.1 | 62 | -25 | 1 | -29 | 61 | 62 | -29 | -1 | -29 | 63 | | 62 | 1.4142 |
| 1.0 | 93 | -3 | 31 | -12 | 62 | 94 | -13 | 28 | -12 | 66 | | 64 | 2.8284 |
| 10.0 | 102 | 20 | 41 | 20 | 61 | 103 | 18 | 44 | 18 | 59 | | 60 | 1.4142 |
| 100.0 | 95 | 26 | 59 | 10 | 36 | 94 | 18 | 52 | 12 | 42 | | 39 | 4.2426 |
| 1,000.0 | 95 | 23 | 62 | 23 | 33 | 99 | 25 | 64 | 23 | 35 | | 34 | 1.4142 |
| 8,000.0 | 65 | 20 | 57 | 19 | 8 | 69 | 19 | 60 | 18 | 9 | | 8.5 | 0.7071 |
| 9,000.0 | 89 | 24 | 79 | 23 | 10 | 90 | 20 | 84 | 19 | 6 | | 8 | 2.8284 |
| 10,000.0 | 99 | 11 | 97 | 23 | 2 | 109 | 21 | 98 | 21 | 11 | | 6.5 | 6.3640 |

## 8.1 Conductive carbon coating

A layer of carbon materials was coated onto the surface of the E-glass fiber fabric. A high-efficiency, electrically-conductive coating material (sheet resistance 10 Ω/m but can be adjusted) was investigated. This material can be easily coated onto substrates with good adhesion via many different coating techniques – spinning off, painting, brushing, spray, pouring, immersing, etc. This coating is tough and robust against scratches and handling and is weather resistant. In this procedure, the conductive layer is coated onto a layer of the E-glass fiber fabric and embedded into the panel. The polyester GFRP panel was made at Armortex. The size of the panel is 32 x 56 in. (Figure 44).

Figure 44. GFRP panel using a layer of conductive carbon coating.

It was shown that this material would provide shielding on the order of 5–10 dB (Table 21). At .1 MHz and 1 MHz, the average was less than 1 dB and at 10 MHz, the average shielding was 5.17 dB. At even higher frequencies, the shielding would average 23 dB.

Table 21. EMI shielding performance of GFRP panel using conductive carbon coating on panel surface.

| Panel A | | | | | | | | | | | | | | | | | |
|---|---|---|---|---|---|---|---|---|---|---|---|---|---|---|---|---|---|
| Date | 7/7/2011 | | | | | 7/12/2011 | | | | | 7/28/2011 | | | | | | |
| Type | Calibration | | Test | | | Calibration | | Test | | | Calibration | | Test | | | | Standard |
| Frequency (MHz) | Signal | Noise | Signal | Noise | | Signal | Noise | Signal | Noise | | Signal | Noise | Signal | Noise | | Avg. | Deviation |
| 0.1 | 81 | -18 | 81 | -16 | 0 | 81 | -20 | 80 | -19 | 1 | 81 | -19 | 81 | -22 | 0 | 0.33333 | 0.5092 |
| 1.0 | 75 | -11 | 75 | -11 | 0 | 75 | -11 | 74 | -13 | 1 | 75 | -12 | 76 | -12 | -1 | 0 | 0.5774 |
| 10.0 | 52 | -12 | 50 | -13 | 2 | 55.5 | -12.5 | 47 | -12 | 8.5 | 55 | -13 | 50 | -13 | 5 | 5.16667 | 3.2504 |
| 0.1 | 72 | -25 | -21 | -28 | 93 | 63 | -18 | -22 | -28 | 85 | 84 | -23 | -6 | -23 | 90 | 89.3333 | 4.0046 |
| 1.0 | 98 | -11 | 32 | -11 | 66 | 94 | 0 | 31 | -11 | 63 | 101 | -5 | 38 | -6 | 63 | 64 | 1.5275 |
| 10.0 | 103 | 17 | 73 | 3 | 30 | 101.5 | 20.5 | 75 | 2 | 26.5 | 101 | 32 | 75 | 63 | 26 | 27.5 | 1.8028 |
| 100.0 | 112 | 12 | 79 | 8 | 33 | 95.5 | 27.5 | 78 | 12 | 17.5 | 98 | 23 | 75 | 10 | 23 | 24.5 | 7.7621 |
| 1,000.0 | 104 | 10 | 73 | 23 | 31 | 96 | 23 | 78 | 23 | 18 | 94 | 23 | 70 | 23 | 24 | 24.3333 | 6.5007 |
| 8,000.0 | 0 | 0 | 0 | 0 | | 61.5 | 22 | 45 | 18 | 16.5 | 66 | 19 | 39 | 19 | 27 | 21.75 | 3.7123 |
| 9,000.0 | 0 | 0 | 0 | 0 | | 86 | 25 | 58 | 22 | 28 | 91 | 23 | 72 | 24 | 19 | 23.5 | 3.1820 |
| 10,000.0 | 0 | 0 | 0 | 0 | | 103 | 18 | 82 | 23 | 21 | 107 | 25 | 75 | 11 | 32 | 26.5 | 3.8891 |

## 8.2 Exclucent™ film

An additional sample panel was tested that was coated with ANI's Exclucent™ material (Figure 45). This material consists of copper lines on a PET substrate. This material was attached to the panel with copper side down with an adhesive for the testing at ERDC-CERL (Table 22). Due to this extra layer of conducting material, this sample was expected to provide a significant amount of shielding (on the order of 40–50 dB). The average shielding was found to 4.33 dB at 100 kHz, 16.3 at 1 MHz, and 39 dB at 10 MHz.

Figure 45. GFRP panel using a layer of conductive Exclucent film on the surface.

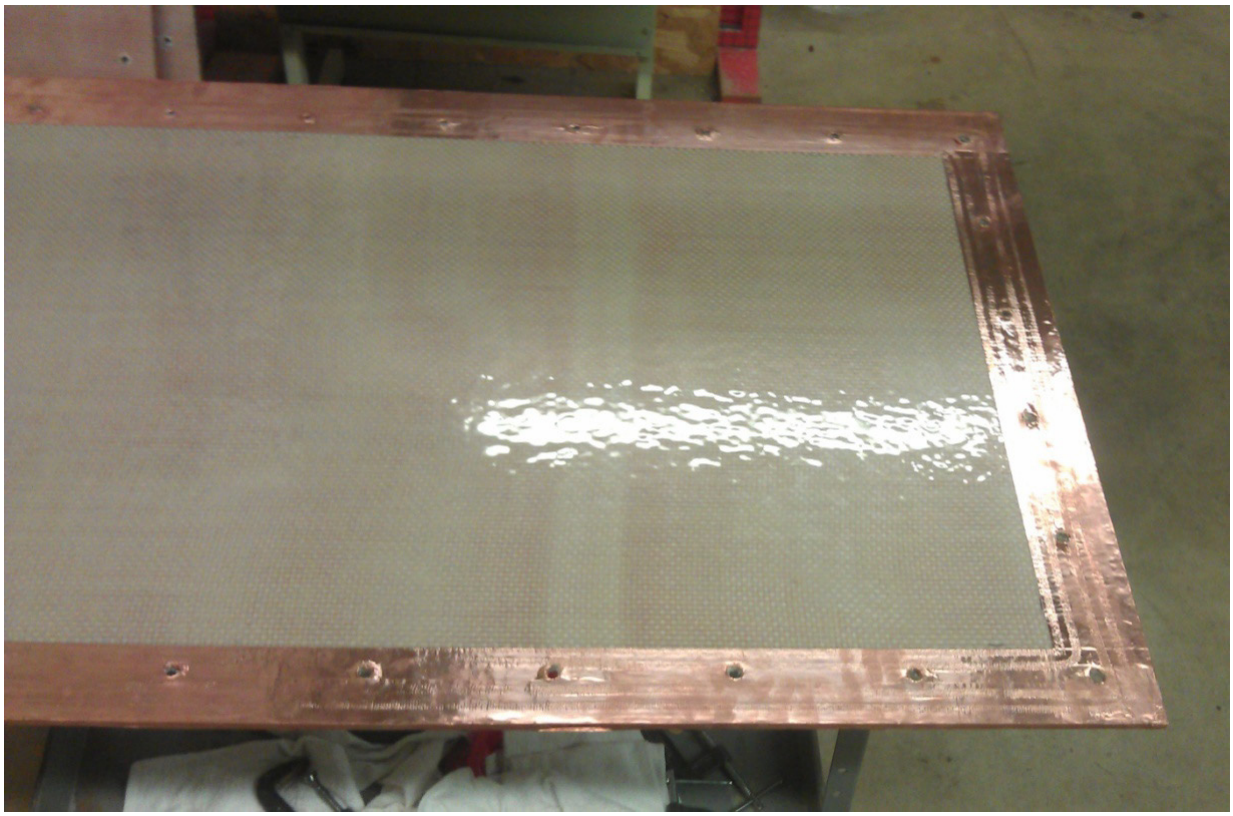

Table 22. EMI shielding performance of GFRP panel using conductive Exclucent film.

| Panel B | | | | | | | | | | | | | | | | | |
|---|---|---|---|---|---|---|---|---|---|---|---|---|---|---|---|---|---|
| Date | 7/8/2011 | | | | | 7/11/2011 | | | | | 7/11/2011 | | | | | | |
| Type | Calibration | | Panel X | | | Calibration | | Panel X | | | Calibration | | Panel X | | | | Standard |
| Frequency (MHz) | Signal | Noise | Signal | Noise | | Signal | Noise | Signal | Noise | | Signal | Noise | Signal | Noise | | Avg. | Deviation |
| 0.1 | 81 | -18 | 78 | -20 | 3 | 81 | -16 | 75 | -21 | 6 | 81 | -19 | 77 | -21 | 4 | 4.33333 | 1.5275 |
| 1.0 | 76 | -11 | 57 | -14 | 19 | 75 | -11 | 60 | -14 | 15 | 75 | -13 | 60 | -14 | 15 | 16.3333 | 2.3094 |
| 10.0 | 54 | -12 | 15 | -15 | 39 | 58 | -13 | 15 | -13 | 43 | 54 | -13 | 19 | -13 | 35 | 39 | 4.0000 |
| 0.1 | 64 | -15 | -9 | -29 | 73 | 73 | -23 | -2 | -17 | 75 | 82 | -12 | 8 | -25 | 74 | 74 | 1.0000 |
| 1.0 | 95 | -1 | 19 | -11 | 76 | 95 | 0 | 25 | -11 | 70 | 96 | 0 | 27 | -10 | 69 | 71.6667 | 3.7859 |
| 10.0 | 100 | 5 | 42 | 20 | 58 | 101 | 17 | 43 | 16 | 58 | 104 | 17 | 49 | 22 | 55 | 57 | 1.7321 |
| 100.0 | 108 | 9 | 47 | -8 | 61 | 96 | 32 | 66 | 12 | 30 | 93 | 20 | 65 | 8 | 28 | 39.6667 | 18.5023 |
| 1,000.0 | 95 | 22 | 56 | 22 | 39 | 104 | 23 | 49 | 23 | 55 | 103 | 23 | 57 | 23 | 46 | 46.6667 | 8.0208 |
| 8,000.0 | 0 | 0 | 0 | 0 | | 67 | 19 | 38 | 19 | 29 | 66 | 19 | 34 | 19 | 32 | 30.5 | 2.1213 |
| 9,000.0 | 0 | 0 | 0 | 0 | | 90 | 21 | 62 | 24 | 28 | 88 | 22 | 58 | 23 | 30 | 29 | 1.4142 |
| 10,000.0 | 0 | 0 | 0 | 0 | | 105 | 23 | 68 | 26 | 37 | 110 | 24 | 65 | 26 | 45 | 41 | 5.6569 |

## 8.3 Embedded layer of conductive carbon

An additional sample panel was tested that had a conductive carbon layer embedded in the GFRP panel (Figure 46). It was shown that this material would provide shielding on the order of 5–10 dB. At 10 MHz, the average shielding was found to be 38.5 dB (see Table 23). At higher frequencies,

the shielding averaged 17 dB which is about 10 dB less than the GFRP panel with coating of the same carbon film on its surface (see Table 21).

Figure 46. Polyester GFRP panel (32 x56 in.) with carbon coating incorporated (left); cross-section view of panel showing continuous carbon coating integrated with the GFRP at the middle of the panel (right).

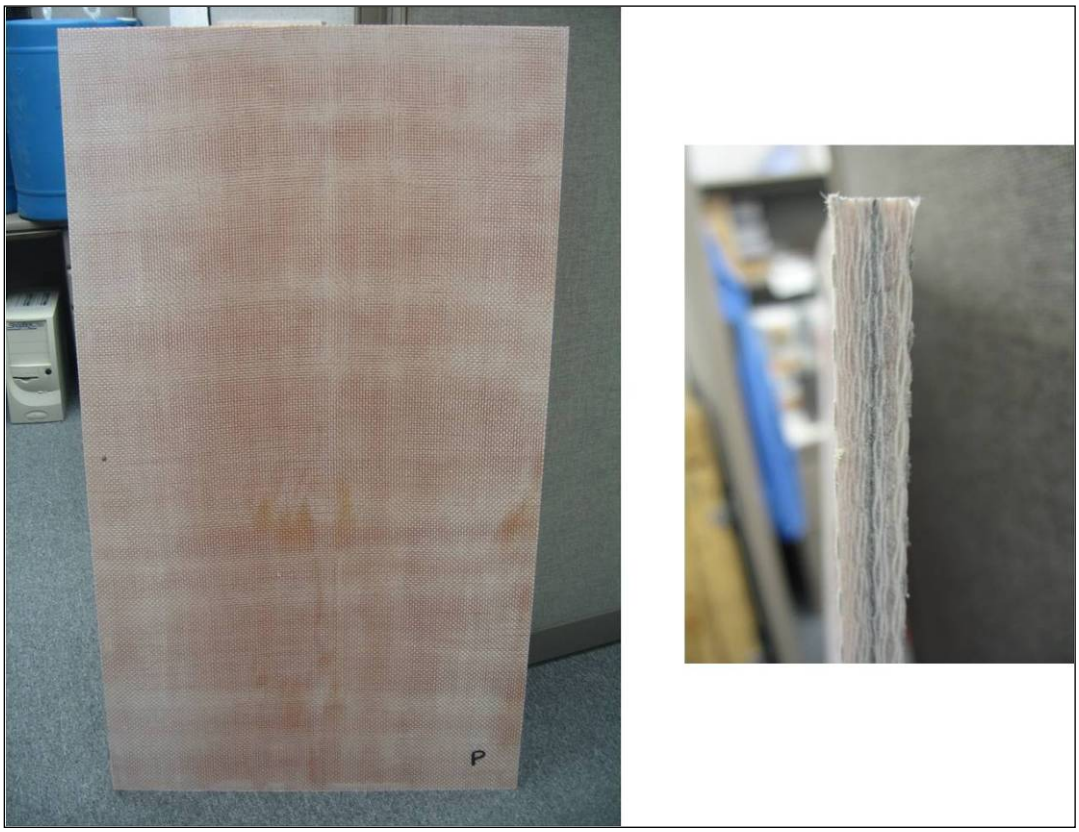

Table 23. EMI shielding performance of the GFRP panel using a conductive carbon coating embedded in the panel.

| Panel D | | | | | | | | | | | | | | | | | |
|---|---|---|---|---|---|---|---|---|---|---|---|---|---|---|---|---|---|
| Date | 7/6/2011 | | | | | 7/14/2011 | | | | | 7/18/2011 | | | | | | |
| Type | Calibration | | Test | | | Calibration | | Test | | | Calibration | | Test | | | | Standard |
| Frequency (MHz) | Signal | Noise | Signal | Noise | | Signal | Noise | Signal | Noise | | Signal | Noise | Signal | Noise | | Avg. | Deviation |
| 0.1 | 81 | -16 | 66 | -10 | 15 | 81 | -19 | 83 | -19 | -2 | 81 | -19 | 82 | -19 | -1 | -1.5 | 0.7071 |
| 1.0 | 75 | -12 | 74 | -16 | 1 | 75 | -12 | 76 | -12 | -1 | 75 | -13 | 76 | -13 | -1 | -1 | 0.0000 |
| 10.0 | 54 | -13 | 70 | -14 | -16 | 59 | -13 | 56 | -12 | 3 | 54 | -13 | 53 | -13 | 1 | 2 | 1.4142 |
| 0.1 | 72 | -12 | -2 | -27 | 74 | 63 | -25 | -10 | -28 | 73 | 82 | -12 | -10 | -28 | 92 | 82.5 | 13.4350 |
| 1.0 | 96 | 0 | 36 | -8 | 60 | 95 | -3 | 40 | -12 | 55 | 96 | 0 | 35 | -12 | 61 | 58 | 4.2426 |
| 10.0 | 101 | 24 | 77 | 21 | 24 | 102 | 11 | 49 | 33 | 53 | 104 | 17 | 80 | 17 | 24 | 38.5 | 20.5061 |
| 100.0 | 111 | 26 | 91 | 16 | 20 | 93 | 8 | 88 | 9 | 5 | 93 | 20 | 89 | 0 | 4 | 4.5 | 0.7071 |
| 1,000.0 | 104 | 22 | 78 | 23 | 26 | 95 | 23 | 81 | 22 | 14 | 103 | 23 | 72 | 23 | 31 | 22.5 | 12.0208 |
| 8,000.0 | 0 | 0 | 0 | 0 | | 65 | 19 | 54 | 19 | 11 | 66 | 19 | 54 | 19 | 12 | 11.5 | 0.7071 |
| 9,000.0 | 0 | 0 | 0 | 0 | | 88 | 22 | 76 | 23 | 12 | 88 | 22 | 85 | 23 | 3 | 7.5 | 6.3640 |
| 10,000.0 | 0 | 0 | 0 | 0 | | 110 | 25 | 93 | 25 | 17 | 110 | 24 | 93 | 25 | 17 | 17 | 0.0000 |

# 9 Properties and Cost for Full-Size Multifunctional Panel Configurations

## 9.1 Panel fabrication

In this effort, a number of large GFRP panels were fabricated to ensure the processes could be scaled up for commercialization. Fabrication included the functionalities listed below:

- Self-healing properties
- CNT reinforcement
- EMI shielding
- Self-decontamination surface (SDS)

Seven GFRP panels were fabricated at a size of 4 x 8 ft (thickness 0.5 in.) to include the functionalities mentioned above plus one multifunctional panel as follows:

- two panels were integrated with self-healing agent;
- two panels were reinforced with CNTs;
- two panels were fabricated with an SDS; and
- one panel featured all functionalities.

All seven GFRP panels were made at Armortex and delivered to the Army (ERDC-CERL) for further examination.

### 9.1.1 Fabrication for self-healing functionality (Panels 1 and 2)

A large-diameter HGF was integrated in the GFRP panel for the self-healing functionality. Loading of the self-healing agent required a large amount of HGFs to be filled with self-healing agent (Figure 47a); one open end of the HGFs was sealed in preparation for filling them with vinyl ester and catalyst (Figure 47b). Then, enough HGFs were filled with the self-healing agent (Figure 47c) to make three 4 x 8 ft GFRP panels. In addition, enough CNT-reinforced polyester resin was prepared, as shown in Figure 48. The HGFs filled with self-healing agent and catalyst were located on the 4 x 8 ft panel of glass fiber fabric (Figure 49). A completed panel with self-healing agent is shown in Figure 50.

A 2.5 wt% loading of the self-healing agent was used in these GFRP panels because this formulation had been shown to achieve the best self-healing efficiency (refer to discussion in Chapter 6). Results showed the flexural strength of the panels decreased 1% while the modulus improved 7%. The compression strength of the GFRP panel with HGF (corresponding to 2.5 wt% loading of the self-healing agent in the panel) was 50.0 MPa;

When tested within 1 hr after impact (impact energy: 30 J), the compression strength of the GFRP panel with 2.5 wt% loading of the self-healing agent was 35.2 MPa; this measurement meant the GFRP panel's strength was damaged about 30% after the impact. This was likely due to the time after impact being too short for the self-healing agent to effectively react with the catalyst.

It was expected that the self-healing agent would effectively react with the catalyst during one week. The compression strength of the GFRP panel with 2.5% loading of the self-healing agent after impact (impact energy: 30 J) when tested one week after the impact was 48.1 MPa. The self-healing efficiency in this case is 96%, and it almost recovers to the compression strength of the undamaged GFRP (50.0 MPa).

Figure 47. Groups of HGFs were prepared in three steps: (a) filled with self-healing agent; (b) filled with catalyst; and (c) filled with self-healing agent and catalyst.

(a)

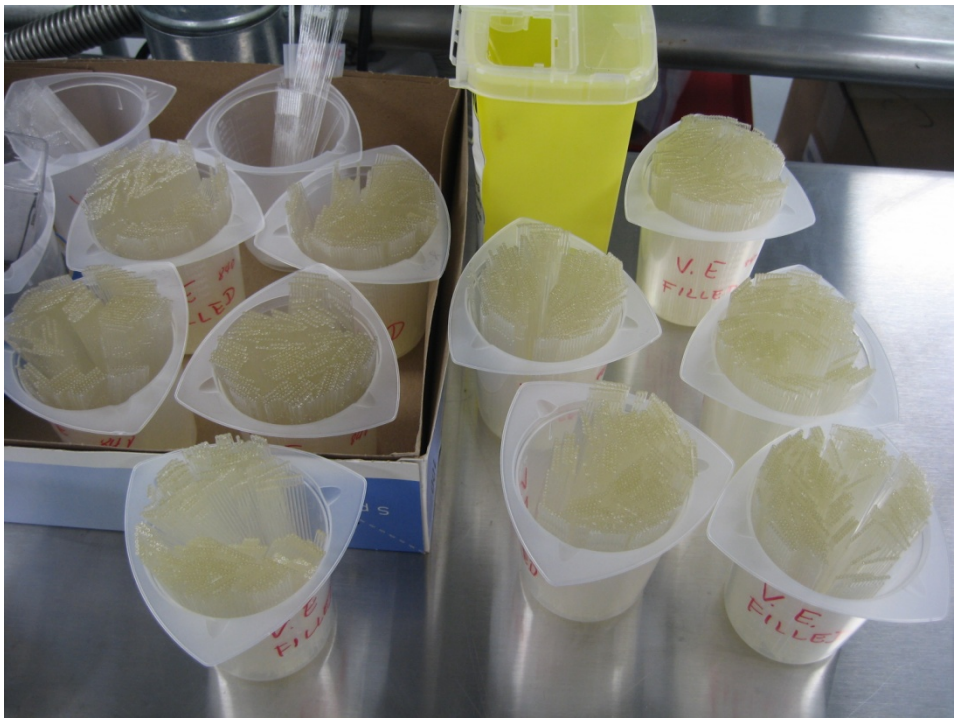

(b)

(c)

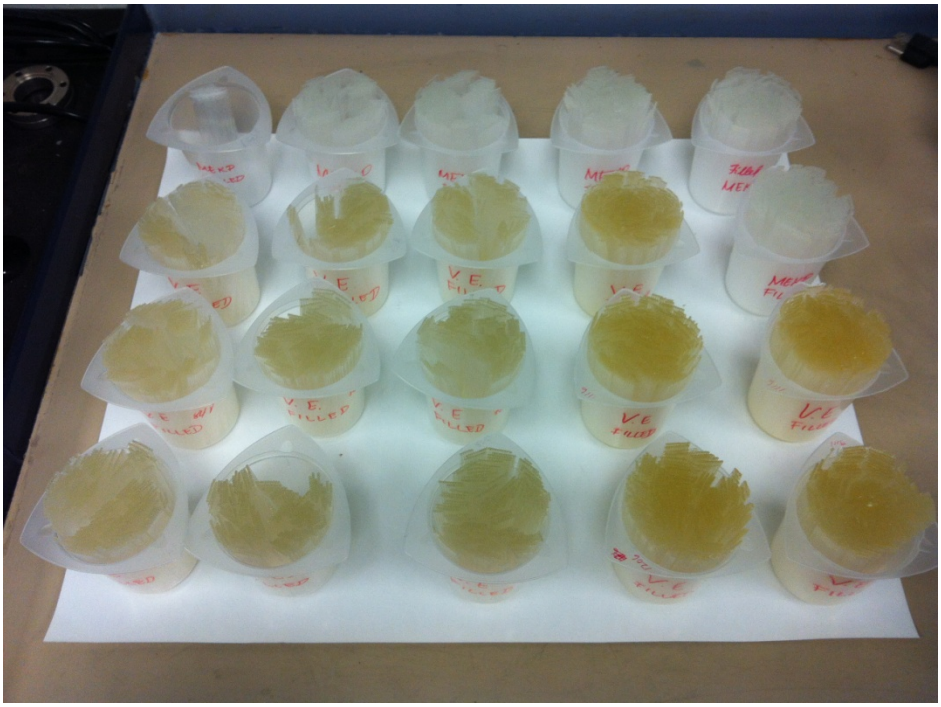

Figure 48. CNT-reinforced polyester resin.

Figure 49. Placing HGFs filled with self-healing agent and catalyst on a 4 x 8 ft panel of glass fiber fabric.

Figure 50. 2 GFRP panels with self-healing agent.

### 9.1.2 Fabrication for CNT reinforcement functionality (Panels 3 and 4)

The base matrix was polyester with E-glass fiber fabric. The polyester was reinforced with the CNTs, using 1 % wt of -COOH functionalized multiwall CNTs because reasonable improvement of mechanical properties was achieved based on that formulation. Results showed the flexural strength improved 10% while the modulus improved 7% as compared with the control GFRP panel. A completed panel with CNT reinforcement is shown in Figure 51.

### 9.1.3 Fabrication for EMI shielding functionality

A layer of CNT sheet was incorporated in the multifunctional panel (Panel 5) to improve electrical conductivity and EMI shielding properties.

Figure 51. One of the two GFRP panels that were reinforced with CNTs.

### 9.1.4 Self-decontamination functionality (Panels 6 and 7)

A biocidal coating was applied over the surface of the GFRP panels to include additional functionality. The coating contains a QUAT. QUATs are known to disrupt cell membranes and are very efficient in killing microorganisms. Antimicrobial coatings containing a variety of additives, including QUATs, are active against a broad-spectrum of potentially pathogenic bacteria (1–7 log kill), enveloped viruses (2–7 log kill), and fungi (1–2 log kill). The coating applied in this task contained 1% wt of hexadecyl-(2-methoxyethyl)-dimethyl-ammonium bromide which is a novel amphiphilic QUAT developed for applications in self-decontaminating surface coatings. The surface of the GFRP panels were coated with a primer and a QUAT-containing water-based acrylic latex topcoat. This task required 1 gal of primer coating (Sherwin Williams waterborne multi-purpose primer was used). The primer was applied by roller and then dried for 24 hr in air at room temperature. Sherwin Williams acrylic latex (43% vol. solids) paint was used, with the addition of 1 wt % of QUAT. At this percentage, 1 gal of paint required the addition of approximately 16.7 g of QUAT. The biocide was preliminarily dissolved in water by using an ultrasonic bath and then added to the paint in the form of an aqueous solution. The acrylic

topcoat also was applied by roller and dried for 24 hr in air at room temperature. The topcoat was purchased to complete this task.

Formulation of the coating for the GFRP panels was in accordance with suggestions from a journal article by Fulmer and Wynne (2012) of the Naval Research Laboratory (NRL). The self-decontaminated coating composition consisted of the following:

1. Topcoat: Sherwin Williams Acrylic Latex (type ProMar 400);
2. Endospores nutrient: Yeast Extract, 1 wt% (Fluka 92144);
3. Germinating agent 1: L-Alanine, 1 wt% (Sigma-Aldrich A7627);
4. Germinating agent 2: L-Methionine, 1 wt% (Sigma-Aldrich M9625);
5. QUAT: Hexadecyl-(2-methoxyethyl)-dimethyl-ammonium bromide, 1 wt% (obtained from Dr. Wynne);
6. PhotoScrub, a $TiO_2$-based photocatalyst (ANI), spray coated at 60 mg/sq ft.

This coating was applied in two layers. In the first layer, 1 gal of topcoat with 47% solid content will require the addition of 24 g of each ingredient (#2–5 from the above list) dissolved in small amounts of water. This topcoat mixture was applied to the panel and then allowed to dry for one day. The second layer consisted of a spray coating of PhotoScrub. Covering the panel with this photocatalyst required 2 g PhotoScrub dispersed in 2 L isopropyl alcohol (IPA) per panel.

The two panels fabricated with SDS coating are shown in Figure 52.

### 9.1.5 Fully multifunctional (Panel 5)

A 1.0 wt% loading of the –COOH functionalized CNTs was used to reinforce the GFRP panels. A 2.5 wt% loading of the self-healing agent was used in the GFRP panels. Results showed the flexural strength improved 2%, while the modulus improved 38%.

Figure 52. One panel reinforced with CNTs (left) and two panels coated with SDS coating (middle and right).


## 9.2 Cost model

The approximate cost was developed for added functionality of each full-size panel (in a lot of 1,000). Table 24 gives cost model details.

Table 24. Unit cost breakout for full-size multifunctional panel (>1000 quantity)

| Items | Cost/unit | Cost ($) |
|---|---|---|
| Resin | $2.0/kg, 16 kg needed | 32.00 |
| E-glass fiber | n/a | 58.00 |
| CNT additive | $1/g, 160 g needed | 160.00 |
| CNT sheet (Nanocomp) | $180/ sq ft, 32 sq ft needed | 5760.00 |
| HGF | $47/250, pieces needed | n/a |
| Self-healing agent/catalyst | n/a | 5.00 |
| Silicone sealant | $850/pint, ¼ pint needed | 212.50 |
| Labor for making CNT/resin | 2 kg/hr, 8 hr @$20/hr needed | 160.00 |
| Self-decontaminating primer | $26.99/gal, 1/5 gal needed | 5.40 |

| Items | Cost/unit | Cost ($) |
|---|---|---|
| Self-decontaminating paint | $58.30/gal, 1/5 gal needed | 11.56 |
| PhotoScrub coating | $21.20/liter, 2 L needed | 42.40 |
| Labor for filling, sealing, and placing the HGFs | $20/hr, 18 hr needed | 360.00 |
| Labor for coating the self-decontaminating paint | $20/hr, 0.5 hr needed (assuming automated process) | 10.00 |
| Labor for making the GFRP panel | 4 hr needed | 358.00 |
| Total | | 7174.86 |

The total weight for a 4 ft x 8 ft x 0.5 in. size GFRP panel is around 80 kg. The resin content is around 20 wt%. It can be seen in the above table that the main cost is the Nanocomp CNT sheet material needed ($5,760). There are much more cost-effective means of adding EMI shielding to the ballistic panel such as CNT-polymer matrix.

## 9.3 Fabrication to test flexural strength and modulus

Some GFRP laminate coupons were fabricated to check the change of flexural strength and modulus by incorporating the self-healing agent and other functionalities mentioned above. Nanocomp's CNT sheet and self-decontamination functionality was not included for this effort, as they were not expected to significantly affect the mechanical performance. The following sample sets were made for flexural strength and modulus testing:

- reference (control) sample (polyester with E-glass fiber);
- sample (GFRP incorporated with self-healing agent); and
- electrical GFRP incorporated with self-healing agent as well as CNT reinforcement.

Each sample set mentioned above included six specimens for mechanical testing (see Table 25).

Table 25. Flexural strength and modulus of the GFRP samples with and without self-healing agent (each sample contained six specimens; average value was taken).

| Samples | Flexural strength (MPa) | Flexural modulus (GPa) |
|---|---|---|
| Control | 222.8 | 14.1 |
| 1.0% -COOH CNT | 244.7 | 15.3 |
| 2.5% self-healing agent/1.0% -COOH CNT | 226.3 | 19.4 |
| 5.0% self-healing agent/1.0% -COOH CNT | 257.7 | 22.6 |
| 10.0% self-healing agent/1.0% -COOH CNT | 187.0 | 21.4 |

Table 25 shows that the GFRP sample containing 5.0% of the self-healing agent had the best mechanical properties. (The results were similar to those shown in Table 18.)

# 10 Summary and Recommendations

## 10.1 Summary

This work investigated methods to improve ballistics-resistant fiberglass panels by improving the mechanical properties of the polymer matrix and by incorporating additional functionalities such as self-healing capabilities, electromagnetic interference (EMI) shielding, and biocidal properties.

An investigation of numerous publications, presentations, and news articles related to ballistic resistance showed that mechanical properties of a polymer matrix that impact factors such as strength, compression, and flexural strength and modulus may be critical for improving the ballistic resistance of GFRP panels. This investigation provided a first focus for work to improve the mechanical and physical properties of a CNT-reinforced polymer matrix.

Incorporating CNTs into the polyester matrix was shown to improve its mechanical properties. Use of -COOH functionalized CNTs at a loading of 1.0 wt% achieved 23% improvement of flexural strength, 4% improvement of the flexural modulus, 26% improvement of compression strength, and 10% improvement of compression modulus; however, the impact strength was decreased about 48%. Better results were obtained from using -OH functionalized CNTs at a loading of 0.5 wt% which achieved 18% improvement of flexural strength, 4% improvement of the flexural modulus, 22% improvement of compression strength, 10% improvement of compression modulus, and 24% improvement of the impact strength. Use of the better-performing resin in fabricating the GFRP panels achieved a 5% improvement of V50 ballistic resistance.

Use of CNT sheets within the panel layers only marginally improved the panel's ballistic resistance, however. It was concluded that other approaches such as CNT-polymer matrix would achieve resistance in a more cost-effective manner.

HGFs filled with self-healing agent and catalyst were used to improve a panel's self-healing functionality because this approach can significantly increase the amount of catalyst and polymer available for the self-repair process. Different sizes of the HGF, different loadings of the self-healing

agent, and different positions of the self-healing layers were studied. Overall, the panels with HGF were weaker than the control panels that did not have HGF by about 5-10% using V50 testing. However, the V50 test performance of panels with self-healing agent that were shot but then allowed to heal exceeded the V50 test performance of the virgin panels using HGF and after 1 week, they even approached the performance of the control panels with no HGF.

Work to improve EMI shielding performance incorporated a copper mesh screen, a conductive carbon coating, and Exclucent material into or onto the panel as appropriate. For the GFRP panels incorporated with copper mesh screen, the EMI shield achieved 60-66 dB between 0.1 to 1000 MHz frequencies. The screen was shown to have less shielding, however, at the 8–10 GHz range. For the GFRP panel coated with a conductive carbon layer, EMI shielding was on the order of 5–10 dB. At 0.1 MHz and 1 MHz, the average was less than 1 dB, and at 10 MHz, the average shielding was found to be 5.17 dB. At higher frequencies, the shielding was averaged 23 dB. For the panel laminated with an Exclucent film on its surface, the average shielding was 4.33 dB at 100 kHz, 16.3 at 1 MHz, and 39 dB at 10 MHz.

To achieve biocidal properties on the panels, a combined QUAT-photocatalytic coating which possesses synergistic biocidal properties was co-developed with a team at NRL. The resulting data shows that the biocides added into the topcoat were not efficient for spore decontamination since it is likely that the chemicals in the paint have blocked the active surface sites or chemical groups of either QUAT or photocatalysts. The photocatalysts sprayed over the dried topcoat showed much better performance. The spore inactivation rate achieved over 180 min of exposure of sunlight was as high as 97.2 % for PhotoScrub V (log kill = 1.56), and it was lower for ZnO-based compositions.

The mechanical properties of the GFRP panels integrated with self-healing agent were tested. Different loadings (2.5%, 5.0%, and 10.0%) of the self-healing agent on compression and CAI were studied. It was found that the self-healing agent could effectively repair the damage of the GFRP panels. At the loading of 2.5% of the self-healing agent, the GFRP panel has the best self-healing efficiency (96%). A number of large GFRP panels (4 ft x 8 ft x 1/2 in.) were fabricated with different functionalities (self-healing agent, CNT reinforcement, self-decontamination, and CNT sheet).

The objective of the research was to develop multifunctional nanocomposite materials with CNTs that have enhanced mechanical properties and electrical properties, as well as capability for self healing and decontamination. The team conceived, developed, and validated a multifunctional nanocomposite technology consisting of innovative new individual components that can be combined with each other and conventional materials to produce a variety of previously unavailable capabilities. The overall intent of this research was to develop a multifunctional nanomaterial capability to use in both carbon fiber reinforced polymer (CFRP) and GFRP composite applications. At the center of this new technology is a nanocomposite material, made of epoxy resin blended with functionalized CNTs that exhibits highly improved flexural strength and electrical conductivity.

Some of the results of this multi-year effort are summarized in the peer-reviewed journal articles and conference proceedings of Barua et al. 2010; Hosur et al. 2012a, 2012b; Rahman et al. 2012a, 2012b,2013a, 2013b; Zainuddin et al. 2009, 2010a, 2010b, 2011; Mantena 2013, 2014.

## 10.2 Recommendations

Based on work done by Prof. Brian Wardle of the Dept. of Aeronautics and Astronautics at the Massachusetts Institute of technology in Cambridge, Massachusetts, it is recommended that CNTs should be grown directly on the fiber instead of adding them to the epoxy matrix (Wicks, Guzman de Villoria and Wardle 2010). This eliminates the difficulty of uniformly distributing the CNTs through the epoxy matrix, which results in a reduction of V50. The attachment of the CNTs to the fiber surface increases energy dissipation modes and increases the V50 value. Wardle et al. grew CNTs directly on alumina fibers and fabricated a composite using these ‘fuzzy fiber’ fabrics. They compared the fuzzy fiber composite to composites made with plain alumina fibers and measured an increase in V50 by 12% with 0.4% CNTs by wt. Furthermore, we have preliminary results that suggest that the V50 value can be increased by using fuzzy fiber glass fabrics as well. Additionally, these glass fabric fuzzy fiber composites also show remarking increases in energy absorption properties compared to plain glass fiber composites. At high strain rates, the specific energy absorption and the rate of specific energy absorption increased by over 100 %.

More work is necessary to optimize the increase in V50, energy absorption, and other mechanical properties by tuning the parameters of the CNT fabrication process.

# References

Abdelkader, M., J.C. Withers, R.O. Loutfy, A. Moravsky, and M. Sennett. 2002. "The Investigation of Carbon Nanotubes for Lightweight Armor Materials." In 23rd Army Science Conference, Orlando, FL. http://mindtel.com/2005/SDSU.Geol600.Sensor_Networks/sensornets.refs/2003.%20ASC.%20Army%20Studies%20Conference/LP-05.pdf

Ahmad, Mohd Rozi, Wan Yunus, Wan Ahmad, Jamil Salleh, and Azemi Samsuri. 2007. "Performance of natural rubber coated fabrics under ballistic impact." *Malaysian Polymer Journal* 2(1): 39-51.

Aliabadi, M. H., Wingfen Li, Li Li, and F. G. Buchholz. 2006. "High-Velocity Impact Characteristic of Carbon Fiber Reinforced Plastic Laminates Using Ballistic Range." *Key Engineering Materials* Vol. 324-325: 1071–1074.

Allen, L., W. F. Walker, and K. K. Siarkiewicz. 1976. "An Investigation of Electromagnetic Properties of Advanced Composite Materials." In IEEE International Symposium on Electromagnetic Compatibility. New York, NY: IEEE.

Anderson, Charles E., and Kathryn A. Dannemann. 2002. "Deformation and Damage of Two Aluminum Alloys from Ballistic Impact." In *AIP Conference Proceedings* 620(1): 1298–1301. College Park, MD: American Institute of Physics.

ASTM D256. "Standard Test Methods for Determining the Izod Pendulum Impact Resistance of Plastics." West Conshohocken, PA: ASTM International.

_____ D695. "Standard Test Method for Compressive Properties of Rigid Plastics." West Conshohocken, PA: ASTM International.

_____ D790. "Standard Test Methods for Flexural Properties of Unreinforced and Reinforced Plastics and Electrical Insulating Materials." West Conshohocken, PA: ASTM International.

_____ D3039. "Standard Test Method for Tensile Properties of Polymer Matrix Composite Materials." West Conshohocken, PA: ASTM International.

Barua, Rajib, Mahesh Hosur, Shaik Zainuddin, Shaik Jeelani, Ashok Kumar, Jonathan Trovillion, and Yadira Perez. 2010. "Processing and Characterization of Epoxy Nanocomposites with MWCNT's/CNT's using thinky and 3-roll shear mixing techniques." *Revista Matéria* 15: 247–253.

Ben-Dor, Gabi, Anotoly Dubinsky, and Tov Elperin. 2005. "Ballistic Impact: Recent Advances in Analytical Modeling of Plate Penetration Dynamics – A Review." *Applied Mechanics Reviews* 58: 355–371.

_____ 2009. "Ballistic Properties of Multilayered Concrete Shields." *Nuclear Engineering and Design* 239(10): 1789–1794.

Blake, C. L. 1976. "Composites–Their Electrical and Electromagnetic Impact." In IEEE International Symposium on Electromagnetic Compatibility. New York, NY: IEEE.

Booth, C. J., Megan Kindinger, Heather R. McKenzie, Jesse Handcock, Alan V. Bray, Gary W. Bealla. 2006. "Copolyterephthalates Containing Tetramethylcyclobutane with Impact and Ballistic Properties Greater than Bisphenol A Polycarbonate." *Polymer* 47(18): 6398–6405.

Brown, J. R., P. J. C. Chappell, and Z. Mathys. 1991. "Plasma Surface Modification of Advanced Organic Fibres: Part II Effects on the Mechanical, Fracture and Ballistic Properties of Extended-Chain Polyethylene/Epoxy Composites." *Journal of Materials Scienc*e 27: 31673172.

Brown, Tania, and Ercan Sevkat. 2008 "Ultrasound Studies of Drop-Weight Impact Responses of Woven Hybrid Glass-Graphite/Toughened Epoxy Composites." In ASME 2008 International Mechanical Engineering Congress and Exposition, Vol. 12: *Mechanics of Solids, Structures and Fluids*. Event held 31 October–6 November at Boston MA.
http://proceedings.asmedigitalcollection.asme.org/proceeding.aspx?articleid=1644026

Chen, Bill, Eric Beckel, and Jerry Chung. 2007a. "Low and Medium Speed Multi-Axial Impact Responses of Fiber Reinforced Thermoplastic and Thermoset Composites." Presented at SAMPE Spring Conference in May at Baltimore, MD.

_____ 2007b. "Effects of Resins on Low and Medium Speed Impact of Glass Fiber Reinforced Composites." Presented at SAMPE Spring Conference held in May 2007 at Baltimore, MD.

Colakoglu, M., O. Soykasap, and T. Ozek. 2007. "Experimental and Numerical Investigations on Ballistic Performance of Polymer Matrix Composites Used in Armor Design." *Applied Composite Materials* 14(1): 47–58.

DuPont. n.d."Science Behind the Story: Ballistic Protection."
http://www.dupont.com/content/dam/dupont/corporate/our-approach/global-challenges/documents/Science%20Behind%20Ballistic%20Protection%20Final%20Formatted.pdf

Edwards, M. R., and H. Waterfall. 2008. "Mechanical and ballistic properties of polycarbonate apposite to riot shield applications." *Plastics, Rubber and Composites* 37(1): 1–6.

Faur-Csukat, G. 2005. "Development of Fibre Reinforced Ballistic Composites." Proceeding of the 8th Polymers for Advanced Technologies International Symposium, held 13-16 September in Budapest, Hungary.

Fink, Richard. 2011. *Improved Ballistic Resistance of E-Glass FRP Panels*. Final report on Contract No. W9132T-10-C-0020 for the U.S. Army. Austin, TX: Applied Nanotech, Inc.

Franks, Lisa Prokurat, ed. 2009. *Advances in Ceramic Armor IV: Ceramic Engineering and Science Proceedings*. Vol. 29, No. 6. Westerville, OH: The American Ceramic Society.

Fulmer, P.A., and J.H. Wynne. 2012. "Coatings Capable of Germinating and Neutralizing Bacillus Anthracis Endospores." *Applied Materials and Interfaces* 2012(4): 738–743.

Gama, Bazle A., S. M. Waliul Islam, and Mostafezur Rahman. 2005. "Punch Shear Behavior of Thick-Section Composites Under Quasi-Static, Low Velocity, and Ballistic Impact Loading." *SAMPE Journal* 41(4): 6–13.

Gama, B. A., S. Y. Yarlagadda, and M. Kubota. 2006. "Low Velocity Impact and Damage Behavior of Kevlar Bonded Carbon/Epoxy Composites Fabricated by Near-IR Irradiation," *In Proceedings of Composites & Polycon 2006*, American Composites Manufacturing Association (ACMA) held 18-20 October in St. Louis, MO.

Genuth, Iddo, and Tomer Yaffe. 2006. "Protecting the Soldiers of Tomorrow." IsraCast: http://www.isracast.com/article.aspx?id=28

Gilde, Gary A. and Jane W. Adams. 2005. *Processing and Ballistic Performance of $Al_2O_3/TiB_2$ Composites*. ARL-TR-3658. Adelphi, MD: Army Research Laboratory.

Gogolowski, Raymond P., and Bruce R. Morgan. 2001. *Ballistic Experiments with Titanium and Aluminum Targets.* DOT/FAA/AR-01/21. Washington, DC: U.S. Department of Transportation, Federal Aviation Administration, Office of Aviation Research.

Gooch, William A., and Matthew S. Burkins. 2001. "Development and Ballistic Testing of a Functionally Gradient Ceramic/Metal Applique." Presented at the PTO AVT Specialists' Meeting on "Cost Effective Application of Titanium Alloys in Military Platforms" held in Loen, Norway, May 7–11.

Grujicic, Mica, B. Pandurangan, D. D. Angstadt, K. L. Koudela, and B. A. Cheeseman. 2007. "Ballistic-Performance Optimization of a Hybrid Carbon-Nanotube/E-Glass Reinforced Poly-Vinyl-Ester-Epoxy-Matrix Composite Armor." *Journal of Materials Science* 42: 5347–5359.

Harel, H., G. Marom, and S. Kenig. 2002. "Delamination Controlled Ballistic Resistance of Polyethylene/Polyethylene Composite Materials." *Applied Composite Materials* Vol. 9: 33–42.

Honeywell. 2015. "Composite Materials (Spectra HT fiber)." http://www.honeywell-advancedfibersandcomposites.com/product/tag/composite-materials/

Hong, S., and D. Liu. 1989. "On the Relationship Between Impact Energy and Delamination Area." *Experimental Mechanics* 29(2): 115–120.

Horsfall, I., C. H. Watson, and C. Boswell. 2007. "Residual Strength of Composites after Ballistic Impact." Presented at 23rd International Symposium on Ballistics, held 16–20 April in Tarragona, Spain.

Hosur, Mahesh V., Mazedul Islam, Aziz Ahmed, and Shaik Jeelani. 2007. "Low Velocity and High Strain Rate Compression Response of Braided Carbon/Epoxy Composites." Presented at SAMPE Spring Conference held in May at Baltimore, MD.

Hosur, Mahesh, Rajib Barua, Shaik Zainuddin, Ashok Kumar, Jonathan Trovillion, and Shaik Jeelani. 2012a. "Effect of Processing Techniques on the Performance of Epoxy/MWCNT Nanocomposites." *Journal of Applied Polymer Science* 127(6): 4211–4244. doi: 10.1002/APP.37990.

_____ 2012b. "Rheology, Flexure and Thermomechanical Characterization of Epoxy/CNF Nanocomposites: Effect of Dispersion Techniques." *Polymers and Polymer Composites* 20(6): 517–530.

Jensen, R. E., and S. H. McKnight. 2004. "Nano-Textured Fiber Coatings for Energy Absorbing Polymer Matrix Composite Materials." In *Proceedings for the 24th Army Science Conference* held 29 Nov–2 Dec in Orlando, Florida. Aberdeen Proving Ground, MD: Army Research Laboratory, Multifunctional Materials Research Branch. http://www.dtic.mil/cgi-bin/GetTRDoc?AD=ADA433232

Jensen, Robert E., Steven H. McKnight, Dave P. Flanagan, Alan R. Teets, and Donovan Harris. 2004. "Hybrid Fiber Sizings for Enhanced Energy Absorption in glass-Reinforced Composites." ARL-TR-3241. Aberdeen Proving Grounds, MD: Army Research Laboratory, Multifunctional Materials Research Branch.

Karahan, Mehmet, Abdil Kus, and Recep Eren. 2008. "An Investigation into Ballistic Performance and Energy Absorption Capabilities of Woven Aramid Fabrics." *International Journal of Impact Engineering* 35(6): 499–510.

Kohlman, William G. 1995. "Ballistic Performance of Polycarbonate/Polyester and Polycarbonate/Styrene-Acrylonitrile Microlayer Sheets." *Polymer Engineering and Science* 35(14): 1191–1195.

Kyziol, Leslaw. 2007. "Shooting Resistance of Non-Metallic Materials." *Polish Maritime Research* 14: 68–73.

Lee, Young S., E. D. Wetzel, and N. J. Wagner. 2003 "The Ballistic Impact Characteristics of Kevlar Woven Fabrics Impregnated with a Colloidal Shear Thickening Fluid." *Journal of Materials Science* 38: 2825–2833.

Mantena, P. Raju, Alexander H. D. Cheng, and Ahmed Al-Ostaz 2010. "Blast and Impact Resistant Composite Structures for Navy Ships." 2010 Office of Naval Research – Solid Mechanics Program. Marine Composites and Sandwich Structures Conference, University of Maryland. doi: 10.13140/2.1.3127.1364.

Mantena, P. R., T. Tadepalli, B. Pramanik, V. M. Boddu, M. W. Brenner, L. D. Stephenson, and A. Kumar. 2013. "Energy Dissipation and the High-Strain Rate Dynamic Response of Vertically Aligned Carbon Nanotube Ensembles Grown on Silicon Wafer Substrate." *Journal of Nanomaterials* Vol. 2013: Article ID 259458. http://dx.doi.org/10.1155/2013/259458

Mantena, P. R., B. Pramanik, T.Tadepalli, V. M. Boddu, M. W. Brenner, and A. Kumar. 2014. "Effect of Process Parameters on the Dynamic Modulus, Damping and Energy Absorption of Vertically Aligned Carbon Nano-Tube (VACNT) Forest Structures." *Journal of Multifunctional Composites* 2: 93–100.

Mao, Dongsheng, and Richard Fink. 2013. Improved Ballistic Resistance of E-Glass FRP Panels. Final report on Contract No. W9132T-12-0014 for the U.S. Army. Austin, TX: Applied Nanotech, Inc.

MIL-DTL-53039D. 2011. "Detail Specification: Coating, Aliphatic Polyurethane, Single Component, Chemical Agent Resistant." Aberdeen Proving Ground, MD: U.S. Army Research Laboratory, Weapons and Materials Research Directorate, Materials Manufacturing, Technology Branch.

MIL-PRF-85582D. 2011. "Performance Specification: Primer Coatings: Epoxy, Waterborne." Washington, DC: Department of Defense, U.S. Navy, Naval Air Warfare Center Aircraft Division.

MIL-STD-662F. 1997."Military Standard: V50 Ballistic Test for Armor." Aberdeen Proving Ground, MD: Department of Defense, U.S. Army Research Laboratory, Weapons & Materials Research Directorate.

Naik, N. K., P. Shrirao, and B. C. K. Reddy. 2005. "Ballistic Impact Behavior of Woven Fabric Composites: Parametric Studies." *Materials Science Engineering: A* 412: 104–116.

Nanocomp Technologies. 2009. "Nanocomp Technologies Reaches New Production Milestones for Carbon Nanotube Yarn and Large Format Mats." Press release. Merrimack, NH: Nanocomp Technolgoies, Inc.

Nycon. n.d. "Nycon-SF Type I." http://nycon.com/nycon-sf-type-i-n/. Fairless Hills, PA: Nycon Corp.

Ostermayer, D., F. L. Beyer, P. G. Dehman, and M. A. Klusewitz. 2001."Measurement of V50 Behavior of a Nylon 6-Based Polymer-Layered Silicate Nanocomposite." ARL-TR-2605. Aberdeen Proving Grounds, MD: Army Research Laboratory.

Patel, B. P., S. K. Bhola, M. Ganapathi, and D. P. Makhecha. 2004. "Penetration of Projectiles in Composite Laminates." *Defense Science Journal* 54(2): 151–159.

Pathomsap, Somsiri, Tharathon Mongkhonsi, Kuljira Sujirote, and Sarawut Rimdusit. 2006. "Development of Light Weight Ballistic Armor from Polybenzoxazine Alloys and Kevlar™ Fiber." Presented at 4th Thailand Materials Science and Technology Conference held 31 Mar.–1 Apr.

Polito, Anthony J., Ronald E. Bailey, William W. Timmons, and Robert H. Bell. 1998. "Ballistic resistant metal armor plate." U.S. Patent 5749140. Washington, DC: U.S. Patent and Trademark Office.

PPG Industries. n.d. "Military Strength Fiberglass." http://www.ppg.com/corporate/governmentsolutions/SiteCollectionDocuments/MilitaryStrengthFiberglass.pdf

Prosser, Robert A., Samuel H. Cohen, and Ronald A. Segars. 2000. "Heat as a Factor in the Penetration of Cloth Ballistic Panels by 0.22 Caliber Projectiles." *Textile Research Journal* 70(8): 709–722.

Quan, Xiangyang, and Naury Birnbaum. 1999. "SPH Simulation of the Ballistic Perforation of GFRP." Presented at 18th International Symposium and Exhibition on Ballistics, held 15-19 Nov. in San Antonio, TX.

Rahman, Muhammad M., Mahesh Hosur, Adriane G. Ludwick, Shaik Zainuddin, Ashok Kumar, Jonathan Trovillion, and Shaik Jeelani. 2012a. "Thermo-Mechanical Behavior of Epoxy Composites Modified with Reactive Polyol Diluent and Randomly-Oriented Amino-Functionalized Multi-Walled Carbon Nanotubes." *Polymer Testing* 31: 777–784.

Rahman, M.M., S. Zainuddin, M. V. Hosur, J.E. Malone, M.B.A. Salam, Ashok Kumar, and S. Jeelani. 2012b. "Improvements in Mechanical and Thermo-Mechanical Properties of E-glass/Epoxy Composites Using Amino Functionalized MWCNTs." *Composite Structures* 94: 2397–2406.

Rahman, M.M., M. Hosur, S. Zainuddin, U. Vaidya, A. Tauhid, A. Kumar, J. Trovillion, and S. Jeelani. 2013a. "Effects of Amino-Functionalized MWCNTs on Ballistic Impact Performance of E-Glass/Epoxy Composites Using a Spherical Projectile. *International Journal of Impact Engineering* 57: 108–118.

Rahman, M. M., S. Zainuddin, M. V. Hosur, C. J. Robertson, Ashok Kumar, Jonathon Trovillion, and S. Jeelani. 2013b. "Effect of $NH_2$-MWCNTs on Crosslink Density of Epoxy Matrix and ILSS Properties of E-glass/Epoxy Composites." *Composite Structures* 95: 213–221.

Raju, Basavaraju, Dongying Jiang, Yushun Cui, Yuanyuan Liu, and Zheng-Dong Ma. 2006. "Simulation and Design of Nanocomposite for Application in Ballistic Protection." STA 7114-E Rev 21, paper presented at Army Science Conference (26th) Held in Orlando, Florida on 1–4 December 2008. Warren, MI: U.S. Army Tank–Automotive and Armament. http://www.dtic.mil/cgi-bin/GetTRDoc?Location=U2&doc=GetTRDoc.pdf&AD=ADA505716

Reddy, G. Madhusudhan, and T. Mohandas. 1996. "Influence of Welding Process and Residual Stress on Ballistic Performance." *Journal of Materials Science Letters* 15, 1633–1635.

Reyes-Villanueva, G., and W. J. Cantwell. 2004. "The High Velocity Impact Response of Composite and FML-Reinforced Sandwich Structures." *Composites Science and Technology* 64: 35–54.

Rincon, Paul. 2007. "Super-strong body armour in sight", http://news.bbc.co.uk/2/hi/science/nature/7038686.stm

Roberts, Gary D., Duane M. Revilock, Wieslaw K. Binienda, Walter Z. Nie, S. Ben Mackenzie, and Kevin B. Todd. 2002. "Impact Testing and Analysis of Composites for Aircraft Engine Fan Cases." NASA/TM-2002-211493. Cleveland, OH: National Aeronautics and Space Administration, Glenn Research Center.

SACMA. 1994. "Compressive Properties of Oriented Fiber-Resin Composites." SACMA Recommended Method SRM 2R-94. (SACMA was replaced 1 June 2000 by the Carbon Fiber Management Council, formed by the Composite Fabricators Association.)

Santulli, C., and A. P. Caruso. 2009. "A Comparative Study on Falling Weight Impact Properties of Jute/Epoxy and Hemp/Epoxy Laminates." *Malaysian Polymer Journal* Vol. 4(1): 19–29.

Sevkat, E., B. M. Liaw, F. Delale, and B. B. Raju. 2007. "Experimental and Numerical Studies of S2-Glass Fiber/Toughened Epoxy Composite Beams Subject to Drop-Weight or Ballistic Impact." 2007 ASME International Mechanical Engineering Congress and Exposition held November 11–15 in Seattle, WA.

Showalter, Dwight D., William A. Gooch, Mathew S. Burkins, and R. Stockman Koch. 2008. *Ballistic Testing of SSAB Ultra-High-Hardness Steel for Armor Applications*. ARL-TR-4632. Adelphi, MD: Army Research Laboratory.

Sun, C. T., and S. V. Potti. 1996. "A Simple Model to Predict Residual Velocities of Thick Composite Laminates Subjected to High Velocity Impact." *International Journal of Impact Engineering* 18: 339–353.

Takazuka, Takeshi. 1979. "Method of mixing steel fiber reinforced concrete." U.S. Patent 4159911. Washington, DC: U.S. Patent and Trademark Office.

Tatum, Malcolm. 2015. "What is Ballistic Nylon?" http://www.wisegeek.com/what-is-ballistic-nylon.htm

Total Security Solutions. n.d. "Bullet Proof Glass and Materials." http://www.tssbulletproof.com/bullet_proof_glass_materials?gclid=CMrw9Nuh96ACFQtM5wodMV4fvw

Trask, R.S., G. J. Williams, and I.P. Bond. 2007. "Bioinspired Self-Healing of Advanced Composite Structures Using Hollow Glass Fibres." *Journal of the Royal Society Interface* (4) 363–371.

Trovilion, J.C., N. Boone, R. Fink, D. Mao. 2010. "Improving the Ballistic Performance of E-glass Composite Panels Using Carbon nanotubes." Presented at the 24th Army Science Conference held 29 Nov–02 Dec in Orlando, FL.

Uddin, M. F., H. Mahfuz, S. Zainuddin, and S. Jeelani. 2009. "Improving Ballistic Performance of Polyurethane Foam by Nanoparticle Reinforcement." *Journal of Nanotechnology* 2009: Article ID #794740.

UL Standard 752. Oct. 2005 (rev). "Standard for Bullet-Resisting Equipment." In Chapter 17, "Ballistics Test" in "Performance Bullet-Resisting Materials" section. Northbrook, IL: UL.

Vanark, Virginia C, Thomas M. Ford, Carlo B. Sonnino. 1996. "Ballistic armor and method of producing the same." U.S. Patent 5483864. Washington, DC: U.S. Patent and Trademark Office.

Velmurugan, R., M. Ganesh Babu, and N. K. Gupta. 2006. "Projectile Impact on Sandwich Panels." *International Journal of Crashworth*iness 11(2): 153–164.

VietnamGear.com. 2006. "Who are you calling chicken." http://www.vietnamgear.com/Article.aspx?Art=91

Walker, James D. 2001. "Ballistic Limit of Fabrics with Resin." 19th International Symposium of Ballistics held 7–11 May Interlaken, Switzerland.

Walsh, Shawn M., Brian R. Scott, David M. Spagnuolo, and James P. Wolbert. 2007. "Examination of Thermoplastic Materials for Use in Ballistic Applications." Presented at SAMPE Spring Conference held May 2007 in Baltimore, MD.

White, S. R., N. R. Sottos, P. H. Geubelle, J. S. Moore, M. R. Kessler, S. R. Sriram, E. N. Brown and S. Viswanathan. 2001. "Autonomic Healing of Polymer Composites." *Nature* 409: 794–797.

Wicks, Sunny S., Roberto Guzman de Villoria, and Brian L. Wardle. 2010. "Interlaminar and Intralaminar Reinforcement of Composite Laminates with Aligned Carbon Nanotubes." ***Composites Science and Technology*** **70(1)**: 20–28.

Wright, S. C.,N. A. Fleck, and W. J. Stronge. 1993. "Ballistic Impact of Polycarbonate: An Experimental Investigation." *International Journal of Impact Engineering* 13(1): 1–20.

Xu, Jifeng, Abe Askari, Olaf Weckner, and Stewart Silling. 2008. "Peridynamic Analysis of Impact Damage in Composite Laminates." *Journal of Aerospace Engineering* 21(3): 187–194.

Zainuddin, S., M. V. Hosur, Y. Zhou, A. Kumar, and S. Jeelani. 2009. "Durability Studies of Montmorillonite Clay Filled Epoxy Composites under Different Environmental Conditions." *Materials Science and Engineering A* 507(1–2): 117–123.

Zainuddin, S., M. V. Hosur, A. Kumar, and S. Jeelani. 2010a. "Durability Study of Neat/Nanophased GFRP Composites Subjected to Different Environmental Conditioning." *Materials Science and Engineering A* 527(13–14): 3091–3099.

Zainuddin, S., M. V. Hosur, Y. Zhou, Alfred T. Narteh, A. Kumar, and S. Jeelani. 2010b. "Experimental and Numerical Investigations on Flexure and Thermal Properties of Nanoclay-Epoxy Nanocomposites." *Materials Science Engineering A* 527: 7920–7926.

Zainuddin, S., M. V. Hosur, R. Barua, Ashok Kumar, and S. Jeelani. 2011. "Effects of Ultraviolet Radiation and Condensation on Static and High Strain Rate Compression Behavior of Nanoclay Infused Glass/ Epoxy Composites." *Journal of Composite Materials* 45(18): 1901–1918.

Zhong, Weizhou, Shuncheng Song, Fangju Zhang, Qingping Zhang, Xicheng Huang, Sizhong Li, and Yonggang Lu. 2008. "Experimental Research on Behavior of Composite Material Projectile Penetrating Concrete Target." In *Transactions of Tianjin University* 14(6), 430–433.

# Abbreviations

| Term | Meaning |
|---|---|
| ANI | Applied Nanotech, Inc. |
| ARL | Army Research Laboratory |
| BA | benzoxazin |
| BAA | Broad Agency Announcement |
| BPA | bisphenol A |
| CAI | compression after impact |
| CARC | chemical agent resistant coatings |
| CBDO | 2,2,4,4-tetramethyl-1,3-cyclobutanediol |
| CFRP | carbon fiber reinforced polymer |
| CNT | carbon nanotube |
| DWNT | double-walled carbon nanotube |
| E-glass | a type of glass fiber; electrical-grade glass |
| EMI | electromagnetic interference |
| ERDC-CERL | Engineer Research and Development Center, Construction Engineering Research Laboratory |
| FRP | fiberglass reinforced polymer |
| FSP | fragment-simulating projectile |
| GFRP | glass fiber reinforced polymer |
| HGF | hollow glass fiber |
| ID | inner diameter |
| IPA | isopropyl alcohol |
| MB | methylene blue |
| MEKP | methyl ethyl ketone peroxide |
| MWNT | multi-walled carbon nanotube |
| $NH_3$ | ammonia |
| NRL | Naval Research Laboratory |
| OD | outer diameter |
| PC | polycarbonate |
| PU | polyurethane elastomer |
| QUAT | quaternary ammonium compound biocide |
| S2 | Type of glass fiber |
| SACMA | Suppliers of Advanced Composite Materials Association |
| SDS | self-decontaminating surface |
| SEM | scanning electron microscope |

| Term | Meaning |
|---|---|
| $SiO_2$ | silicon dioxide |
| SPH | smooth particle hydrodynamics |
| SRM | SACMA Recommended Method |
| TiN | titanium nitride |
| $TiO_2$ | titanium dioxide |
| VE | vinyl ester |
| $WS_2$ | tungsten disulfide |
| wt% | percentage by mass |

# REPORT DOCUMENTATION PAGE

*Form Approved*
*OMB No. 0704-0188*



| 1. REPORT DATE (DD-MM-YYYY) | 2. REPORT TYPE | 3. DATES COVERED (From - To) |
|---|---|---|
| 15-May-2015 | Final | |

**4. TITLE AND SUBTITLE**
Multifunctional Nanocomposites for Improved Sustainability and Protection of Facilities

**5a. CONTRACT NUMBER**

**5b. GRANT NUMBER**

**5c. PROGRAM ELEMENT NUMBER**
RDT&E 622784 T41

**6. AUTHOR(S)**
Dongsheng Mao, Igor Pavlovsky, and Richard L. Fink, Jonathan C. Trovillion, Veera M. Boddu, L.D. Stephenson, Debbie J. Lawrence, and Ashok Kumar

**5d. PRO JECT NUMBER**
#157067 and #331695

**5e. TASK NUMBER**

**5f. WORK UNIT NUMBER**

**7. PERFORMING ORGANIZATION NAME(S) AND ADDRESS(ES)**
U.S. Army Engineer Research and Development Center
Construction Engineering Research Laboratory
P.O. Box 9005
Champaign, IL 61826-9005

**8. PERFORMING ORGANIZATION REPORT NUMBER**
ERDC/CERL TR-15-6

**9. SPONSORING / MONITORING AGENCY NAME(S) AND ADDRESS(ES)**
Headquarters
US Army Corps of Engineers
441 G Street NW
Washington DC 20314-1000

**10. SPONSOR/MONITOR'S ACRONYM(S)**
HQUSACE

**11. SPONSOR/MONITOR'S REPORT NUMBER(S)**

**12. DISTRIBUTION / AVAILABILITY STATEMENT**
Approved for public release; distribution is unlimited.

**13. SUPPLEMENTARY NOTES**

**14. ABSTRACT**

The U.S. Army makes worldwide use of high-performance ballistic-resistant fiberglass composite panels for force protection and other applications. This widespread use creates a need for an improved panel material that offers better bullet resistance at a lighter weight while still meeting existing ballistic resistance standards. The team's work to solve the Army's need included conceiving, developing, and validating a new nanocomposite material that is made of epoxy resin blended with functionalized carbon nanotubes (CNTs) that exhibits highly improved flexural strength and electrical conductivity for improving ballistic resistance in lighter weight glass fiber reinforced polymer (GFRP) ballistic panels. In addition, the team's work tested various options for adding self-healing, CNT reinforcement, EMI shielding, and self-decontaminating properties for GFRP panels. Results of separate studies included in this report are: loading panels with CNTs by using different mass fractions and functionalization methods; introducing a self-healing agent directly to the matrix or contained in embedded hollow glass fibers; using layers of proprietary CNT sheeting in the GFRP composite; testing the electromagnetic impulse (EMI) shielding effects of introducing conductive materials; and adding a biocide-containing coating to finished panels.

**15. SUB JECT TERMS**
glass fiber reinforced polymer (GFRP); ballistic-resistant fiberglass panels; nanocomposite materials; ballistics; carbon nanotube (CNT)

| 16. SECURITY CLASSIFICATION OF: | | | 17. LIMITATION OF ABSTRACT | 18. NUMBER OF PAGES | 19a. NAME OF RESPONSIBLE PERSON |
|---|---|---|---|---|---|
| a. REPORT | b. ABSTRACT | c. THIS PAGE | | | 19b. TELEPHONE NUMBER (include area code) |
| U | U | U | UU | 111 | |